



**NTNU – Trondheim**  
Norwegian University of  
Science and Technology

# Magnetic Design for High Temperature, High Frequency SiC Power Electronics

**Torbjørn Sørsdahl**

Master of Energy and Environmental Engineering

Submission date: July 2013

Supervisor: Tore Marvin Undeland, ELKRAFT

Norwegian University of Science and Technology  
Department of Electric Power Engineering



## 1 Summary

Power electronic components which can operate at high temperatures would benefit a large number of different applications such as in petroleum exploration, aviation and electrical vehicles. Silicon carbide semiconductors have in the recent years been introduced commercially in the market. They are opening up new possibilities to create high temperature devices, due to its superior properties over silicon. Design of high temperature magnetic components is still a tedious process compared to normal temperature levels due to little information and software to simplify this process.

The purpose of this thesis is to develop analytical software for high frequency magnetic design in the temperature range from 130°C, and up to 200°C. Care has been taken into developing temperature dependent loss models and thermal design. The software is primarily for inductors, but most of the theory and discussion are also valid for transformers. Prototypes have been built and tested against the software predictions and good correlation has been observed.

A brief introduction to magnetic materials that can be used at elevated temperatures have been included focusing on powder cores and ferrites, since other high frequency materials could not operate at 200°C. It was found that for most materials, it is the laminations and binder agents that introduce the temperature limit. Materials are designed for specific temperatures which make it likely that when there is a larger commercial interest for higher temperatures, new materials will be developed. Core characterization of ferrites and powder cores was performed with a Brochause steel tester up to 10 kHz, and the losses up to 100 kHz were measured using an oscilloscope and amplifier approach. The characterization was performed at 20°C 108°C and 180°C.

The measurements show that the analytical loss data provided by the manufacturers underestimates the losses in Sendust and MPP materials, while there is a good correlation in High Flux, R-ferrite and N27. New Steinmetz parameters were calculated for MPP and Sendust for 20 kHz. Temperature primarily influences only Sendust up to 180 °C by a factor of 10-20 %, the little temperature dependence is in powder cores due to very high curie temperature.

Winding configurations have been investigated, and Litz wire for 200°C do not seem to exist commercially at this date, however wire for 130°C was successfully used in several 180°C experiments, but permanent degradation was observed in wires which had been exposed for several hours. It was found that the insulation in enamel coated round conductors have problems at elevated temperatures under the rated temperature in the areas where the wire was bent, this was not observed in Litz wire.

It has been shown that parallel connection of smaller powder cores can in some cases be used to obtain smaller designs with better thermal dissipation than with a single core. Leakage capacitance has been measured in several designs and by inserting an air gap between layers the capacitance was reduced in the same order as a Bank winding.

Output filter for  $dv/dt$ , Sinus, and a step down converter have been calculated and built. The step down filter has been tested in a buck converter, and compared to analytical data.

## 2 Preface

This thesis was started as a summer job at SmartMotor in Trondheim 2012, and continued during my final year in Energy and Environment. The thesis has been very interesting and I have learned much on how to design magnetic components at higher temperatures, and how often laboratory equipment do not work as planned.

During my work on this specialization project there are many people I would like to thank. First I would like to thank my supervisor Professor Tore M. Undeland for giving me the possibility to work on this topic, and he's support. Second the invaluable help of Dr. Richard Lund and his practical experience in filter and inductor design. Third Professor Arne Nysveen, Edris Agheb and Amir Hayati Soloot for helping me out with lab equipment, and spending time to show me how to use it. Finally everyone in the mechanical workshop and the service lab for always being able to help me.

Torbjørn Sørtdahl  
Trondheim Norway  
July 2013

## Table of Contents

<b>1</b>	<b>SUMMARY .....</b>	<b>I</b>
<b>2</b>	<b>PREFACE.....</b>	<b>II</b>
<b>3</b>	<b>LIST OF FIGURES.....</b>	<b>VII</b>
<b>4</b>	<b>LIST OF TABLES.....</b>	<b>XI</b>
	<b>NOMENCLATURE.....</b>	<b>XIII</b>
	<b>ABBREVIATION.....</b>	<b>XV</b>
<b>1</b>	<b>INTRODUCTION.....</b>	<b>1</b>
1.1	BACKGROUND.....	1
1.2	PROBLEM DESCRIPTION.....	2
1.3	REPORT OUTLINE .....	3
<b>2</b>	<b>SILICON CARBIDE .....</b>	<b>5</b>
2.1	SILICON CARBIDE IN POWER ELECTRONICS.....	5
2.2	COMPARISON OF SIC TO CONVENTIONAL SWITCHES.....	7
2.3	REFERENCES .....	8
<b>3</b>	<b>COMPONENTS IN SINUS FILTERS AND DV/DT FILTERS.....</b>	<b>9</b>
3.1	INTRODUCTION .....	9
3.2	FILTER THEORY .....	10
3.3	CRITICAL CABLE LENGTH .....	11
3.4	DV/DT FILTER .....	12
3.5	SINUS OUTPUT FILTER .....	13
3.6	SIMULATION MODEL.....	14
3.7	REFERENCES .....	16
<b>4</b>	<b>MAGNETIC MATERIALS .....</b>	<b>17</b>
4.1	POWDER CORES.....	18
4.2	SOFT FERRITES .....	22
4.3	SHAPE .....	23
4.4	PERMEABILITY.....	23
4.5	CORE LOSS .....	26
4.6	REFERENCES .....	28
<b>5</b>	<b>CORE LOSS .....</b>	<b>29</b>
5.1	FLUX WAVEFORMS.....	29
5.2	LOSS MODELS .....	30
5.3	PARAMETERS INFLUENCING CORE LOSS.....	33
5.4	REFERENCES .....	34
<b>6</b>	<b>WINDING CONFIGURATION .....</b>	<b>35</b>
6.1	INTRODUCTION .....	35
6.2	LITZ WIRE.....	38
6.3	ROUND WIRE.....	39

6.4	FOIL WINDING.....	40
6.5	PARASITIC CAPACITANCES.....	41
6.6	REFERENCES .....	44
<b>7</b>	<b>THERMAL ASPECTS &amp; MODELS.....</b>	<b>45</b>
7.1	INTRODUCTION .....	45
7.2	THERMAL MODELING.....	46
7.3	COMSOL MODEL .....	46
7.4	HEAT TRANSFER BY CONDUCTION.....	47
7.5	HEAT TRANSFER BY CONVECTION .....	48
7.6	NATURAL CONVECTION AND FORCED CONVECTION .....	48
7.7	HEAT TRANSFER BY RADIATION .....	53
7.8	MOUNTING .....	54
7.9	EMPIRICAL THERMAL MODEL.....	55
7.10	MODEL COMPARISON.....	56
7.11	WINDING THERMAL RESISTANCE .....	57
7.12	CORE THERMAL RESISTANCE.....	59
7.13	THERMAL MODEL FOR TOROID MAGNETIC COMPONENTS .....	60
7.14	EXTERNAL THERMAL RESISTANCE.....	62
7.15	REFERENCES .....	63
<b>8</b>	<b>INDUCTOR SOFTWARE .....</b>	<b>64</b>
8.1	SHORT INTRODUCTION.....	64
8.2	LIMITATIONS && GOAL.....	64
8.3	INPUT PARAMETERS .....	64
8.4	OUTPUT PARAMETERS .....	69
8.5	EXPERIMENTAL RESULTS.....	69
8.6	REFERENCES .....	70
<b>9</b>	<b>FILTER DIMENSIONS.....</b>	<b>71</b>
9.1	FILTER FOR A BUCK CONVERTER .....	71
9.2	SINUS AND DV/DT FILTER .....	73
9.2.1	<i>RLC Dv/dt Filter.....</i>	<i>73</i>
9.2.2	<i>Sinus Filter .....</i>	<i>75</i>
9.3	FILTER COMPARISON .....	76
9.4	REFERENCES .....	77
<b>10</b>	<b>LABORATORY SETUP .....</b>	<b>78</b>
10.1	SAMPLES.....	78
10.2	CORE LOSS CHARACTERIZATION .....	78
10.2.1	<i>Measurement setup BROCHAUS MPG.....</i>	<i>78</i>
10.2.2	<i>Core characterisation at 180.5°C .....</i>	<i>81</i>
10.3	100 KHZ MEASUREMENTS.....	82
10.3.1	<i>Core Loss measurements .....</i>	<i>82</i>
10.3.2	<i>Fundamental waveform with a high frequency ripple .....</i>	<i>84</i>
10.3.3	<i>Non-sinusoidal losses .....</i>	<i>84</i>
10.4	MEASUREMENTS WITH A BUCK CONVERTER.....	84
10.5	LEAKAGE CAPACITANCE .....	85
10.6	REFERENCES .....	87

<b>11</b>	<b>MEASUREMENTS AND DISCUSSION .....</b>	<b>88</b>
11.1	CORE LOSS .....	88
11.1.1	Core loss in KoolM $\mu$ 5 kHz – 9 kHz .....	88
11.1.2	Core loss in KoolM $\mu$ 5 kHz – 100 kHz .....	90
11.1.3	Core loss in High Flux 160 5 kHz – 9.9 kHz .....	92
11.1.4	Core loss in High Flux 160 5 kHz – 100 kHz .....	93
11.1.5	Core loss in High Flux 125 5 kHz- 9.9 kHz .....	94
11.1.6	Core loss in MPP 5 kHz- 9 kHz .....	95
11.1.7	Core loss in MPP 5 kHz- 100 kHz .....	95
11.1.8	Core loss in N27 Ferrite .....	97
11.1.9	Core loss in R Ferrite.....	98
11.2	BUCK CONVERTER .....	99
11.2.1	Inductor measurements and comparison .....	99
11.2.2	Paralleling of inductors .....	100
11.3	LEAKAGE CAPACITANCE .....	101
11.3.1	Reducing the leakage capacitance.....	101
11.3.2	Parallel connection between two inductors.....	102
11.3.3	Minimum leakage capacitance .....	103
11.3.4	Enamel windings .....	104
11.3.5	Leakage capacitance in a hybrid winding of enamel and Litz wire .....	105
11.3.6	Temperature and Leakage capacitance .....	105
11.4	REFERENCES .....	106
<b>12</b>	<b>CONCLUSIONS.....</b>	<b>107</b>
<b>13</b>	<b>FURTHER WORK.....</b>	<b>109</b>
<b>A</b>	<b>APPENDIXES.....</b>	<b>110</b>
<b>B</b>	<b>APPENDIX SOFTWARE FOR DESIGN OF POWDER CORES INDUCTORS.....</b>	<b>111</b>
I.	URNS .....	111
II.	FILL FACTOR.....	111
III.	MEAN LENGTH PER TURN .....	111
IV.	HDC.....	113
V.	FLUX DENSITY .....	113
VI.	PERMEABILITY CORRECTION .....	113
VII.	THE POWER HANDLING CAPABILITY OF THE CORE .....	113
VIII.	RESISTANCE .....	114
IX.	POWER LOSS .....	114
X.	SURFACE AREA .....	115
XI.	THERMAL.....	115
XII.	LAYERS .....	115
XIII.	LEAKAGE INDUCTANCE .....	115
XIV.	STACKING CORES .....	116
XV.	ITERATIVE PROCESS .....	116
XVI.	REFERENCES .....	117
<b>C</b>	<b>APPENDIX SOFTWARE TO DESIGN FERRITE INDUCTORS.....</b>	<b>118</b>
I.	ENERGY STORAGE CAPABILITY.....	118
II.	PERMEABILITY.....	118

III.	REFERENCES .....	119
<b>D</b>	<b>APPENDIX MEASUREMENTS &amp; CALCULATIONS .....</b>	<b>120</b>
I.	MEASUREMENTS UP TO 100 KHz 20°C.....	120
II.	MEASUREMENTS UP TO 100 KHz 180°C.....	125
III.	NON-SINUSOIDAL LOSSES .....	127
V.	FILTER FOR BUCK CONVERTER .....	128
VI.	DV/DT OUTPUT INDUCTOR FOR DIFFERENTIAL NOISE .....	129
VII.	SINUS OUTPUT FILTER .....	130
VIII.	PARALLEL CONNECTION OF INDUCTORS IN A BUCK CONVERTER.....	132
IX.	N27 .....	133
<b>E</b>	<b>APPENDIX PYTHON .....</b>	<b>134</b>
<b>F</b>	<b>MECHANICAL MEASUREMENTS MLT.....</b>	<b>135</b>
<b>G</b>	<b>THERMAL RESISTANCES .....</b>	<b>136</b>
I.	NATURAL CONVECTION.....	136
II.	FORCED CONVECTION.....	137
III.	RADIATION .....	137
<b>H</b>	<b>PICTURES FROM THE LABORATORY .....</b>	<b>140</b>
<b>I</b>	<b>PYTHON SOURCE CODE.....</b>	<b>142</b>



### 3 List of Figures

Figure 1-1 Down-hole system.....	1
Figure 3-1 Differential and Common mode noise [2].....	10
Figure 3-2 Low pass filter [1] .....	10
Figure 3-3 RLC Filter .....	11
Figure 3-4 RLC filter at the inverters output .....	12
Figure 3-5 Different sinus filter configurations [7].....	13
Figure 3-6 The PSCAD model of a Buck converter .....	14
Figure 3-7 The PSCAD model of the converter with a sinus filter .....	15
Figure 4-1 Typical B-H Loops for some magnetic materials [3].....	17
Figure 4-2 Some powder core shapes .....	18
Figure 4-3 High magnification of a powder material .....	18
Figure 4-4 Core loss limited at $100 \text{ mWcm}^{-3}$ for $15.6 \text{ cm}^3$ cores at 5 kHz .....	20
Figure 4-5 Core losses for $15.6 \text{ cm}^3$ cores up to saturation at 5 kHz.....	20
Figure 4-6 Core loss limited at $100 \text{ mWcm}^{-3}$ for $15.6 \text{ cm}^3$ cores at 100 kHz .....	20
Figure 4-7 Core losses for $15.6 \text{ cm}^3$ cores up to saturation at 100 kHz.....	20
Figure 4-8 Core loss with sinus 50 mT peak at 100 kHz compared to rated saturation flux density ....	21
Figure 4-9 Current measurement in an inductor experiencing a .....	21
Figure 4-10 Comparison of the inductance in KoolM $\mu$ with increasing $I_{dc}$ .....	24
Figure 4-11 Comparison of the inductance in HighFlux with increasing $I_{dc}$ .....	24
Figure 4-12 Permeability versus dc bias in KoolM $\mu$ .....	25
Figure 4-13 Permeability versus dc bias for XFlux.....	25
Figure 4-14 Permeability versus dc bias for High Flux.....	25
Figure 4-15 Permeability versus dc bias for MPP .....	25
Figure 4-16 Measured loss in N27 at 5 kHz .....	26
Figure 4-17 Measured loss in R ferrite at 5 kHz .....	26
Figure 4-18 Measured loss in KoolM $\mu$ at 20 kHz.....	27
Figure 4-19 Measured loss in KoolM $\mu$ at 50 kHz.....	27
Figure 4-20 Measured loss in HighFlux at 20 kHz.....	27
Figure 4-21 Measured loss in HighFlux at 100 kHz.....	27
Figure 4-22 Measured loss in MPP at 20 kHz .....	27
Figure 4-23 Measured loss in MPP at 50 kHz .....	27
Figure 5-1 Flux waveforms [5] .....	30
Figure 6-1 100 k Hz skin depth at different temperatures.....	35
Figure 6-2 Proximity effect in multilayer windings .....	36
Figure 6-3 $R_{ac}/R_{dc}$ for $O_d = 1.25 \text{ mm}$ at $25 \text{ }^\circ\text{C}$ .....	37
Figure 6-4 $R_{ac}/R_{dc}$ for $O_d = 1.25 \text{ mm}$ at $200 \text{ }^\circ\text{C}$ .....	37
Figure 6-5 Square fitting.....	39
Figure 6-6 Hexagonal fitting .....	39
Figure 6-7 Damage to enamel insulation operated at $170 \text{ }^\circ\text{C}$ .....	40
Figure 6-8 Damage to enamel insulation operated at $180.5 \text{ }^\circ\text{C}$ .....	40
Figure 6-9 Inductor equivalent circuit.....	42

Figure 6-10 Impedance versus frequency for a normally wound core .....	43
Figure 6-11 Impedance versus frequency for a bank winding .....	43
Figure 6-12 Impedance versus frequency for a winding with air gap between the layers .....	43
Figure 7-1 Toroid mesh .....	47
Figure 7-2 Simulation results.....	47
Figure 7-3 Boundary layer fluid velocity profile perpendicular to a wall.....	48
Figure 7-4 Boundary layer Temperature profile perpendicular to a wall .....	48
Figure 7-5 The total distance of the boundary layer $L_t = a+b+2(d^2+e^2)^{0.5}$ .....	49
Figure 7-6 COMSOL model of a core including only radiation .....	54
Figure 7-7 Horizontal and vertical mounted cores.....	55
Figure 7-8 Heat conduction in a single layer .....	58
Figure 7-9 Heat Conduction in two layers.....	58
Figure 7-10 Heat conduction in three layers.....	58
Figure 7-11 Heat conduction in ten layers .....	58
Figure 7-12 Thermal conductivity for different fill factors [11] .....	59
Figure 7-13 Heat conduction for non-ideal windings.....	59
Figure 7-14 Heat conduction in the core with $d_{ins} = 0.5$ mm .....	60
Figure 7-15 Heat conduction in the core with $d_{ins} = 2$ mm .....	60
Figure 7-16 Equivalent thermal circuit .....	61
Figure 8-1 GUI of the Inductor designer.....	65
Figure 9-1 Buck converter [1].....	71
Figure 9-2 Buck converter in continues mode [1].....	71
Figure 9-3 Circuit topology of the RLC filter model.....	74
Figure 9-4 The voltage waveform before and after the filter .....	74
Figure 9-5 The voltage and current waveform before the load.....	74
Figure 9-6 Zoomed in view of the voltage before and after the filter .....	74
Figure 9-7 Zoomed in view of the voltage and current at the load .....	74
Figure 9-8 Circuit topology of the Sinus filter model .....	75
Figure 9-9 The voltage at the load and current.....	75
Figure 9-10 Filtered and unfiltered line to line voltage.....	75
Figure 10-1 Control principle for electric sheet measuring instrument [2] .....	79
Figure 10-2 The heating chamber rated for 0°C to 200°C.....	80
Figure 10-3 The plugin system for ring cores in BROCHAUS MPG 100D.....	80
Figure 10-4 Measured loss in High Flux at 5 kHz.....	83
Figure 10-5 Measured loss in KoolM $\mu$ at 5 kHz.....	83
Figure 10-6 Impedance plot for 16 Turns Litz wire 240 strands.....	86
Figure 10-7 Impedance plot for KoolM $\mu$ 41 Turns Litz wire 120 strands.....	86
Figure 10-8 Impedance plot for 136 Turns enamel.....	86
Figure 10-9 Impedance plot for 165 Turns Litz 120 strands.....	86
Figure 11-1 Measured loss in KoolM $\mu$ at 3 kHz.....	88
Figure 11-2 Measured loss in KoolM $\mu$ at 5 kHz.....	89
Figure 11-3 Measured loss in KoolM $\mu$ at 7 kHz.....	89
Figure 11-4 Measured loss in KoolM $\mu$ at 10 kHz.....	89
Figure 11-5 Measured loss in KoolM $\mu$ at 5 kHz.....	90

Figure 11-6 Measured loss in KoolM $\mu$ at 20 kHz.....	90
Figure 11-7 Measured loss in KoolM $\mu$ at 50 kHz.....	90
Figure 11-8 Measured loss in KoolM $\mu$ at 100 kHz.....	90
Figure 11-9 Comparison of new Steinmetz parameters for 5 - 20 kHz at 20 kHz .....	91
Figure 11-10 Comparison of new Steinmetz parameters for 20 - 50 kHz at 20 kHz .....	91
Figure 11-11 Measured loss in HighFlux 160 at 3 kHz.....	92
Figure 11-12 Measured loss in HighFlux 160 at 5 kHz.....	92
Figure 11-13 Measured loss in HighFlux 160 at 7 kHz.....	92
Figure 11-14 Measured loss in HighFlux 160 at 9.9 kHz.....	92
Figure 11-15 Measured loss in High Flux at 5 kHz.....	93
Figure 11-16 Measured loss in High Flux at 20 kHz.....	93
Figure 11-17 Measured loss in High Flux at 50 kHz.....	93
Figure 11-18 Measured loss in High Flux at 100 kHz.....	93
Figure 11-19 Measured loss in HighFlux 125 at 3 kHz.....	94
Figure 11-20 Measured loss in HighFlux 125 at 5 kHz.....	94
Figure 11-21 Measured loss in HighFlux 125 at 7 kHz.....	94
Figure 11-22 Measured loss in HighFlux 125 at 9.9 kHz.....	94
Figure 11-23 Measured loss in MPP 125 at 3 kHz .....	95
Figure 11-24 Measured loss in MPP 125 at 5 kHz .....	95
Figure 11-25 Measured loss in MPP 125 160 at 7 kHz .....	95
Figure 11-26 Measured loss in MPP 125 at 9.9 kHz .....	95
Figure 11-27 Measured loss in MPP at 5 kHz .....	96
Figure 11-28 Measured loss in MPP at 20 kHz .....	96
Figure 11-29 Measured loss in MPP at 50 kHz .....	96
Figure 11-30 Measured loss in MPP at 100 kHz .....	96
Figure 11-31 Comparison of new Steinmetz parameters for 5 - 20 kHz at 20 kHz .....	97
Figure 11-32 Comparison of new Steinmetz parameters for 20 - 50 kHz at 20 kHz .....	97
Figure 11-33 Measured loss in N27 at 3 kHz.....	97
Figure 11-34 Measured loss in N27 at 5 kHz.....	97
Figure 11-35 Measured loss in R ferrite at 3 kHz .....	98
Figure 11-36 Measured loss in R ferrite at 5 kHz .....	98
Figure 11-37 Measured loss in R ferrite at 7 kHz .....	98
Figure 11-38 Measured loss in R ferrite at 9 kHz .....	98
Figure 11-39 Measured permeability with increasing dc current in 0077715A7 (KoolM $\mu$ ) .....	100
Figure 11-40 Measured permeability with increasing dc current C058583A2 (High Flux 160) .....	100
Figure 11-41 Analytical permeability with increasing dc current in 0077715A7 (KoolM $\mu$ ) .....	101
Figure 11-42 Analytical permeability with increasing dc current in C058583A2 (High Flux 160) .....	101
Figure 11-43 Impedance versus frequency for a normally wound core .....	101
Figure 11-44 Impedance versus frequency for a bank winding .....	101
Figure 11-45 Impedance versus frequency for a winding with air gap between the layers.....	102
Figure 11-46 A single 100 turn KoolM $\mu$ core.....	102
Figure 11-47 Parallel connection of two 100 turn KoolM $\mu$ core.....	102
Figure 11-48 A 1 turn Litz wire on a KoolM $\mu$ core NB add 20 db to the amplitude.....	103
Figure 11-49 A 5 turn KoolM $\mu$ core NB add 20 db to the amplitude .....	103

Figure 11-50 A 8 turn KoolM $\mu$ core NB add 20 db to the amplitude .....	103
Figure 11-51 A 11 turn KoolM $\mu$ core NB add 20 db to the amplitude .....	104
Figure 11-52 A 100 turn koolM $\mu$ core with 100 turns of Litz wire 120 x 0.1mm .....	104
Figure 11-53 A 136 turns high flux 160 core with 136 turns of enamel wire 1 x 1.15 mm .....	104
Figure 11-54 A 100 turn KoolM $\mu$ core with 100 turns of Litz wire 120 x 0.1mm .....	105
Figure 11-55 A 100 turn KoolM $\mu$ core with 100 turns of Litz wire 120 x 0.1mm and 10 turns of enamel 1 x 1.15 mm 20 db need to be added to the vertical axis .....	105
Figure 11-56 A 100 turn KoolM $\mu$ core with 100 turns of Litz wire 120 x 0.1mm at 20°C .....	106
Figure 11-57 A 100 turn High Flux core with 136 turns of Litz wire 1 x 1.15 at 20°C .....	106
Figure 11-58 A 100 turn KoolM $\mu$ core with 100 turns of Litz wire 120 x 0.1mm at 118°C .....	106
Figure 11-59 A 100 turn High Flux core with 136 turns of Litz wire 1 x 1.15 at 118°C .....	106
Figure 13-1 Toroid winding configuration .....	112
Figure 13-2 (a) Square fitting (b) hexagonal fitting [4] .....	112
Figure 13-3 Simple flow chart of the Iterative process .....	117
Figure 13-4 The loss measurement setup with a Brochause steel tester .....	140
Figure 13-5 The heating chamber .....	140
Figure 13-6 Buck converter .....	141
Figure 13-7 The 100 kHz amplifier setup .....	142

## 4 List of Tables

Table 1-1 Drive Specification .....	2
Table 2-1 SiC Commercial products with largest breakdown voltage in the market 2012 [6] .....	5
Table 2-2 SiC material properties compared to Si [8] .....	5
Table 2-3 Temperature problems in semiconductors [10] .....	6
Table 3-1 Magnetic components in power electronic applications .....	9
Table 3-2 Desired properties for CM and DM inductors .....	10
Table 3-3 Filter parameters for RLC filters [2] .....	12
Table 3-4 Cable parameters .....	14
Table 4-1 Magnetic Properties of some powder Cores [1][9] .....	19
Table 4-2 Magnetic Properties of some powder HT Ferrites .....	22
Table 4-3 Examples of absolute maximum NI that should be applied to magnetics® powder cores... ..	24
Table 6-1 Advantages and disadvantages with Litz wires [2] .....	38
Table 6-2 Advantages and disadvantages with round wires .....	39
Table 6-3 Advantages and disadvantages with foil windings .....	40
Table 6-4 Measured values for a normal winding .....	43
Table 6-5 Measured values for a Bank winding .....	43
Table 6-6 Measured values an inductor with air gap between layers .....	43
Table 7-1 Thermal classes for inductive modules .....	45
Table 7-2 COMSOL Model inputs .....	46
Table 7-3 Thermal conductivity for some materials [7] .....	47
Table 7-4 Thermal conductivity examples .....	52
Table 7-5 Thermal properties of Air and Oil [8] T in Celcius .....	52
Table 7-6 Emissivity of some surfaces [7] .....	53
Table 7-7 Radiation at different temperatures .....	53
Table 7-8 COMSOL model data for C058583A2 .....	56
Table 7-9 Comparison of temperature increase in C058583A2 for natural convection .....	56
Table 7-10 C058583A2 including windings .....	57
Table 7-11 Temperature comparison in C058548A2 with 106 turns of 120 x 0.1 Litz wires with natural convection cooling .....	57
Table 7-12 Temperature comparison in C058548A2 with 106 turns of 120 x 0.1 Litz wires with natural convection cooling at 100 °C ambient temperature .....	57
Table 7-13 COMSOL model data for the windings .....	58
Table 7-14 Thermal conductivity for different configurations with 50 % fill factor .....	59
Table 7-15 COMSOL model data for core thermal resistance .....	59
Table 8-1 Output Parameters .....	69
Table 9-1 Buck filter specifications .....	72
Table 9-2 Drive specification .....	73
Table 9-3 Dv/dt filter values .....	73
Table 9-4 Sinus filter values .....	75
Table 9-5 Input parameters .....	76

Table 9-6 Software recommendations.....	76
Table 10-1 Core materials .....	78
Table 10-2 Lab equipment.....	79
Table 10-3 Core loss samples .....	80
Table 10-4 Winding resistance before and after the high temperature tests .....	81
Table 10-5 Lab equipment for 100 kHz .....	82
Table 10-6 Equations to calculate the flux density in the core .....	82
Table 10-7 Lab equipment Buck converter .....	84
Table 10-8 Inductance and resistivity measurements in some inductors.....	85
Table 10-9 Lab equipment for Leakage capacitance.....	85
Table 10-10 Leakage capacitance and SRF in some different inductors .....	86
Table 11-1 KoolM $\mu$ new Steinmetz parameters.....	91
Table 11-2 MPP new Steinmetz parameters.....	96
Table 11-3 Buck filter properties.....	99
Table 11-4 Comparison of analytical design and measured values for inductors.....	99
Table 11-5 Comparison of analytical design and measured values for inductors.....	100
Table 11-6 Measured values for a normal winding.....	101
Table 11-7 Measured values for a Bank winding .....	101
Table 11-8 Measured values an inductor with air gap between layers .....	102
Table 11-9 Parameters of a single 100 turn KoolM $\mu$ core .....	102
Table 11-10 Parameters of a parallel connection of two 100 turn KoolM $\mu$ core .....	102
Table 11-11 Parameters for a 1 turn KoolM $\mu$ core .....	103
Table 11-12 Parameters for a 5 turn KoolM $\mu$ core .....	103
Table 11-13 Parameters for a 5 turn KoolM $\mu$ core .....	103
Table 11-14 Parameters for a 5 turn KoolM $\mu$ core .....	104
Table 11-15 Litz wire and enamel comparison.....	104
Table 11-16 100 Litz wire versus hybrid winding of 100 turn Litz with 10 turns enamel .....	105
Table 11-17 Leakage capacitance comparison at elevated temperatures.....	106
Table 13-1 The permeability stability in a ferrite air gap 0.26mm le 138mm and $\mu$ 2300.....	118
Table 13-2 measurements from 5 – 100 kHz at 20°C.....	120
Table 13-3 measurements from 5 – 100 kHz at 180°C.....	125
Table 13-4 Inductor analytical data and measured values .....	129
Table 13-5 Inductor analytical data and measured values .....	129
Table 13-6 some values for LC in different filters .....	130
Table 13-7 KoolM $\mu$ 70 turns inductance at dc bias from 0-16 A.....	132
Table 13-8 KoolM $\mu$ two 100 turns inductors parallel connected.....	132
Table 13-9 HighFlux 40 turns inductance at dc bias from 0-16 A.....	132
Table 13-10 HighFlux two 50 turns inductors parallel connected .....	132
Table 13-11 N27 Geometric Data.....	133

## Nomenclature

Symbol	Description	Unit
$W$	Energy	$J \cdot s^{-1}$
$Al$	Nominal inductance	$nH \cdot N^{-2}$
$B_g$	Flux density in the air gap	$Wb \cdot m^{-2}$
$B_c$	Flux density in the magnetic material	$Wb \cdot m^{-2}$
$\mu_r$	Relative permeability	1
$\mu_0$	Permeability of free space defined to be $4\pi 10^{-7}$ Henries	$H \cdot m^{-1}$
$\mu$	Permeability	$H \cdot m^{-1}$
$A_g$	Cross section area of the air gap	$m^2$
$Le$	Mean magnetic path	m
$N$	Number of turns	-
$B$	Magnetic flux density	$Wb \cdot m^{-2}$
$R_{th,c}$	Core thermal resistance	$K \cdot W^{-1}$
$R_{th,w}$	Winding thermal resistance	$K \cdot W^{-1}$
$R_{th,e}$	External thermal resistance	$K \cdot W^{-1}$
$P_c$	Power loss core	W
$P_w$	Power loss winding	W
$T_{th,a}$	Ambient temperature	K
$T_{th,s}$	Surface temperature	K
$T_{th,\infty}$	Flow temperature	K
$T$	Temperature	K
$\Delta T$	Temperature gradient	$K \cdot m^{-1}$
$\alpha_{th}$	Heat transfer coefficient	$W \cdot m^{-2} K^{-1}$
$d$	Height of the magnetic component	m
$n$	Constant	-
$C$	Constant	-
$U_\infty$	Velocity of the flow outside the boundary layer	$ms^{-1}$
$A_t$	The area the flow see of the magnetic component	$m^2$
$L_t$	Total distance of the boundary layer	m
$A_{eff}$	Effective enveloped surface	$m^2$
$r_{wire}$	Radius of the wire	m
$D_{ow}$	Core outer diameter including wire	m
$D_{iw}$	Core inner diameter including wire	m
$H_w$	Core height including wire	m
$D_y$	Core outer diameter	mm
$D_i$	Core inner diameter	mm
$H$	Height of the magnetic component	mm
$\rho_{th}$	Density	$m^{-3} kg$
$\mu_{th}$	Dynamic viscosity	$N \cdot s \cdot m^{-2}$
$Pr$	Prandtl number	-
$\nu$	Kinematic viscosity	$m^2 s^{-1}$
$C_p$	The constant pressure specific heat capacity	$J kg^{-1} K^{-1}$
$\lambda$	Thermal conductivity	$Wm^{-1} K^{-1}$
$Gr$	Grashof number	-
$L$	The characteristic length	m
$g$	Gravity constant	$ms^{-2}$
$\beta_{th}$	The thermal volume expansion coefficient	$K^{-1}$
$\kappa$	The thermal diffusivity	$m^2 s^{-1}$

$Re$	Reynolds number	-
$Nu$	Nusselt number	-
$\epsilon$	Permittivity	$F \cdot cm^{-2}$
$t_{rmax}$	Rise time	s
$\omega_0$	Resonance frequency	$m^{-1}$
$f_{sw}$	Switching frequency	$m^{-1}$
$f_{eq}$	Equivalent frequency	$m^{-1}$
$f_r$	Relative frequency	$m^{-1}$
$\beta$	Parameter in the Steinmetz equation for flux density change	-
$\alpha$	Parameter in the Steinmetz equation for frequency change	-
$K$	Parameter in the Steinmetz equation a constant	-
$\lambda$	Thermal conductivity	$W \cdot m^{-1} \cdot ^\circ C^{-1}$
$E_g$	Band-gap	eV
$E_c$	Critical field	$V \cdot cm^{-1}$
$\mu_n$	Electron mobility	$cm^2 V^{-1} \cdot s^{-1}$
$n_i$	Intrinsic concentration	$cm^{-3}$
$N_a$	Ionized acceptor density	$cm^{-3}$
$N_d$	Ionized donor density	$cm^{-3}$
$\tau_p$	Majority carrier lifetime	s
$\tau_n$	Minority carrier lifetime	s
$q$	Electron charge	C
$K$	Boltzmann's constant	$J \cdot K^{-1}$
$\epsilon_0$	Permittivity of vacuum	$F \cdot cm^{-2}$
$\epsilon_r$	Relative permittivity	-
$S_{win}$	Area between the windings	$m^2$
$d_{win}$	Distance between the different windings	m
$\dot{q}$	Heat flux	$Wm^{-2}$
$w$	Fluid velocity	$ms^{-1}$
$L$	Inductance	H
$V_o$	Output voltage	V
$t_{off}$	Time period the switch is off	s
$\Delta I_l$	Current ripple	A
$T_s$	Switching period	s
$C$	Capacitance	F
$l_{cr}$	Critical cable length	m
$L_{cab}$	Cable inductance	H
$C_{cab}$	Cable capacitance	C



## Abbreviation

Parameter	Description
SiC	Silicon Carbide
Si	Silicon
EMC	Electromagnetic Compatibility
PCB	Printed circuit board
ESR	Equivalent series resistor
HT	High Temperature (defined here as above 150°C)
DM	Differential mode noise
CM	Common mode noise
SRF	Self-resonance frequency

# 1 Introduction

## 1.1 Background

High temperature power devices such as converters and inverters are becoming more and more important in applications like petroleum exploration, aviation and electrical vehicles. The trend is to push the devices into even harsher environments. Electrification of down-hole drilling equipment is a promising area which requires electrical components that are able to withstand the high ambient temperatures, and pressure several kilometers subsurface. SmartMotor and Badger Explorer are developing a motor drive for a down-hole drilling tool with the concept as following:

*“The Badger Explorer is a revolutionary method to obtain subsurface data for oil gas exploration, mapping of hydrocarbon resources and long-term surveillance. The Badger Explorer drills and buries underground, carrying a unique package of logging and monitoring sensors, at a substantially lower risk, cost and complexity of utilizing an expensive drilling rig.”*

Figure 1-1 shows a possible overview of this concept.

The conventional switching technology is based on silicon (Si) devices which is limited in a range of properties compared to silicon carbide (SiC). SiC offers better thermal conductivity, band gap, breakdown field and are capable of being operated at high junction temperatures. However the main deceleration factors in developing new applications are the packing technology, control electronics and passive components.

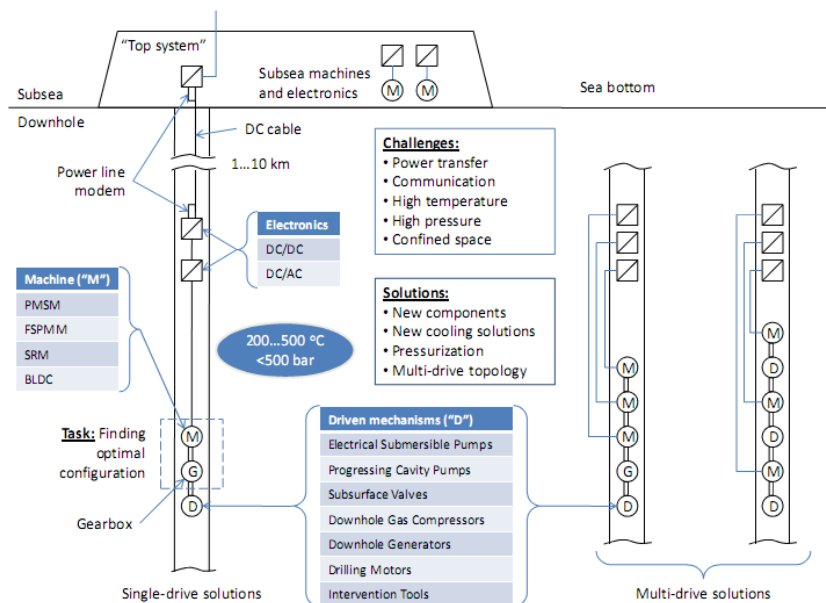


Figure 1-1 Down-hole system

## 1.2 Problem description

This master thesis will focus on the design of fast magnetic components for high temperature power devices, the task description is as follows:

*The aim is to develop an analytical design tool in Python for fast magnetic/electrical/ thermal calculation of typical magnetic components used in high temperature power electronics. Due to wide operating temperature ranges exact temperature dependent loss models are required. Also, compactness requires more accurate thermal models and effective cooling.*

*Comparison of SiC and conventional switches in terms of influence on the magnetic components should be carried out. The analytical results should be compared with experimental results.*

The materials required to design magnetic components for temperatures up to 200°C will be surveyed. A comparison between SiC and Si will be performed. Loss models for magnetic materials will be compared to lab measurements performed at 20°C and 200°C in the frequency range from 3 kHz to 100 kHz. A thermal model for inductors will be developed and compared to measurements, and the information gathered will be used to create an analytical design tool for high temperature and frequency up to 100 kHz.

The tool will be used to design sinus and dv/dt filters for the electrical specification in Table 1-1, and the cores recommended by the tool will be tested and evaluated.

Table 1-1 Drive Specification

Drive Specification	
$V_{dc}$	600 V
$S$	3000 VA
$f_{sw}$	Up to 100 kHz
$T_{amb}$	150 °C
$\frac{dv}{dt} \max$	1 kV/ $\mu$ s
<b>Where</b>	$V_{dc}$ is the Dc-link voltage $S$ is the apparent power delivered $f_{sw}$ is the switching frequency $T_{amb}$ is the downhole ambient temperature $dv/dt$ is the maximum voltage change over given time

## 1.3 Report outline

### Chapter 2

This chapter presents silicon carbide and compares the theoretical properties to silicon. Theory on semiconductor devices is used to perform a comparison on the influence of using SiC over Si on the magnetic components.

### Chapter 3

Different magnetic components will be introduced and filter theory for  $dv/dt$  and sinus will be explained. Simulation of the different filters will be performed to some extent with a focus on reducing the component physical size.

### Chapter 4

Magnetic materials for inductor design are presented, and the most common materials are explained. Thereafter suitable ferrites and powder materials for 200°C power electronics is investigated. Theory and some recommendations for reducing the core size in powder materials is then explained, and finally core losses measured in the materials is presented, and compared to the analytical data up to 100 kHz.

### Chapter 5

Core losses and flux waveforms are explained in more detail, and analytical models on how to calculate core loss is presented. The most recent models are listed and different parameters that affect the core losses are mentioned.

### Chapter 6

The possible winding options for inductors are explained with a focus on Litz, round and foil windings. Thereafter experience and problems with using round enamel windings and Litz wire at 180°C is briefly covered. The last section covers theory and ways to reduce parasitic capacitance.

### Chapter 7

Basic thermal modelling in inductors is explained and the thermal conductivity of Litz wire and multilayer windings is investigated with COMSOL Multiphysics. A thermal model of round cores is developed for forced and natural convection, and simulated in COMSOL Multiphysics. Lab measurements of a high frequency Litz wire windings is performed and compared to the analytical results at 22°C and 100°C.

### Chapter 8

Chapter 8 presents the analytical design tool. Input and output parameters are explained and ways to input data for different applications is explained. Some analytical designs are compared to experimental measurements.

### Chapter 9

The design tool and information from chapter 3 is used to design sinus, buck and  $dv/dt$  filters.

**Chapter 10**

This chapter covers the different lab setups which was performed, and explains relevant theory and error sources. There were four different lab setups:

- Core characterization 3 kHz -10 kHz
- Core characterization 5 kHz -100 kHz
- Inductor measurements in a buck converter
- Leakage capacitance in windings

**Chapter 11**

Chapter 11 presents the measurement results in more details than the other chapters and the results are evaluated and discussed.

**Chapter 12**

Chapter 12 presents the conclusion.

**Chapter 13**

Chapter 13 covers further work.

## 2 Silicon Carbide

Silicon (Si) is the conventional material used in the production of power devices, while Silicon carbide (SiC) is a material which has proven to have superior properties and has recently become commercially available, but still lags behind Si in some aspects by as much as 20 years. However some applications can have tremendous benefits from SiC due to higher temperature limit and very low losses.

### 2.1 Silicon Carbide in power electronics

The main advantages SiC provide over silicon is thinner drift region, and higher doping, which lower the theoretical on-resistance by up to 1000 times see Table 2-2 for the material properties. A high intrinsic temperature limit allow for high temperature operation [8], which enables the production of higher temperature equipment. Some of the possible applications for this are down-hole applications, hybrid vehicles, and space ships. The high temperature rating means that the components like the heat sink can be reduced if it is operated at a higher temperature, and higher switching frequency can reduce the filter components.

The SiC market is still at an early stage and the commercially available switches are the Schottky, GTO, JFET, BJT and Mosfet see Table 2-1. These switches are made for voltage levels at around 1200 volts and current of 10-20 ampere. There is development on a SiC IGBT but due to issues with high resistivity and low performance of the oxide layer it is not believed they will be commercialized within the next decade [7]. Table 2-2 summarizes standard properties of some commonly used SiC polytypes and Si.

Table 2-1 SiC Commercial products with largest breakdown voltage in the market 2012 [6]

Manufacturer		Schottky	MOSFET	JFET	BJT/SJT	GTO	Ref
CREE	[V]	1700	1200				[1]
Rohm	[V]	1200	1200				[2]
Infineon	[V]	2400		1200			[3]
GeneSiC	[V]				1200	6500	[4]
TranSiC/Fairchild	[V]				1200		[5]

Table 2-2 SiC material properties compared to Si [8]

		Si	4H-SiC	6H-SiC	3C-SiC
Band-gap $E_g$	[eV]	1.12	3.2	3.0	2.4
Intrinsic conc. $n_i$	[ $\text{cm}^{-3}$ ]	$2.5 \cdot 10^{10}$	$8.2 \cdot 10^{-9}$	TBD	TBD
Critical field $E_c$	[ $\text{MVcm}^{-1}$ ]	0.25	2.2	2.5	2
Electron mobility $\mu_n$	[ $\text{cm}^2\text{V}^{-1}\text{s}^{-1}$ ]	1350	950	500	1000
Permittivity $\epsilon_r$	[-]	11	10	10	9.7
Thermal conductivity $\lambda$	[ $\text{Wcm}^{-1}\text{K}^{-1}$ ]	1.5	5	5	5

One of the advantages of SiC is that it enables for higher operation temperatures which affect the parameters listed in Table 2-3.

Table 2-3 Temperature problems in semiconductors [10]

**Physics problems in semiconductors operating at elevated temperatures**

1. Increasing intrinsic carrier density.
2. Increasing junction leakage current.
3. Variations in device parameters.
4. Availability of adequate wide-temperature-range device models for circuit simulators

The intrinsic carrier density  $n_i$  in a semiconductor device depends on the temperature and the band gap of the material described by Equation 2-1 [9].

$$n_i^2 = C \exp\left(-\frac{qE_g}{kT}\right) \quad \text{Equation 2-1}$$

$T$	Temperature
$C$	Constant
$k$	Boltzmann's constant
$q$	Electron charge

The current density can be explained by Equation 2-2.

$$J = qn_i^2 \left[ \frac{L_n}{N_a \tau_n} + \frac{L_p}{N_d \tau_p} \right] \left[ e^{\frac{qV}{kT}} - 1 \right] \quad \text{Equation 2-2}$$

$L_n, L_p$	The minority/ majority carrier diffusion length
$N_a, N_d$	ionized acceptor/donor densities
$\tau_p, \tau_n$	Electron charge

Assuming a one dimensional non-punch through unipolar junction, the on resistance can be expressed as [11]:

$$R_{on} = \frac{4V_B^2}{\epsilon_r \mu_n E_c^3} \quad \text{Equation 2-3}$$

$V_B$	Represents breakdown voltage over the junction
$\mu_n$	Electron mobility
$E_c$	Critical electrical field
$\epsilon_r$	Permittivity

SiC have higher critical electrical field compared to Si which results in a reduced  $R_{on}$ .

## 2.2 Comparison of SiC to conventional switches

The theoretical effects of introducing Sic switches on the magnetic components are as follows:

1. According to Equation 2-1 it can be seen that the intrinsic carrier density is exponentially decreasing with increased band gap, which coupled with Equation 2-2 means that a Sic switch will have several magnitudes lower leakage current than a Si switch. The effects of this on the magnetic components are a smaller dc leakage current, but on the other hand the leakage current in a Si switch is so low that this should have low practical impact, other than in high temperature operation where leakage current is increasing with temperature.
2. Breakdown voltage in a minority carrier device depends on the intrinsic carrier density that according to Equation 2-1 is exponentially decreasing with increased band gap. Therefore a Sic device can be operated at higher temperature than a Si device which could be used to minimize designs however this requires passive components to be designed for higher temperatures.
3. The on resistance of a SiC switch can as previously mentioned be up to 1000 times smaller than the comparable Si switch. This low resistance results in lower internal dampening for the component resulting in larger ringing effects.
4. The high critical field strength in SiC allows for a shorter drift region in minority carrier devices, and shorter carrier lifetime's results in faster switching, which increase dv/dt effects that have to be controlled by the appropriate filter see more in section 3.1.
5. SiC allows for higher switching frequencies than the Si counterpart, and with lower losses. This can be used to lower the harmonic distortion or reduce the size of filter components.



## 2.3 References

- [1] <http://www.cree.com/power/products>
- [2] <https://www.rohm.com/web/global/sic>
- [3] <http://www.infineon.com/cms/en/product/index.html>
- [4] <http://www.genesicsemi.com/index.php/sic-products>
- [5] <http://www.transic.com/>
- [6] Zetterling, C. -M, "Present and future applications of Silicon Carbide devices and circuits," *Custom Integrated Circuits Conference (CICC), 2012 IEEE* , vol., no., pp.1,8, 9-12 Sept. 2012
- [7] June 2012 IEEE Industrial Electronics Magazine 17
- [8] I. Abuishmais "Sic Power Diodes and junction field effect transistors" Doctoral theses 2012.
- [9] N. Mohan and T. M. Undeland, *Power Electronics Converters, Applications, and Design*: John Wiley & sons, 2003.
- [10] Dreike, P.L.; Fleetwood, D.M.; King, D.B.; Sprauer, D.C.; Zipperian, T.E.; , "An overview of high-temperature electronic device technologies and potential applications," *Components, Packaging, and Manufacturing Technology, Part A, IEEE Transactions on* , vol.17, no.4, pp.594-609, Dec 1994  
doi: 10.1109/95.335047
- [11] Øyvind Holm Snefjellå, "Silicon Carbide Technologies for High Temperature Motor Drives", Master thesis, June 2011.

### 3 Components in sinus filters and dv/dt filters

Magnetic materials in power electronic applications are a large subject and therefore only the main points have been listed in Table 3-1, including the optimal properties in different applications. The focus of this chapter will be on sinus filters and dv/dt filters for switch mode power supplies. And in later chapters these components will be designed, and tested see chapter 9. The two filter configurations will be compared both on losses and filter volume, and the main goal is to minimize the size of the total filter configuration while keeping the losses reasonable low.

Table 3-1 Magnetic components in power electronic applications

Application	Purpose	Magnetic Material properties
<b>Filter</b>	Suppresses signals above the cutoff frequency.	Low losses Known temperature factor. Stable.
<b>Interference suppression</b>	Suppresses unwanted high frequency signals.	High impedance over the frequency range.
<b>Pulse delaying</b>	Leading edge on a signal is delayed until the inductor is saturated.	High permeability.
<b>Storage of energy</b>	Necessary in switch mode power supply applications. Stores energy in the on periods and delivers it to the load in the off periods.	High saturation.
<b>General purpose transformer</b>	Isolation between output and input, and can change the voltage level.	High permeability. Low hysteresis factor. Low dc-bias sensitivity.
<b>Power transformer</b>	Transmits energy while providing isolation.	Low power losses. High saturation.

#### 3.1 Introduction

In many normal applications it might not be necessary to filter the output from a switch mode power supply, but the advances in semiconductor technology have enabled high frequency switching operation with rise time below  $0.1 \mu\text{s}$ . In 480 V applications, the differential and common mode voltage can in uncontrolled circuits reach  $7000 \text{ V}/\mu\text{s}$  at the motor terminals [7].

SiC semiconductors can have rise time of the voltage pulses is in the range of nanoseconds for example the SiC mosfet CMF20120 from CREE have a rise time of 38 ns which equals  $25.44 \text{ kV}/\mu\text{s}$  (according to NEMA). The purpose of filters is to control these rapid voltages and currents changes, and decrease the total harmonic distortion, or mitigate other forms of undesired noise.

**Differential mode noise (DM):** Undesired current or voltage line to line. See  $I_{DM}$  in Figure 3-1, this noise is transferred by stray capacitance or inductance.

**Common mode noise (CM):** Undesired current or voltage measured between a line and ground. See  $I_{CM}$  in Figure 3-1. The noise is transferred to the ground due to stray capacitance of the lines.

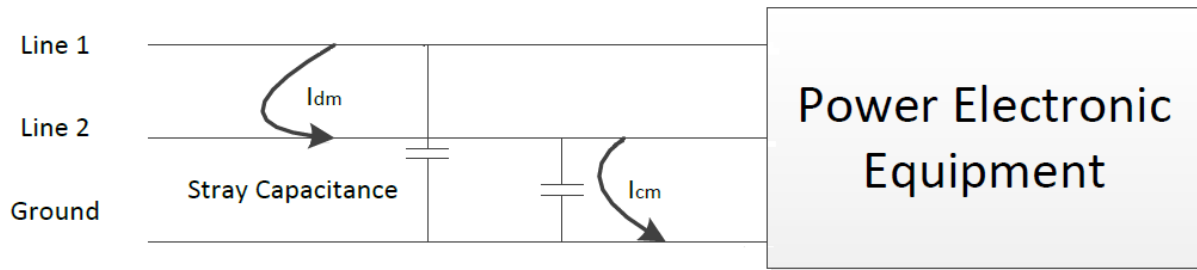


Figure 3-1 Differential and Common mode noise [2]

The filter for CM noise is wound with two windings of the same number of turns and connected between the lines in such a way that the line currents cancel out the fluxes induced, leaving the core unbiased which reduces the component size. While in a DM filter the core only have a single winding which requires the core to support the whole line current without saturating see optimal design properties for CM and DM inductors in Table 3-2.

Table 3-2 Desired properties for CM and DM inductors

Application	Purpose	Magnetic Material properties
CM Inductor	Suppresses noise between lines	High permeability
DM Inductor	Suppresses noise between lines and earth	Low permeability High saturation flux density Low leakage capacitance

### 3.2 Filter theory

A common filter topology in switch mode power supplies is a low pass filter which consists of an inductor and capacitor as shown in Figure 3-2. The filter acts in such a way that all amplitudes above the cutoff frequency  $f_0$  are suppressed.

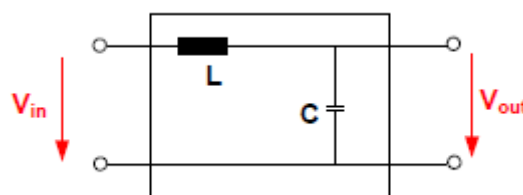


Figure 3-2 Low pass filter [1]

A dv/dt filters purpose is to controls the rise time of an inverters output voltage. This is can be done with a simple circuit such as Figure 3-2 but with this configuration, the circuit is undamped and a sinusoidal voltage overshoot with a possible peak of twice the output voltage is possible [1]. Adding an additional dampening resistance will solve this, see Figure 3-3 [2] however this increases the losses.

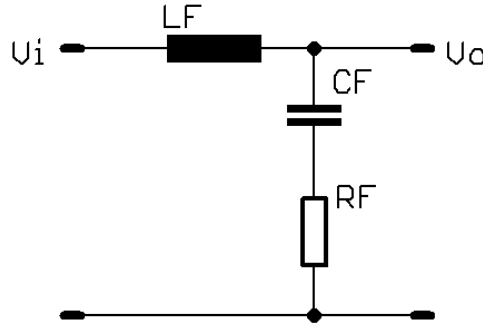


Figure 3-3 RLC Filter

The transfer function for a standard RLC filter such as in Figure 3-3 is given by Equation 3-1.

$$H_f(S) = \frac{SR_f C_f + 1}{S^2 L_f C_f + SR_f C_f + 1} \quad \text{Equation 3-1}$$

Equation 3-2 is Equation 3-1 written on standard form.

$$H_f(S) = \frac{\frac{S\zeta}{\omega_0} + 1}{\frac{S^2}{\omega_0^2} + \frac{2S\zeta}{\omega_0} + 1} \quad \text{Equation 3-2}$$

The relative dampening frequency  $\zeta$  is defined as Equation 3-3 and a good choice for this factor is somewhere between 1 and 2, this recommendation come from [2].

$$\zeta = \frac{1}{2} R_f \sqrt{\frac{C_f}{L_f}} \quad \text{Equation 3-3}$$

The resonance or cutoff frequency  $f_0$  can be calculated with Equation 3-4. This is the frequency where the output signal have been reduced with a minimum  $\sqrt{2}$  of the fundamental component meaning the power output has been reduced by 50 percent or more.

$$f_0 = \frac{1}{2\pi\sqrt{L_f C_f}} \quad \text{Equation 3-4}$$

### 3.3 Critical cable length

A critical cable length can be defined, representing the maximum length a cable can have before a voltage pulse travels to the motor terminals and returns to the inverter doubling the voltage at the motor see Equation 3-5.

$$l_{cr} = \frac{t_r}{2\sqrt{L_{cab} C_{cab}}} \quad \text{Equation 3-5}$$

In the case of a silicon carbide inverter with  $t_r$  of 38 ns the critical cable length for a 2 mm<sup>2</sup> cable with  $L = 0.698 \mu\text{H/m}$  and  $C = 137.79 \text{ pF/m}$  (parameters from [2]) would be 1.98 m. Therefore in nearly any silicon carbide drives using this semiconductor it would be necessary to have a filter to reduce the

voltage overshoot at the motor. High dv/dt leads to an overvoltage at the motor and the two main options are matching the load impedance to the cable characteristics or increase the voltage pulse rise time. The solutions that will be covered in the next sections are filters at the inverter terminals which changes the pulse rise time.

### 3.4 Dv/dt Filter

Dv/dt filters are known as an effective solution for differential and common mode noise attenuation. They can have passive, and active components the passive filter have high reliability and low costs and is the most common. However the active filter can have improved performance [10].

A good criterion for LC filters is that the filter inductance and capacitance should be equal or higher than the total inductance and capacitance of the cable, this way the filter dominates the system [10]. Dv/dt filters can be used for both common mode and differential mode voltage system or in a combination with sine wave filter which will be covered in the next section.

#### Output choke

An output choke is operating as a small dv/dt filter with only an inductor near the inverters output however this is not a real filter due to not containing a filter capacitor. They are cheap and simple suited for smaller drives.

**RC filter** is a dv/dt filter which consists of a resistor and capacitor, this reduces the ringing effects.

#### RLC Filter

A RLC dv/dt filter are used to limit the rise time of the inverters output and consists of inductances, resistances and capacitors. According to [2] RLC filters can be designed based on the parameters in Table 3-3. This will be performed and simulated in chapter 9. The biggest disadvantage with a RLC filters is that the resistive element leads to losses.

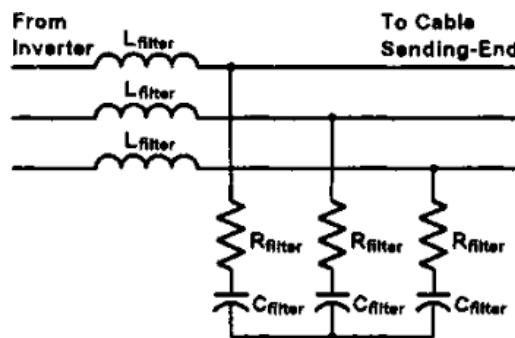


Figure 3-4 RLC filter at the inverters output

The derivation of the filter values can be found in [2]  $R_f$  is the filter resistance,  $f_{co}$  the cut off frequency,  $C_f$  the capacitor value and  $L_f$  the filter inductance.

Table 3-3 Filter parameters for RLC filters [2]

$$R_f = \frac{Z_c}{2} = \frac{1}{2} \sqrt{\frac{L_c}{C_c}} [\Omega] \quad f_{co} = \frac{1}{27l_c \sqrt{L_c C_c}} [Hz] \quad C_f = \frac{2\sqrt{18}}{\pi R_f f_{co}} [F] \quad L_f = C_f \left(\frac{R_f}{4}\right)^2 [H]$$

### 3.5 Sinus output filter

A sinus output filter is inserted into an inverter to obtain a sinusoidal output waveform and therefore suppresses all amplitudes in the switching frequency range and above. The filter consists of capacitors and inductors with the difference from a dv/dt RLC filter being the choice of the resonance frequency which in a sinus filter is chosen between the fundamental and the switching frequency.

The optimal is often  $\frac{f_{sw}}{3} = f_o$  with a filter inductor in the range of 1-10% Pu [2]. If the resonance frequency is chosen to be too low it could be excited by the fundamental frequency while if it is too high the suppression of the pulse frequency might be insufficient. It is recommended by some other sources that there should at least be a factor of ten between the fundamental and the resonance frequency and another factor of ten to the switching frequency [7] which means operation below 5 kHz is not recommended with a 50 Hz fundamental.

There exist different kinds of sinus filters see Figure 3-5 which is presented in [7].

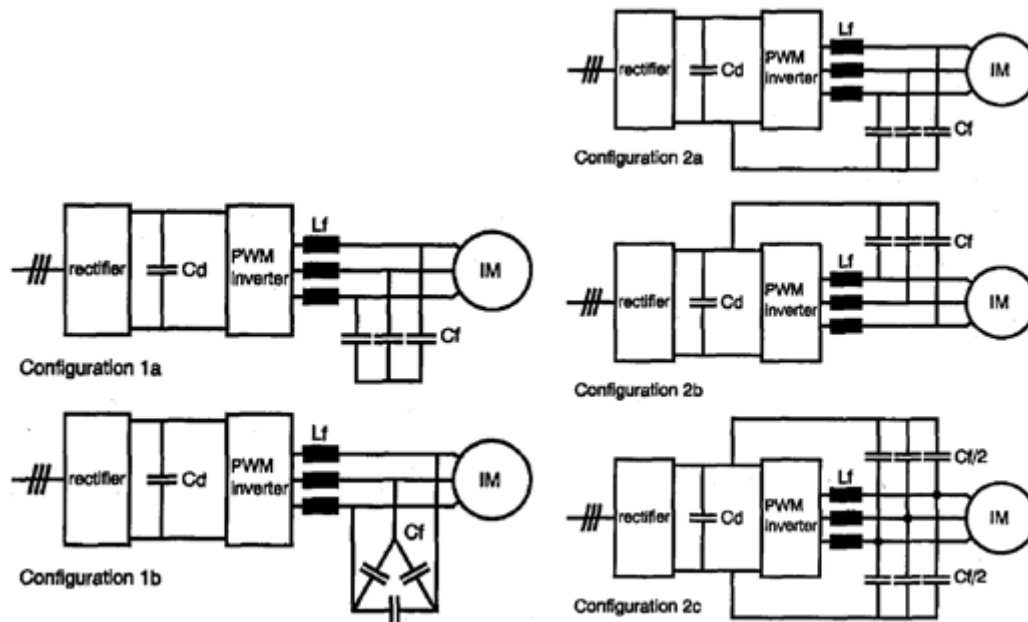


Figure 3-5 Different sinus filter configurations [7]

Due to the low resonance frequency in a sinus filter the filter inductor causes a large voltage drop at the fundamental frequency which in general applications can be up to 6% [1]. The sinus filters do not include a filter resistance which means that the overall power losses will be reduced and the difference between a sinus filter and a dv/dt filter's inductance is low. This could mean that in some applications it would be better to just use a sinus filter however leakage capacitance might create difficulties.

### 3.6 Simulation model

A three phase inverter and a buck converter model were created to study dv/dt and sinus filters see Figure 3-6 and Figure 3-7. The model was created based on a free PSCAD model which provided the control system and overhead topology however it did not take into account any cable effects. PSCAD modeling of common mode can be viewed in [12].

The cable system was modeled with lumped parameters with adequate number of segments. In systems with wires longer than the critical length several lumped elements have to be used and according to [11] the critical length of each segment for a 14 AWG wire with rise time of 50 ns is 40 mm with reasonable high accuracy. However this would be to computational expensive and only useful to show the unfiltered waveform, therefore the critical rise time was set 1000 ns which is the specified rise time the motor can handle see Table 1-1. This means only one lumped element is necessary for each meter after the filter. The rise time before the filter is still given by the rise time of the semiconductor however comparison to experiments showed good correlation with only using pi sections of 1 meter in the buck converter, and therefore the effects of incorrectly modeling this section of the cable do not seem to influence the results.

Table 3-4 Cable parameters

Parameter	Value
Resistivity	8.267 mΩ/m
Inductivity	0.698 μH/m
Capacitance	137.79 pF/m

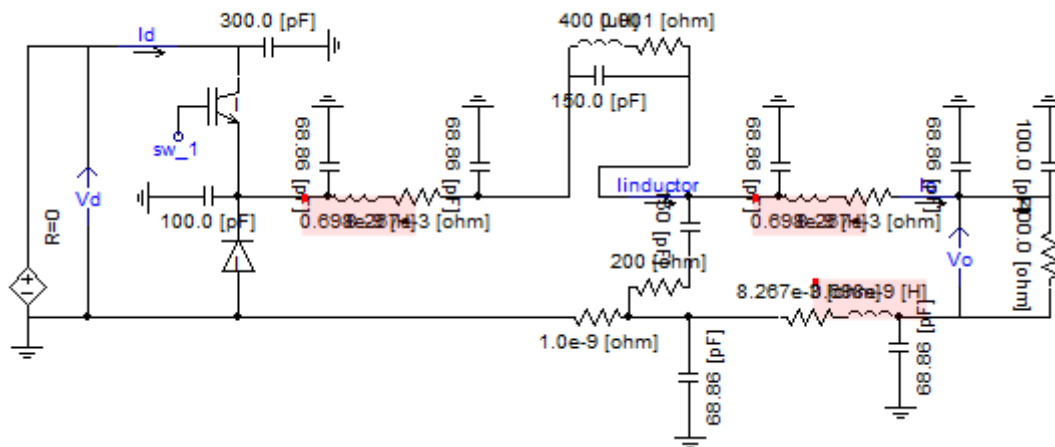


Figure 3-6 The PSCAD model of a Buck converter

The model seen in Figure 3-6 represents the buck converter which will be used in section 11.2 to measure relevant inductor parameters, and simulations of the filters in chapter 9. The model output was compared to measured values for some filter configurations with good correlation. However some smaller transients did not match completely, this is likely due to the leakage capacitance of the dc-link was not measured and only assumed to be 300 pF as described in [12].

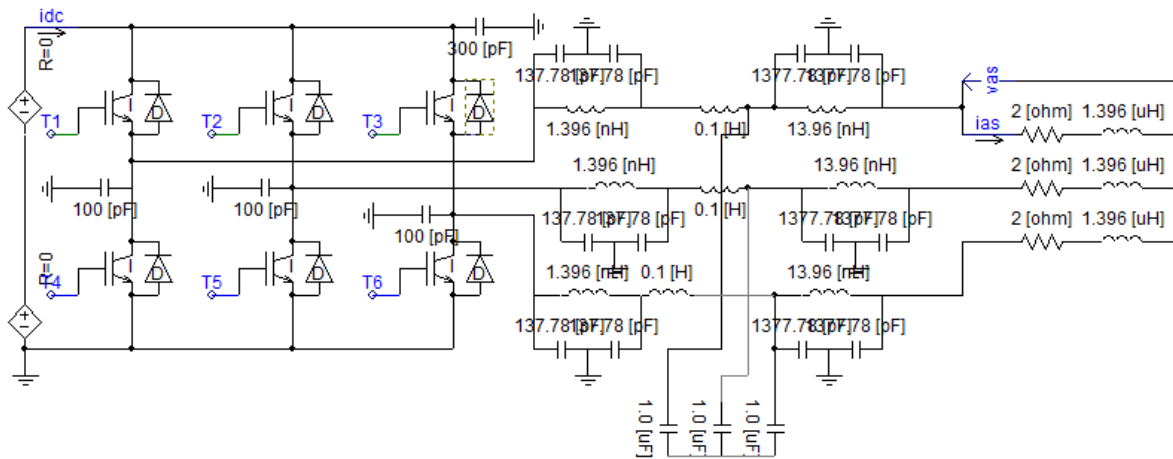


Figure 3-7 The PSCAD model of the converter with a sinus filter

The three phase model consists of a split dc source of 300 V, connected to an inverter. A 300 pF leakage capacitance was assumed to be between the dc link and ground. The cable section from the inverter to the filter was assumed to be 1 meter however only one pi section was used to model this due to software constraints. It was shown with the measurements in the buck inverter that this section should have small influence on the model results after the filter. The cable to the motor was modelled as 1 meter long pi, and the load a 2Ω 1.396 μH however these parameters was changed depending on the load necessary. The simulation time step was set to 1 ns which was necessary to have stable system which accurately simulated most transients, at least in the buck converter case.



### 3.7 References

- [1] NEK IEC/TS 61800-8
- [2] Tigest Atnafseged Adamu "Electromagnetic Interference in Downhole Applications"
- [3] R. Lund Memo "Output Filter Consideratons In High Switching Inverters"
- [4] N. Mohan and T. M. Undeland, Power Electroncis Converters, Applications, and Design: John Wiley & sons, 2003.
- [5] Ferroxcube Data Handbook "Soft Ferrites and Accessories" 2008
- [6] Jonas Muhlethaler "Optimal Design of inductive components Based on Accurate Loss and Thermal Models"
- [7] Rendusara, D.; Enjeti, P.; , "New inverter output filter configuration reduces common mode and differential mode dv/dt at the motor terminals in PWM drive systems," *Power Electronics Specialists Conference, 1997. PESC '97 Record., 28th Annual IEEE* , vol.2, no., pp.1269-1275 vol.2, 22-27 Jun 1997
- [8] Magnetics® Technical Bulleting "Magnetic Cores For Switching Power Supplies"
- [9] <http://www.cpes.vt.edu/public/showcase/hybridcmdm.php> [02.07.2013]
- [10] Dzhankhotov, V.; Pyrhonen, J., "Passive LC Filter Design Considerations for Motor Applications," *Industrial Electronics, IEEE Transactions on* , vol.60, no.10, pp.4253,4259, Oct. 2013
- [11] A. F. Moreira, T. A. Lipo, G. Venkataramanan, and S. Bernet, "Modeling and evaluation of dv/dt filters for AC drives with high switching speed", *Proc. 9th European Conf. Power Electronics and Applications (EPE'01)*, 2001
- [12] Flávio, C.C.; Diab, V.R.; Assunção, C.B.C.; Moreira, A.F., "PSCAD/EMTDC® model for overvoltage and common mode current analysis in PWM motor drives," *Industry Applications (INDUSCON), 2010 9th IEEE/IAS International Conference on* , vol., no., pp.1,6, 8-10 Nov. 2010

## 4 Magnetic Materials

Soft magnetic materials can be divided up into five main groups depending on their magnetic properties. Ferrites is a ceramic material consisting of an oxide mixture of iron and Mn, Zn, Ni or Co, which have a low saturation flux compare to the other groups. However on the other hand have high electric resistivity making them ideal in high frequency applications. The last four groups have low electric resistivity with high saturation flux density. Laminated cores are electrically isolated steel sheets which are limited to lower frequency applications (a few kHz), powder iron cores consist of iron particles isolated from each other, Amorphous alloys are liquid magnetic materials similar to glass with magnetic properties. Nanocrystalline materials are FeSi grains embedded in an amorphous phase [2]. Figure 4-1 show the B-H loops for some common materials used in magnetic designs. Along the horizontal axis the magnetic field intensity or H-field is displayed while the flux density up to saturation is on the vertical axis.

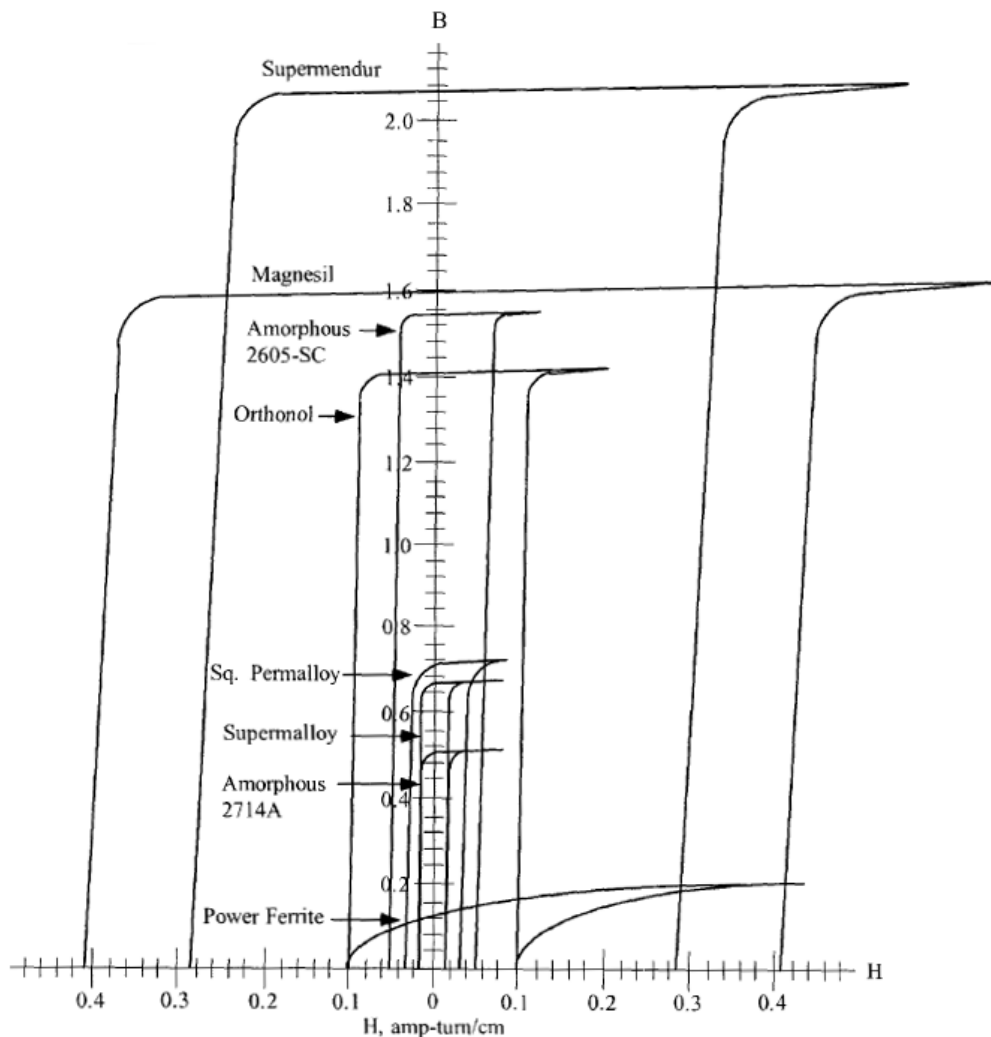


Figure 4-1 Typical B-H Loops for some magnetic materials [3]

The magnetic field intensity  $H$  is also proportional to the flux density by  $\mu H$  and can in magnetic components be calculated by equation Equation 4-1. So for example a core of Orthonol with a mean magnetic path length of 10 cm and 10 turns will go into saturation at 0.1 A. This value is so low that in inductors the material cannot be used without having an air gap in series with the material.

$$H = \frac{NI}{l_e} \quad \text{Equation 4-1}$$

$N$  Number of turns in the winding  
 $I$  Current  
 $l_e$  Mean magnetic path length

The further discussion in this thesis is limited to magnetic powder cores and ferrites, which according to the initial study [1] are the commercially available possibilities in a high temperature and frequency designs and also possible options in CM and DM filters.

#### 4.1 Powder cores

Powder cores consist of high permeability alloys like Orthonol and Permalloy (see Figure 4-1) which have been grinded down into particles, and is treated with an insulating medium. This reduces the eddy losses to a point, where this loss can be ignored as long as the penetration depth is much larger than the particles. According to [3] the eddy losses can be ignored for most powder materials today up to frequencies of around 200 kHz. There are four standard materials for powder cores; this includes Molypermalloy powder (MPP) which is made from Permalloy metal; High flux powder cores is made from Orthonol which result in high saturation flux and therefore large energy storage; Sendust is made from a ferrous alloy resulting in large energy storage for a cheap price at the cost of higher core losses. Xflux have the highest saturation flux of the categories [1].

The powder metallurgy process applied to produce a powder core traditionally used organic materials to electrically insulate each particle in the powder, however recent development have led to powder cores without organic materials significantly increasing the saturation flux density, permeability and reduced the hysteresis losses. Thermal ageing is also removed by removing the organic binder. The new development has made powder cores a viable alternative to electrical steel and ferrites in some applications [5].

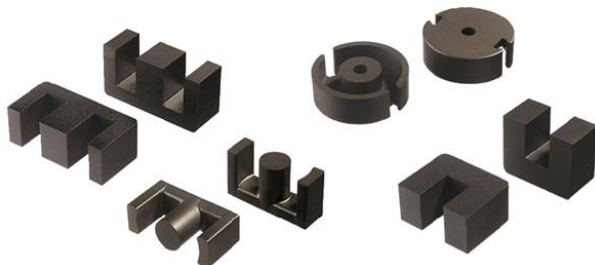


Figure 4-2 Some powder core shapes



Figure 4-3 High magnification of a powder material

The magnetic properties of the materials are reported somewhat different depending on the producers this can be found in Table 4-1. The variation is likely due to small differences in the production process.

Table 4-1 Magnetic Properties of some powder Cores [1][9]

Magnetic material type	Manufacturer	Material	Composition	Bsat[T] @ 25°C	Rel. Permeability (100 °C @ 20 k [Hz])	Curie temp. [°C]	Continuous operating temperature [°C]	Thermal conductivity [W/(mK)]	Density [g/cm <sup>3</sup> ]	Core Loss @ 0.1T, 20 k[Hz] 60 μW/Cm <sup>3</sup>	Core Loss @ 0.1T, 100 k[Hz] 60 μmW/Cm <sup>3</sup>
Powder Core	Magnetics®	MPP	Fe-Ni-Mo	0.75	14-550	460	200	8	8.2	45	590
Powder Core	Magnetics®	High Flux	Fe-Ni	1.5	14-160	500	200	8	7.7	116	1300
Powder Core	Magnetics®	KoolMu	Fe-Al-Si	1.05	26-125	500	200	8	6.8	83	700
Powder Core	Magnetics®	Xflux	Fe-si	1.6	26-60	700	200	8	7.5	200	2000
Powder Core	Magnetics®	AmoFlux	Fe-Si-B-C	1.0	60	400	155	8	6.2 <sup>2</sup>	80	700
Powder Core	Chang Sung Corp.	MPP	Fe-Ni-Mo	0.7	26-200	450	200	8 <sup>1</sup>		65	
Powder Core	Chang Sung Corp.	High Flux	Fe-Ni	1.5	26-160	500	200	8 <sup>1</sup>		100	
Powder Core	Chang Sung Corp.	Sendust	Fe-Al-Si	1	26-125	500	200	8 <sup>1</sup>		76	
Powder Core	Chang Sung Corp.	Mega Flux	Fe-si	1.6	26-90	725	200	8 <sup>1</sup>	6.8	186	
Powder Core	Arnold Magnetics	Fe-si 6%	Fe-si	1.5	14-147	500	200	8 <sup>1</sup>		240	
Powder Core	Ferroxcube	MPP	Fe-Ni-Mo	0.75	14-300	460	200	8 <sup>1</sup>	8.7		
Powder Core	Ferroxcube	High-Flux	Fe-Ni	1.5	14-160	500	200	8 <sup>1</sup>	8.2		
Powder Core	Ferroxcube	Sendust	Fe-Al-Si	1.05	26-125	500	200	8 <sup>1</sup>	7	83	

<sup>1</sup>Similar materials assumed to be 8 or close to it. <sup>2</sup> values range from 6.2 to 6.7 [9]

**Molypermalloy Powder (MPP)** is the name for Fe-Ni-Mo cores which is made from Permalloy metal. The untreated metal have relative permeability in the range of 10,000 – 200,000. Low permeability is gained by grinding the metal into dust and insulating the particles from each other. Depending on the manufacturing process the losses and saturation flux varies, and from the data in Table 4-1 [10]. Magnetics® provide the lowest losses in this category [10].

Primary use: chokes and power inductors

**High flux** is the common name for Fe-Ni cores made from Orthonol. They have higher possible saturation flux than MPP and therefore have a higher energy storage capacity. This also allow for a large dc-bias. Generally High flux has larger losses than MPP and Chang Sung Corp. promises the lowest losses [10].

**Sendust/KoolMμ** is the common name for Fe-Al-Si cores made from ferrous alloy. They provide large energy storage at a cheap price, but the losses are higher than with MPP. Chang Sung Corp. reports the lowest losses [10].

**Xflux** is the common name for Fe-Si cores and have a larger saturation flux density than high flux, and Chang Sung Corp. promises the lowest losses.

**AmoFlux** was introduced by Magnetics® late 2012 and is made from Fe-Si-C, a low loss amorphous metal which is grinded into powder and pressed into a toroid. The resulting properties give low losses and a high dc bias rating ideal for power factor correction and output chokes. The downside with AmoFlux is that it have relatively low continues operation temperature of 155 °C, and only available with a permeability rating of 60, but since this a recently introduced product these properties might change making it in the future a possible material [9].

**Powder Core comparison:** The core loss up to the saturation limit is shown in Figure 4-5 for Magnetics® 125 $\mu$  MPP, High Flux, and KoolMu at 5 kHz. According to [4] magnetic materials are either saturation limited if the core losses are lower than 100 mWcm<sup>-3</sup>, otherwise the cores are thermally limited. The maximum flux density that leads to saturation limited designs can be found in Figure 4-4 for 5 kHz and Figure 4-6 shows the same limit at 100 kHz. This might seem low but it is very important to remember that this is the peak of the ripple current, which should not be very high. In the rest of the thesis when core losses is discussed it is primary the ripple flux which is considered. In Figure 4-5 the losses up to saturation have been plotted for 5 kHz and in Figure 4-7 the same for 100 kHz. It is not normal to operate powder cores up to saturation due to large losses and reduction in permeability. Figure 4-8 summarizes the core losses with a 100 kHz ripple of 50 mT and compares it to the rated saturation flux density.

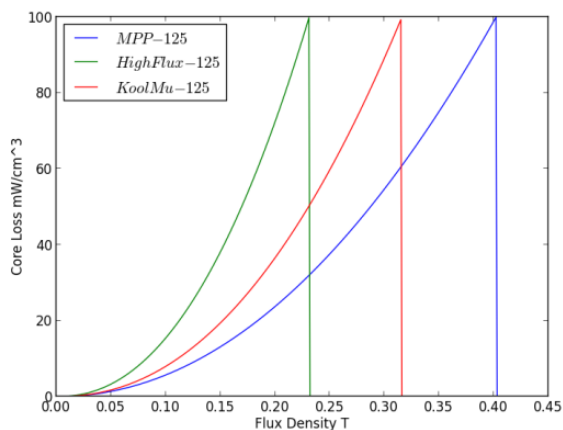


Figure 4-4 Core loss limited at 100 mWcm<sup>-3</sup> for 15.6 cm<sup>3</sup> cores at 5 kHz

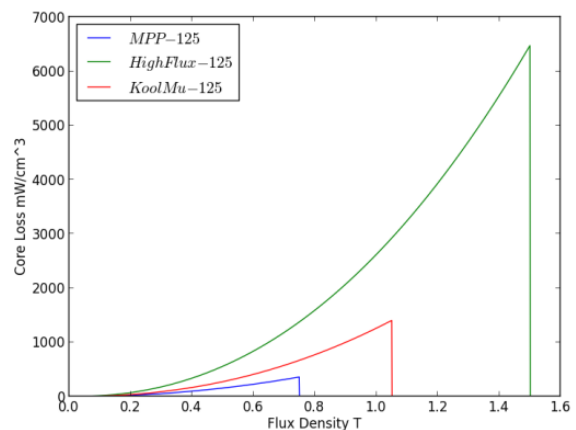


Figure 4-5 Core losses for 15.6 cm<sup>3</sup> cores up to saturation at 5 kHz

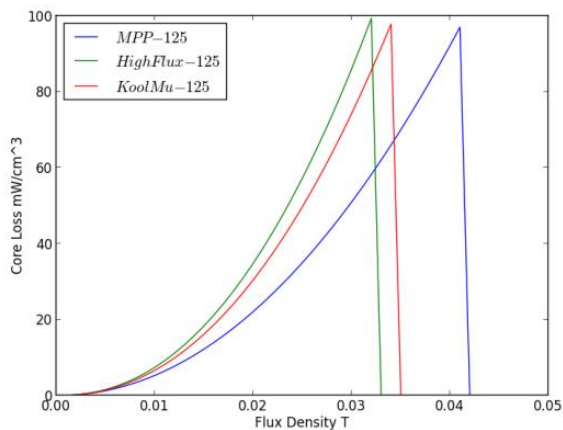


Figure 4-6 Core loss limited at 100 mWcm<sup>-3</sup> for 15.6 cm<sup>3</sup> cores at 100 kHz

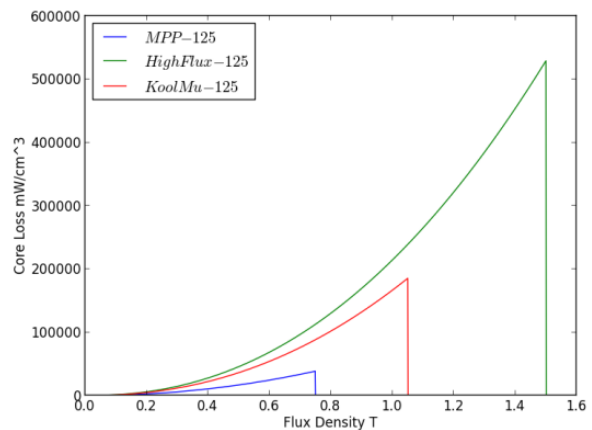


Figure 4-7 Core losses for 15.6 cm<sup>3</sup> cores up to saturation at 100 kHz

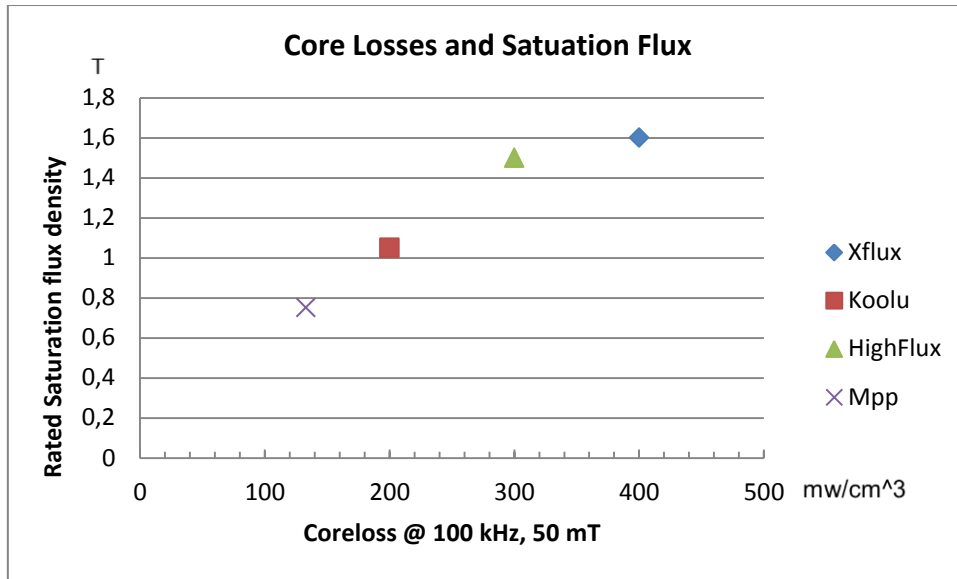


Figure 4-8 Core loss with sinus 50 mT peak at 100 kHz compared to rated saturation flux density

Powder core have a permeability which is heavily dependent on the direct current, and therefore large permeability changes will happened over the fundamental period seen by the high frequency ripple. Assuming 10 % of the current is in the high frequency component, a filter designed for removing the high frequency will experience a dc bias peak of 90% of the current. This bias is time dependent and therefore will vary from zero to the peak resulting in a filter inductance which depends on time, and therefore a varying ripple current. Figure 4-9 shows this effect when an inductor has a fundamental and high frequency ripple. At the time the fundamental current is zero the ripple is around three times as lower than at the peak. Permeability will be covered in more detail in section 4.4.

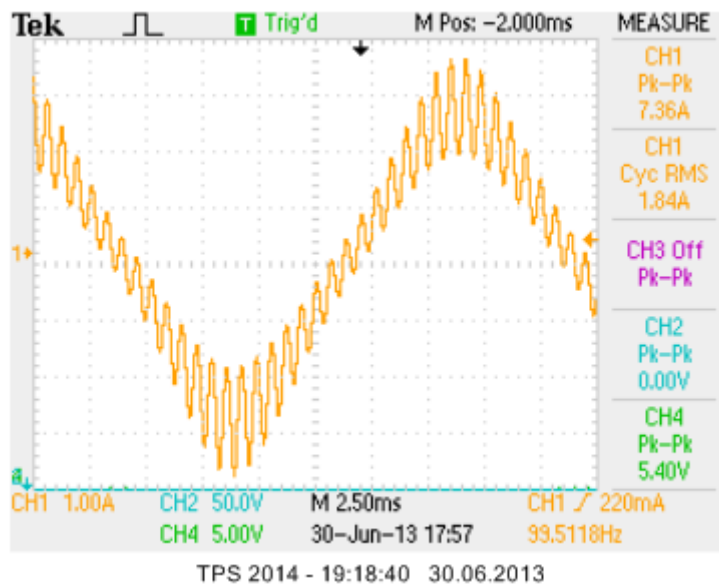


Figure 4-9 Current measurement in an inductor experiencing a 1.5 kHz ripple superimposed on a 50 Hz voltage.

## 4.2 Soft Ferrites

Ferrites are ceramic materials composed of iron oxide that can be used at frequencies from kilo hertz to several hundred megahertz. The oxide structure reduces the eddy losses and therefore these losses can be ignored up to several hundred kilo hertz. This makes ferrites optimal in design which requires high permeability, and low energy storage over a large frequency specter. On the other hand soft ferrites have a low saturation flux. Soft ferrites are usually a good choice in general purpose transformers, EMI filters, pulse delaying and other application requiring high permeability. In applications where low permeability is wanted an air gap can be added however this can lead to large fringing fields and losses in the windings.

The curie temperature for most ferrites are rather low which means that the saturation flux density is likely to change noticeable from the initial given values when the temperature increases. The magnetic properties of ferrites change depending on the materials and manufacturing process used. Different application needs can be satisfied like stable permeability over a wide temperature range, low losses, high temperature stability and other properties depending on the material chosen. The initial survey of higher temperature ferrites yielded the materials shown in Table 4-2 [1].

Table 4-2 Magnetic Properties of some powder HT Ferrites

Magnetic material type	Manufacturer	Material	Composition	Bsat[T] @ 25°C	Rel. Permeability (100 °C @ 20 k[Hz])	Curie temp. [°C]	Thermal conductivity [W/(mK)]	Continuous operating temperature [°C]	Density [g/cm <sup>3</sup> ]	Core Loss @ 0.1T, 20 k[Hz] mW/cm <sup>3</sup>	Core Loss @ 0.1T, 100 k[Hz] mW/cm <sup>3</sup>
Ferrite	Magnetics®	L		0.42	900	300	3.5-5 <sup>1</sup>	Na	4.8		
Ferrite	Magnetics®	R		0.47	2300	210	3.5-5 <sup>1</sup>	Na	4.8	5	70
Ferrite	Magnetics®	P		0.47	2500	210	3.5-5 <sup>1</sup>	Na	4.8	8	96
Ferrite	Magnetics®	F		0.47	3000	210	3.5-5 <sup>1</sup>	Na	4.8	12.39	119
Ferrite	Magnetics®	T		0.53	3000	220	3.5-5 <sup>1</sup>	Na	4.8		65
Ferrite	Ferroxcube	3F4 5	MnZn	0.42	900	300	3.5-5	Na	4.8		
Ferrite	Ferroxcube	3F5	MnZn	0.38	650	300	3.5-5	Na	4.75		
Ferrite	Siemens	N27	MnZn	0.5	2000*	220	3.5-5	Na	4.8	24	200

<sup>1</sup>Assumed

Ferrites are brittle and therefore strong forced cooling can lead to high temperature gradient inside the material causing thermal stress, which can break the ferrite and reduce the lifetime of insulation [7]. The initial permeability of ferrites usually affects the design less than in the case of a powder core inductor, because it is necessary to gap the ferrite to obtain the required relative permeability while in a transformer only high saturation and low losses is important.

### 4.3 Shape

Optimal shape of a magnetic core depends on what kind of application it is intended for, the most common shapes according to [11] are as follows:

<b>Pot Core</b>	The pot core consists of a bobbin which the winding is wound around and shielded by an outer layer lowering the EMI. Disadvantages are low thermal dissipation, high costs, and only available for low power ratings.
<b>E I Core</b>	E cores and similar consist of a simple bobbin with wide windows leading to good thermal dissipation and are simple to wind which reduces costs.
<b>PQ Core</b>	PQ cores have large windows and are quite similar to E cores. The PQ cores are mainly for higher power applications.
<b>Toroid</b>	The toroid shape leads to low leakage flux but high winding costs. Heat dissipation is poor due to the winding filling the middle hole however this depends somewhat on the filling factor.

In magnetic components with the toroid shape it is according to [6] simple to vary the cores height due to no necessity of changing tooling option leading to possible custom shapes that could lead to better utilization of space, Micrometals report that they do this at no extra charge while a custom diameter have some costs.

### 4.4 Permeability

The permeability in ferrites is not often an important parameter in inductors since it is necessary to insert an air gap, to control the effective permeability. However in powder cores the permeability is given by the material properties and depending on the turns and current this permeability change, and this happens long before the material go into saturation.

In a filter which purpose is to remove a high frequency ripple, and output a fundamental waveform or a constant this permeability dependence is hard to avoid. In the case of a fundamental waveform the permeability seen by the high frequency will depend on where on the fundamental waveform it is, at that time. When the fundamental is at the peak value the high frequency ripple will experience a large dc-bias. The results is that if you design the high frequency filter assuming there is no permeability change you can get a much larger ripple than anticipated.

The H-field is used by some core manufactures to analytical express how much the permeability has changed by a given field. This means that at one point increasing the number of turns will actually decrease the inductance, and any turns above this should be avoided, since it decreases inductance and increases the losses. From the analytical data given by Magnetics® this usually happened when the permeability has reached around 20 to 30 % of the initial value. The H field depends on the product of turns and current divided by the magnetic path length which means that for a given core the maximum NI that should be applied can be calculated. In Table 4-3 there are three examples of this limit for some different cores from Magnetics®, if you have 77 turns on the MPP and 10 A peak you would reach this limit. However the analytical data is not reliable at very high permeability



change like this, but it provides some insight into the limits of the materials. This data can be viewed in Figure 4-12 to Figure 4-15.

Table 4-3 Examples of absolute maximum NI that should be applied to magnetics® powder cores

Core Number	Maximum NI [A·T]	H [A·T/cm]
C055089A2 (MPP)	771	86.14
0077715A7 (KoolM $\mu$ )	862	67.8
C058583A2 (HighFlux)	774	86.48
C058548A2 (HighFlux)	1104	135.6

This means in a powder core design you have to decide at what point on the fundamental waveform you want your high frequency filter to be designed at for example halfway to saturation or when the permeability have decreased to 75 %. That means that in cases where you have large NI the magnetic path length need to be long, which with toroid components increase the area taken up by the magnetic material by a large factor. However a core which can support large NI could be built by I blocks thereby taking up less space and having better cooling.

A toroid shape has some benefits, and therefore an idea to increase the maximum NI would be to parallel two cores and wind them separately. This decreases the NI in each but also decreases the total inductance by a factor of two, however since inductance increases by the power of two in some applications this could be a very viable option instead of increasing the core size. Dividing the core into two separate also provides better cooling of the component, but care need to be used to make sure the current is divided evenly.

Paralleling benefits of inductors have been verified by measurements, and can be viewed in section 11.2.2 where a KoolM $\mu$  and a High Flux core was tested for increasing dc-bias and compared to a parallel connection of cores with twice the inductance. This has been plotted in Figure 4-10 and Figure 4-11. In the case of high flux with only 40 turns the inductance of a parallel connection of two 50 turns' cores gave an increased total inductance at 12 A dc bias. This might not seem like a lot but the product of NI is 600 so at 100 turns this positive shift would already happen at 6 A dc-bias which is not so large for the peak of a fundamental waveform. One drawback is a large increase in leakage capacitance, but these results depend on material and core size and should be further investigated.

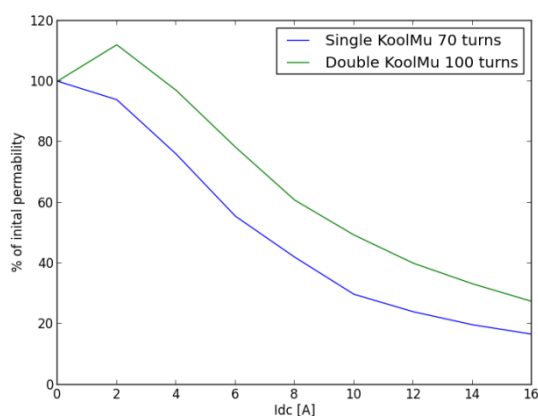


Figure 4-10 Comparison of the inductance in koolM $\mu$  with increasing Idc

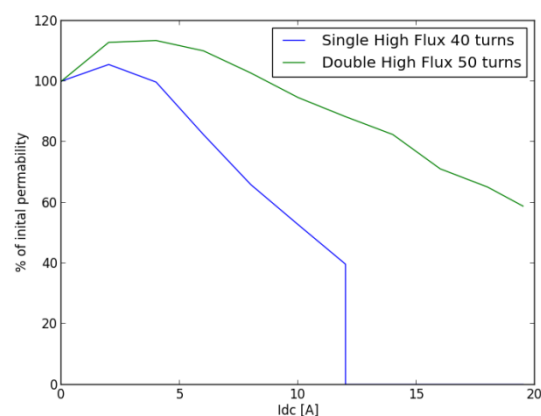


Figure 4-11 Comparison of the inductance in HighFlux with increasing Idc

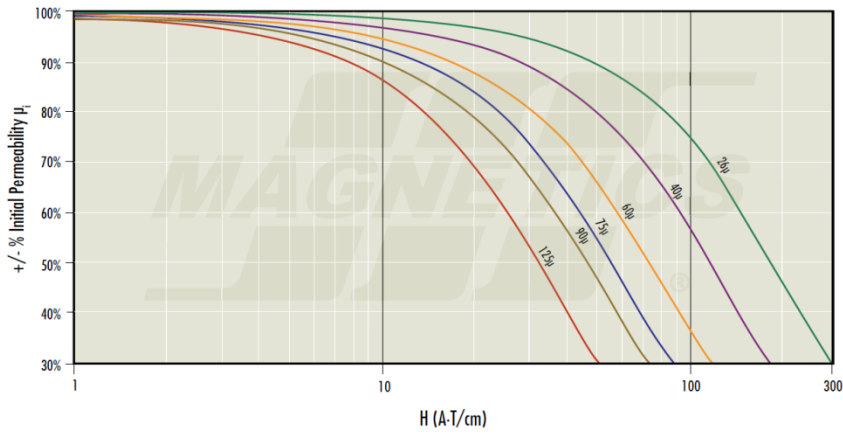


Figure 4-12 Permeability versus dc bias in KoolMμ

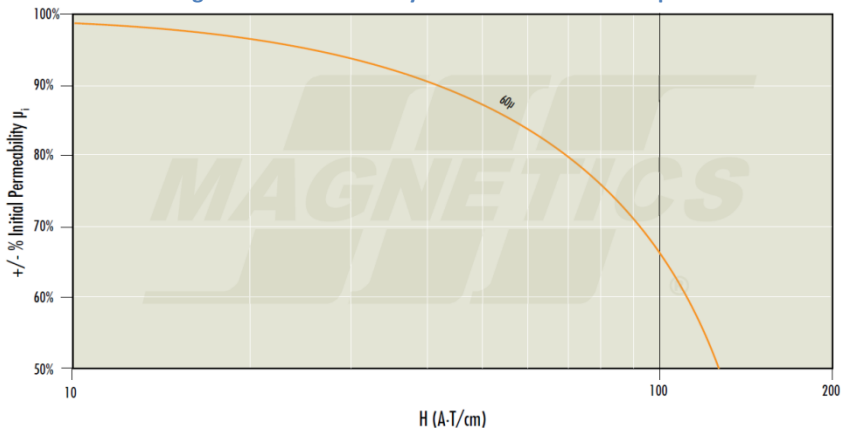


Figure 4-13 Permeability versus dc bias for XFlux

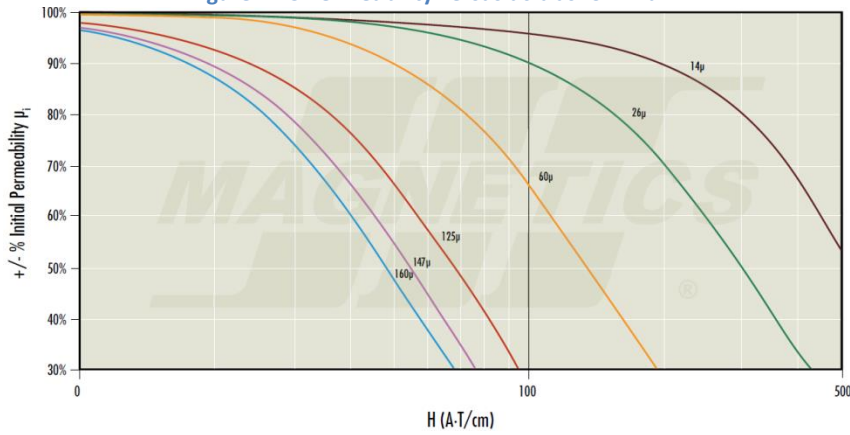


Figure 4-14 Permeability versus dc bias for High Flux

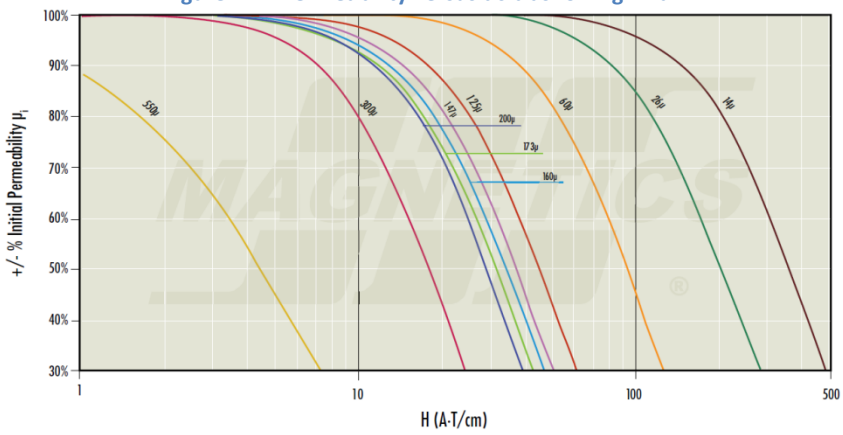


Figure 4-15 Permeability versus dc bias for MPP

Some cases where paralleling might be benefit able (mainly only when a smaller design is wanted):

- Minimum size design: The permeability reduction is primary given by  $H = NI/l_e$  therefore by splitting the current between two cores  $l_e$  can also be divided by two. This increases the losses and the leakage capacitance and therefore only applicable in designs where the core temperature is lower than the thermal limit.
- When the optimal core size for the design falls between two standard cores, however some manufactures can provide custom sizes at higher costs.
- When there are space issues and there is a maximum radius the core can have. Splitting a large core into several smaller could fit into tighter spaces.
- When the core temperature is high.
- The core losses increase by around the square of the peak flux density which means that splitting the ripple over two cores might reduce the total core losses, but this need to be further investigated.

#### 4.5 Core loss

Core loss in general is covered in chapter 5, however this section will briefly explain the actual measured losses in powder cores and ferrites see section 10.2 for the measurement setup, and the more in depth results and discussion see section 11.1. Figure 4-16 and Figure 4-17 show the core losses in N27 and R ferrite for three different temperatures. It can be observed that the losses have a minimum at around 108°C which is common to avoid thermal runaway. The analytical data is accurate however it most likely predicts the losses for some other temperature point than what's been plotted. In Figure 4-18 - Figure 4-17 the measured core losses have been plotted for different temperatures and flux density. It can be seen that KoolM $\mu$  have a large temperature dependency up to 180°C while the losses in High Flux and MPP do not significantly change with temperature. The analytical data provided by the manufacturer [12] underestimates the losses by a large factor for both KoolM $\mu$  and MPP however some of this could be due to the inaccuracy in measuring core loss when the loss is very low. The analytical data is based on the Steinmetz equation and do not take temperature into consideration and can in some cases be inaccurate due to allot of interpolation this will be further explained in the next chapter. In Chapter 11 new Steinmetz parameters for the analytical data will be calculated.

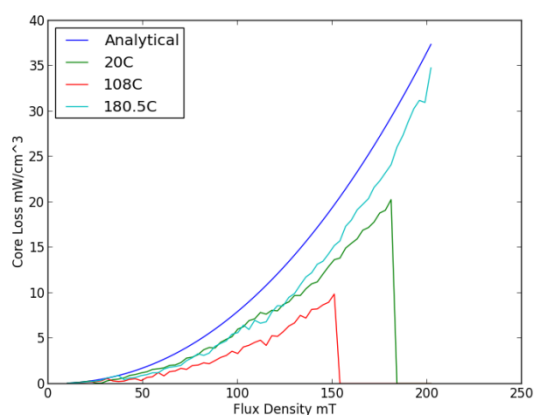


Figure 4-16 Measured loss in N27 at 5 kHz

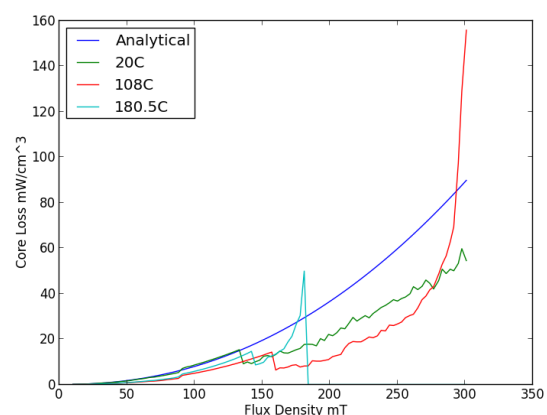


Figure 4-17 Measured loss in R ferrite at 5 kHz

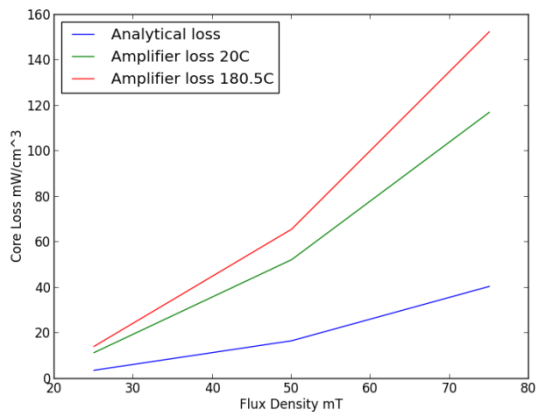


Figure 4-18 Measured loss in KoolM $\mu$  at 20 kHz

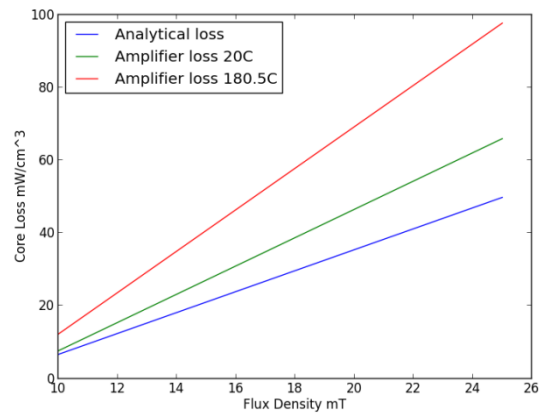


Figure 4-19 Measured loss in KoolM $\mu$  at 50 kHz

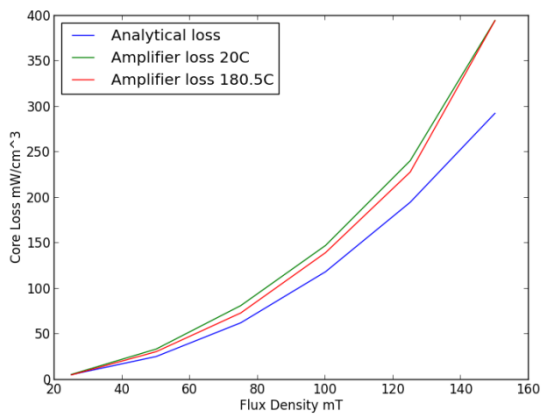


Figure 4-20 Measured loss in HighFlux at 20 kHz

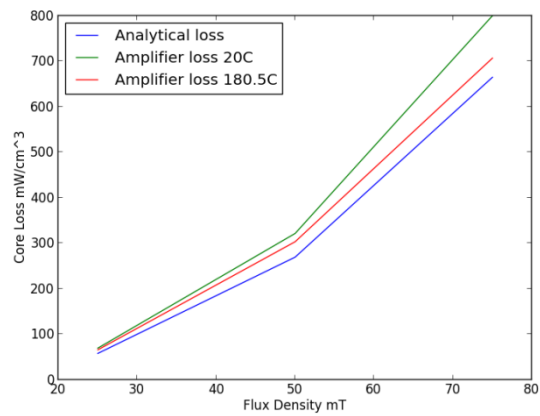


Figure 4-21 Measured loss in HighFlux at 100 kHz

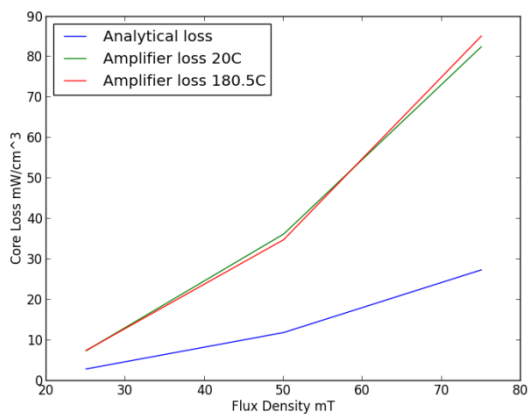


Figure 4-22 Measured loss in MPP at 20 kHz

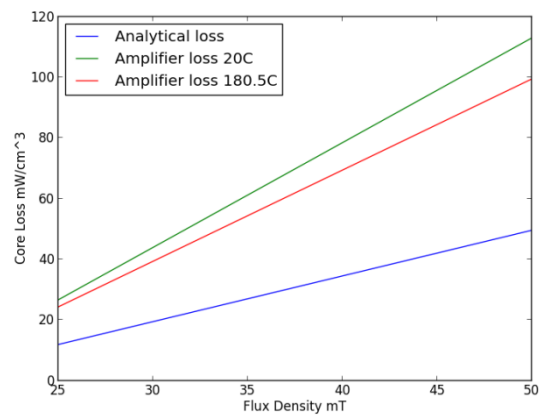


Figure 4-23 Measured loss in MPP at 50 kHz

## 4.6 References

- [1] Specialization Project Torbjørn Sørsdahl Magnetic Components In High Temperature SiC Converters 2012
- [2] Jonas Muhlethaler "Optimal Design of inductive components Based on Accurate Loss and Thermal Models"
- [3] C. McLyman Transformer and Inductor Design Handbook
- [4] Lloyd H. Dixon "Magnetic Design Handbook" Texas Instruments 2001
- [5] <http://www.hoganas.com/en/Segments/Somaloy-Technology/Technology/SMC-materials/> 09.04.2013
- [6] MICROMETALS Technical Bulletin "Practical Construction Tips For Coils Using Iron Powder Cores" revised 2001
- [7] Nicol, D.J., "Plain and simple design details regarding the application of iron powder cores," *Electrical Insulation Conference and Electrical Manufacturing & Coil Winding Conference, 1999. Proceedings* , vol., no., pp.241,247, 1999
- [8] <http://www.kdm-mag.com/products/Sendust-Cores/> 01.04.2013
- [9] <http://www.mag-inc.com/company/news/amoflux> 8.04.2013
- [10] Magnetics® Technical Bulletin "Magnetic Cores For Switching Power Supplies"
- [11] Chan, H.L.; Cheng, K.W.E.; Cheung, T.K.; Cheung, C.K.; , "Study on Magnetic Materials Used in Power Transformer and Inductor," *Power Electronics Systems and Applications, 2006. ICPEA '06. 2nd International Conference on* , vol., no., pp.165-169, 12-14 Nov. 2006
- [12] Magnetics® Technical Bulletin "Powder Core Catalog" 2012

## 5 Core Loss

Core loss is primary generated by two components dominating at different frequencies. Hysteresis losses dominate at lower frequency and are caused by the change in alignment of magnetic materials when a voltage is applied. Eddy current losses dominate at high frequency and in cores with high conductivity. Dc current does not directly contribute to losses in the core.

### *Hysteresis loss*

Magnetic materials can be considered to be built up by large number of smaller regions with a north and south pole which follows the magnetic field, when the field changes according to faradays law. The particles rotate into alignment which takes time and due to friction energy is lost. In an ideal magnetic core this process starts with saturating the shortest flux pathways and moving outward creating a sharp boundary where the magnetic fields are opposite. The speed of this boundary depends on the flux density and frequency [1]. The increase in the magnetic field from the poles is termed relative permeability and is constant as long the average path of the flux density is constant this means that in a non-ideal core the relative permeability will be changing especially just before complete magnetization.

### **Eddy loss**

Eddy losses are created in materials which are exposed to a time varying magnetic field. Following faradays law of induction a voltage will be induced and circulating currents will occur. The magnitude of the currents depends on the resistance of the material which makes it important to maximize the resistivity, especially in high frequency applications. Without laminations even at low frequencies such as 50 Hz the losses will be excessive in low resistive materials. One important point which is often overlooked is that eddy current losses actually are depending on flux density change. In a material operating at constant frequency the loss can be explained with Equation 5-1 where  $V_{ind}$  is the induced voltage  $T_s$  the period, D the duty cycle and R the resistance of the material [1].

$$P_{loss} = \frac{V_{ind}^2 T_s}{RD} \quad \text{Equation 5-1}$$

### **Excess loss**

The losses which are not explained by hysteresis and eddy losses is often summed into a term called excess loss and the exact mechanisms leading to them is not very well understood [2].

### 5.1 Flux waveforms

Magnetic components are usually designed assuming sinusoidal flux waveforms to simplify the design procedure, according to [4] this has been shown underestimate losses especially in ferrites. The waveform will depend allot upon the actual design, and have to be calculated on a case to case basis to obtain an improved analytical model of the system.

In the case of an output inductor the flux change will depend on the voltage over the component which can be described by Equation 5-2

$$v_{ripple} = v_o - v_{o1} \quad \text{Equation 5-2}$$

The component will experience the fundamental output waveform and the ripple which can be non-sinusoidal. The resulting flux waveform will have a major loop and a large number of minor dc biased loops [5]. The main possible waveform formations can be seen in Figure 5-1.

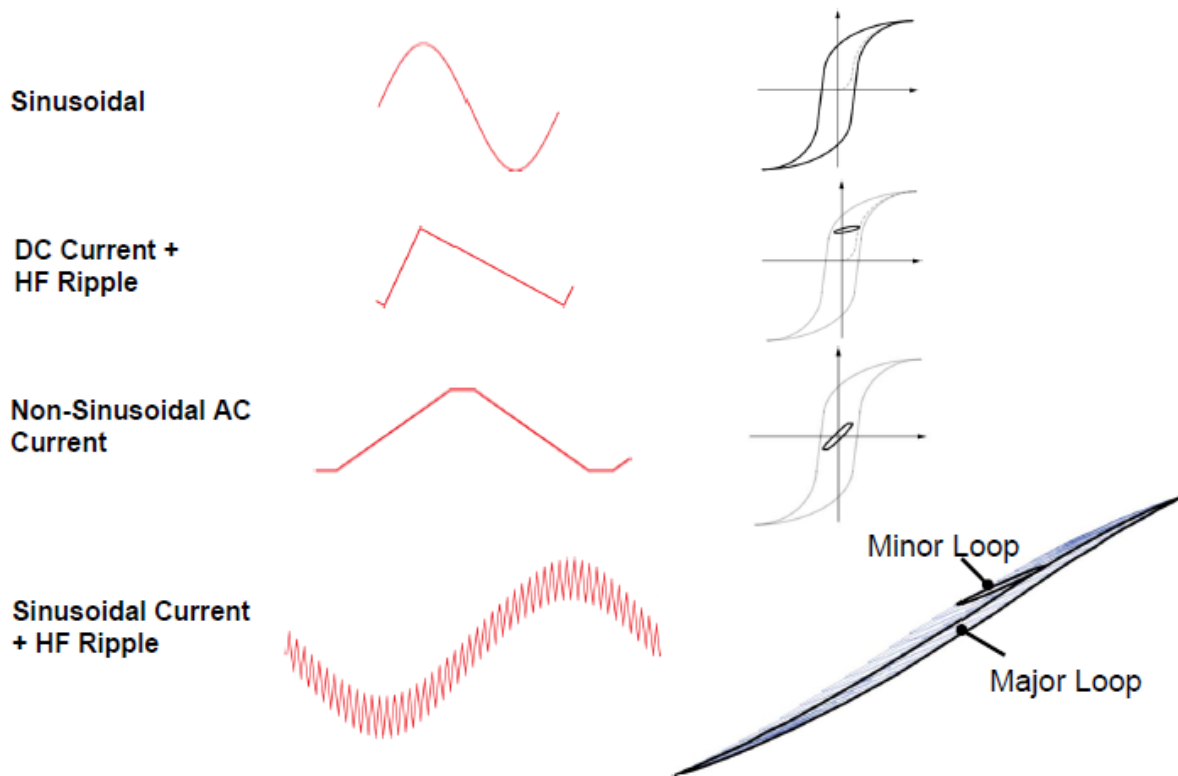


Figure 5-1 Flux waveforms [5]

## 5.2 Loss models

There are three main approaches to core loss determination: hysteresis models, loss separation, and empirical models. The problem with the two first approaches is that they are based on parameters which are not usually available. The most common model is the empirical original Steinmetz equation (OSE) see Equation 5-3 which is based on curve fitting of measured loss data.

$$P_v = k f^\alpha \hat{B}^\beta \quad \text{Equation 5-3}$$

Where  $P_v$  is the time average loss per unit volume,  $\hat{B}$  is the peak flux  $f$  is the frequency of the sinusoidal excitation,  $k$ ,  $\beta$  and  $\alpha$  is material constants, normally available from manufactures which is only valid over a limited frequency and flux density change. Equation 5-3 can be solved for three operating points to determine  $k$ ,  $\alpha$  and  $\beta$  keeping frequency and temperature constant [3][11].

The drawback with the Steinmetz equation is that it assumes sinusoidal waveforms which are normally not the case in power electronics see section 5.1 and in some cases it has been shown that at the same frequency and amplitude the losses with non-sinusoidal ripple waveforms can be twice as much as the OSE predicts [4]. To determine loss for a wider spectrum of waveforms several models have been developed to overcome the limitations in the Steinmetz equation. The models

have been verified on ferrites, however in powder cores the non-sinusoidal losses have little effect [16].

### I. Modified Steinmetz Equation (MSE)

The MSE is based on a hypothesis that core losses is related to the change in magnetic induction and replaces the frequency in Equation 5-3 with an equivalent frequency  $f_{eq}$ . To determine  $f_{eq}$  the induction change is averaged over a remagnetization cycle  $B_{max}$  to  $B_{min}$  and back, if the remagnetization is repeated with a frequency equal  $f_r$  the power loss will be Equation 5-5 [5].

$$f_{eq} = \frac{2}{\Delta B^2 \pi^2} \int_0^T \left( \frac{dB(t)}{dt} \right)^2 dt \quad \text{Equation 5-4}$$

$$P_v = (k f_{eq}^{\alpha-1} \hat{B}^\beta) f_r \quad \text{Equation 5-5}$$

#### Main limitations

- The  $f_{eq}$  averaging is arbitrary and limits accuracy.
- The equation breaks down for sinusoidal waveforms.

### II. Generalized Steinmetz Equation (GSE)

The MSE breaks down for sinusoidal waveforms and the GSE was introduced considering both the instantaneous value and the rate of change of magnetic induction. The proposed equation can be seen in Equation 5-7. The GSE has been experimentally verified as more accurate than the MSE method especially for waveforms with small fundamental amplitudes and at duty cycle near 0.5 [2].

$$P_v = \frac{1}{T} \int_0^T k_1 \left| \frac{dB(t)}{dt} \right|^\alpha |B(t)|^{\beta-\alpha} dt \quad \text{Equation 5-6}$$

If we choose  $k_1$  as Equation 5-7 the result will equal the Steinmetz equation for sinusoidal waveforms.

$$k_1 = \frac{k}{(2\pi)^{\alpha-1} \int_0^{2\pi} |\cos(\theta)|^\alpha |\sin(\theta)|^{\beta-\alpha} d\theta} \quad \text{Equation 5-7}$$

The angle  $\theta$  is the phase angle of the sinusoidal waveform.

#### Main limitations

- Not accurate for all waveforms and sometimes worse than MSE.

### III. Improved Generalized Steinmetz Equation (IGSE)

The IGSE is a continuation of the GSE which start to deviate from measured data at the point where the flux waveform start to have minor hysteresis loops therefore the IGSE calculates the loss separately for each minor loop and major loop taking into account the history of the



material. The IGSE modifies Equation 5-6 with  $\Delta B$  which is the peak to peak flux density at that point for that minor/ mayor loop [6].

$$p_v = \frac{1}{T} \int_0^T k_1 \left| \frac{dB(t)}{dt} \right|^\alpha |\Delta B|^{\beta-\alpha} dt \quad \text{Equation 5-8}$$

$$k_1 = \frac{k}{(2\pi)^{\alpha-1} \int_0^{2\pi} |\cos(\theta)|^\alpha 2^{\beta-\alpha} d\theta} \quad \text{Equation 5-9}$$

The IGSE requires summation of loops and this has been implanted in a Matlab program [7] dc bias has been shown to vary the loss in ferrite cores and this has only by accident been taken into account into the IGSE model [6].

#### Main limitations

- Dc bias is not accounted for.
- Relaxation effects.

#### IV. Improved-Improved Generalized Steinmetz Equation (I<sup>2</sup>GSE)

The I<sup>2</sup>GSE was published February 2012 and the newest loss model published this is a continuation of the IGSE. In most of the previous models it has been assumed that there aren't losses during periods of constant flux. Measurements have shown that this is not true. It is hypothesized that this is due to relaxation mechanisms which readjust the magnetic poles in the material to

The I<sup>2</sup>GSE need 5 new parameters to explain the relaxation mechanisms and the parameters are only valid for limited ranges of flux density and frequency, this make it unsuitable for a modeling approach based on Steinmetz parameters.

#### V. The Waveform Coefficient Steinmetz Equation (WcSE)

The WcSE [9] correlate the losses for non-sinusoidal waveform to a sinusoidal by using a coefficient which describes the difference of area between the waveforms. See Equation 5-10 where a triangular waveform has been used.

$$F_{WC} = \frac{A_{tri}}{A_{sin}} = \frac{\frac{1}{2}}{\frac{2}{\pi}} = \frac{\pi}{4} \quad \text{Equation 5-10}$$

The correction factor is applied to the original Steinmetz equation.

#### Main limitations

- Less accurate than IGSE in some situations[14]

### 5.3 Parameters influencing core loss

The loss models previously mentioned can be affected by a large number of outside parameters and this section presents the main parameters and if there have been observed any influence on the loss.

#### I. Duty Cycle

The duty cycle affects the error in the analytical approaches to modeling core losses as mentioned earlier. The loss of accuracy at higher duty cycle can be explained that the Steinmetz parameters being only valid for a limited range of frequency's and at 0.95 duty cycle the slope of excitation would act as the slope of a 0.5 duty cycle at 10 times the real frequency, this was verified by some experimental data [2].

#### II. Dc Bias and low frequency

Power electronic components is often exposed to dc or a low frequency magnetization which according to [11] have a large effect on ferrites and nanocrystalline materials while the effect in molypermalloy powder cores and silicon steel is small. The Steinmetz parameters  $\beta$  and  $k$  need to be adjusted with the dc-bias present, but do not affect frequency parameter  $\alpha$ . This has been verified for several materials in [11].

#### III. Modulation Technique

Influence of modulation technique on losses has have been investigated in [10] which mentions that in three phase inverters this phenomena is absent and is only found in single phase.

#### IV. Power Factor

The power factor influences on losses have been measured for an ac inductor ferrite in [12] which showed that the iron losses were not influenced much by the power factor.

#### V. Geometric Factors

[15] Investigates the effect of geometric factors on power loss and concludes that the radial flux change in toroid have little influence. However in laminated cores the losses increase in small toroid's.

#### VI. Temperature

The temperature affects the core losses substantially and need to be considered in any analytical approach [11] but little documentation on how this influence the models have been found.

## 5.4 References

- [1] Lloyd H. Dixon "Magnetic Design Handbook" Texas Instruments 2001
- [2] Jieli Li; Abdallah, T.; Sullivan, C.R.; , "Improved calculation of core loss with nonsinusoidal waveforms," *Industry Applications Conference, 2001. Thirty-Sixth IAS Annual Meeting. Conference Record of the 2001 IEEE* , vol.4, no., pp.2203-2210 vol.4, Sept. 30 2001-Oct. 4 2001
- [3] Muhlethaler, J.; Biela, J.; Kolar, J.W.; Ecklebe, A.; , "Improved core loss calculation for magnetic components employed in power electronic system," *Applied Power Electronics Conference and Exposition (APEC), 2011 Twenty-Sixth Annual IEEE* , vol., no., pp.1729-1736, 6-11 March 2011
- [4] Van den Bossche, A.; Valchev, V.C.; Georgiev, G.B.; , "Measurement and loss model of ferrites with non-sinusoidal waveforms," *Power Electronics Specialists Conference, 2004. PESC 04. 2004 IEEE 35th Annual* , vol.6, no., pp. 4814- 4818 Vol.6, 20-25 June 2004
- [5] Reinert, J.; Brockmeyer, A.; De Doncker, R.W.A.A.; , "Calculation of losses in ferro- and ferrimagnetic materials based on the modified Steinmetz equation," *Industry Applications, IEEE Transactions on* , vol.37, no.4, pp.1055-1061, Jul/Aug 2001
- [6] Venkatachalam, K.; Sullivan, C.R.; Abdallah, T.; Tacca, H.; , "Accurate prediction of ferrite core loss with nonsinusoidal waveforms using only Steinmetz parameters," *Computers in Power Electronics, 2002. Proceedings. 2002 IEEE Workshop on* , vol., no., pp. 36- 41, 3-4 June 2002
- [7] "Dartmouth Magnetic Component Research" [Online]. Available: <http://engineering.dartmouth.edu/inductor/coreloss.shtml>. [Accessed 11 10 2012].
- [8] Lin, D.; Zhou, P.; Fu, W.N.; Badics, Z.; Cendes, Z.J.; , "A dynamic core loss model for soft ferromagnetic and power ferrite materials in transient finite element analysis," *Magnetics, IEEE Transactions on* , vol.40, no.2, pp. 1318- 1321, March 2004
- [9] Wei Shen, "Design of high-density transformers for high-frequency high-power converters", Ph.D dissertation, Virginia Polytechnic Institute, July 2006.
- [10] Boglietti, A.; Ferraris, P.; Lazzari, M.; Pastorelli, M.; , "Influence of modulation techniques on iron losses with single phase DC/AC converters," *Magnetics, IEEE Transactions on* , vol.32, no.5, pp.4884-4886, Sep 1996
- [11] Muhlethaler, J.; Biela, J.; Kolar, J.W.; Ecklebe, A.; , "Core Losses Under the DC Bias Condition Based on Steinmetz Parameters," *Power Electronics, IEEE Transactions on* , vol.27, no.2, pp.953-963, Feb. 2012
- [12] "Magnetics®," [Online]. Available: <http://www.mag-inc.com/products/powder-cores/learn-more-about-powder-cores>. [Accessed 17 10 2012].
- [13] Shimizu, T.; Kakazu, K.; Takano, K.; Ishii, H.; , "Loss evaluation of AC filter inductor core on a PWM converter," *Power Electronics and ECCE Asia (ICPE & ECCE), 2011 IEEE 8th International Conference on* , vol., no., pp.1047-1052, May 30 2011-June 3 2011
- [14] Villar, I.; Viscarret, U.; Etxeberria-Otadui, I.; Rufer, A.; , "Global Loss Evaluation Methods for Nonsinusoidally Fed Medium-Frequency Power Transformers," *Industrial Electronics, IEEE Transactions on* , vol.56, no.10, pp.4132-4140, Oct. 2009
- [15] Grimmond, W.; Moses, A.J.; Ling, P.C.Y.; , "Geometrical factors affecting magnetic properties of wound toroidal cores," *Magnetics, IEEE Transactions on* , vol.25, no.3, pp.2686-2693, May 1989
- [16] Thottuvelil, V.J.; Wilson, T.G.; Owen, H.A., Jr., "High-frequency measurement techniques for magnetic cores," *Power Electronics, IEEE Transactions on* , vol.5, no.1, pp.41,53, Jan 1990

## 6 Winding Configuration

Significant reduction in the copper losses, leakage inductance and temperature can be achieved by optimal winding configuration. This chapter will cover high frequency losses in the windings by Dowell's equation, present Litz wire, Round wire and foil wire and some considerations that should be taken at high temperature design. The last section will cover parasitic inductance.

### 6.1 Introduction

The most basic relationship to configure the windings for high frequency components is the penetration depth Equation 6-1. As the frequency increases eddy currents are induced in the middle of the wire leads to an opposing current flowing. This reduces the current in the middle of the wire and more of the current flows on the surface. The simplest way to counteract this is to use Litz wires where a large number of smaller insulated wires is bundled together to form a single wire, see chapter 0.

Equation 6-1 assumes that by the depth  $D_{pen}$  the current density has decreased to  $e^{-1}$  of the surface current density. In this area it is assumed that the current is constant and deeper it is zero. As it can be seen in the equation the penetration depth increases with higher resistivity in the wire so in a high temperature design, larger Litz wires can be used compared to a normal temperature. Larger wires increase the thermal conductivity and fill factor however some problems might happen as the component is heated up to the operation temperature. The penetration depth from 0 to 100 kHz at 50°C, 200°C and 400°C is plotted in Figure 6-1.

$$D_{pen} = \sqrt{\frac{\rho}{\pi \mu f}} \quad \text{Equation 6-1}$$

$D_{pen}$	Penetration depth
$\rho$	Resistivity at the operating temperature
$\mu$	Permeability

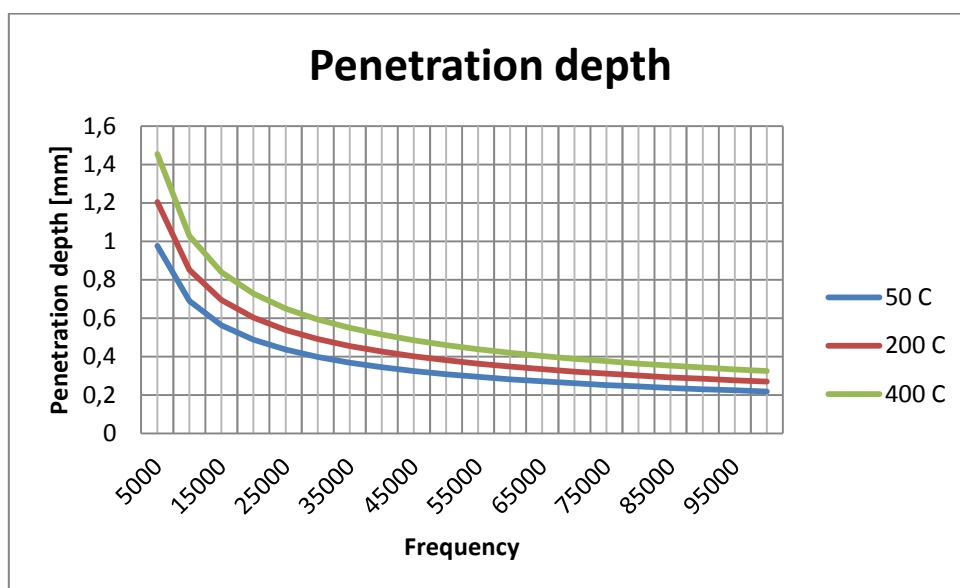


Figure 6-1 100 k Hz skin depth at different temperatures

In a high frequency design the magnetic field configures itself to have the lowest losses which mean it is no longer the resistive effects deciding how the current will flow but the inductive. In a multilayer winding where most of the current is flowing along the surface of each wire, the lowest magnetic potential is obtained when current in one layer negates the current in the next. This effect leads to current on one side of the wire ( $I_1$ ) to flow in the opposite direction of the current on the other side ( $I_2$ ) even if this leads to large resistive losses. The total current still needs to equal the generated current and therefore a larger current flow in  $I_1$  this effect is called the proximity effect. See Figure 6-2 and can be modelled by Dowels equations Equation 6-2 - Equation 6-6 in the case of sinusoidal current. Dowels equations are accurate in round conductor designs while in Litz wire they are only accurate up to when the penetration depth is twice as large as the wire size.

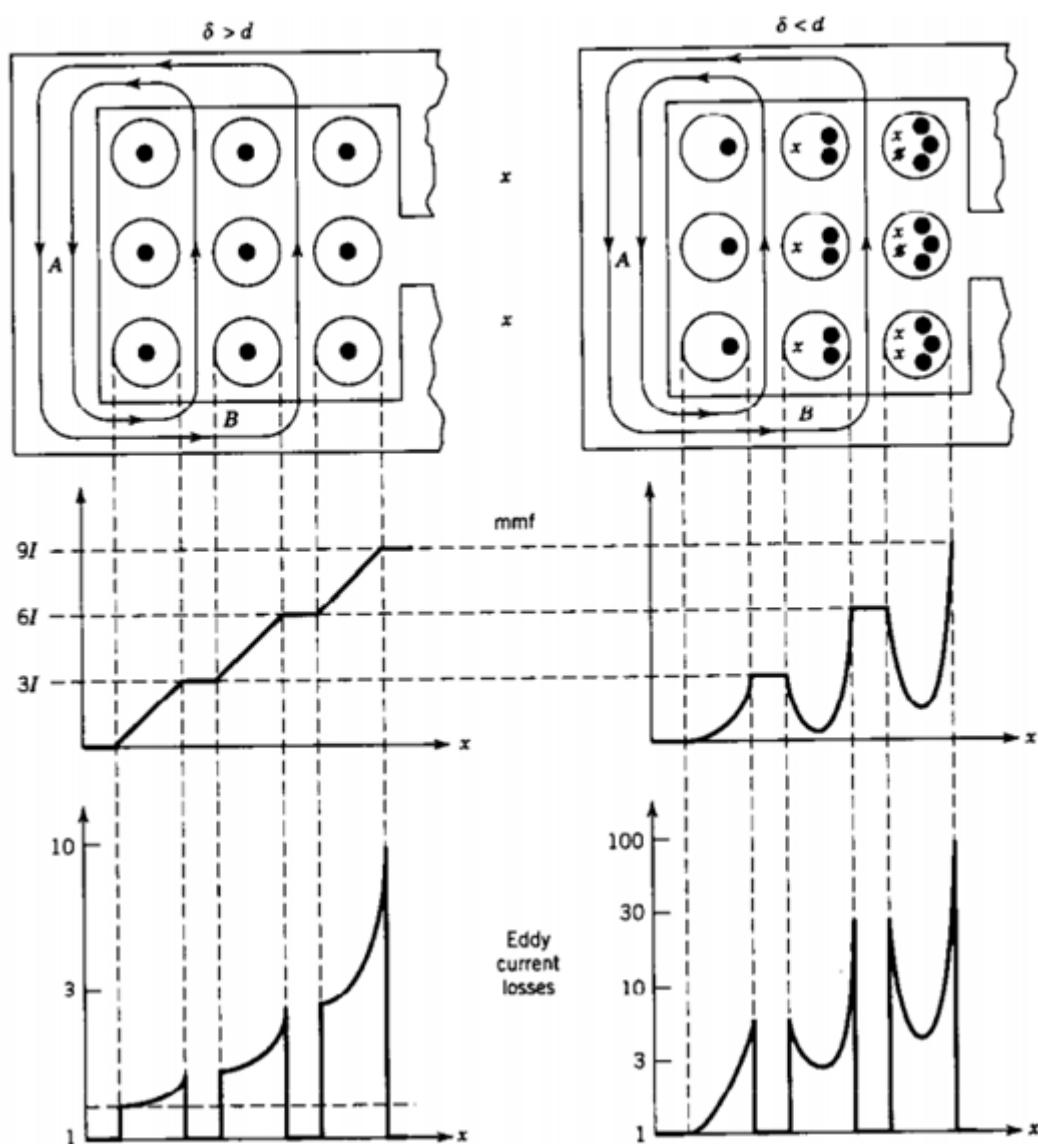


Figure 6-2 Proximity effect in multilayer windings

$$x = \frac{r_{wire}}{D_{pen}} \quad \text{Equation 6-2}$$

$x$  Factor  
 $r_{wire}$  Radius of the wire

$$M = x \left( \frac{\sinh(2x) + \sin(2x)}{\cosh(2x) - \cos(2x)} \right) \quad \text{Equation 6-3}$$

$M$  Factor

$$D = \frac{2x(\sinh(x) - \sin(x))}{\cosh(x) + \cos(x)} \quad \text{Equation 6-4}$$

$D$  Factor

$$Fr = M + D(m^2 - 1)/3 \quad \text{Equation 6-5}$$

$Fr$  Factor  
 $m$  Number of layers

$$R_{ac} = FrR_{dc} \quad \text{Equation 6-6}$$

$R_{ac}$  Ac resistance  
 $R_{dc}$  Dc resistance

$R_{ac}$  equals  $R_{dc}$  at lower frequencies but as frequency and the number of layers increase  $R_{ac}$  can become very large, see Figure 6-3 and Figure 6-4 where  $R_{ac}/R_{dc}$  have been plotted for 25°C and 200°C. The temperature dependency in the skin effect decreases the relative resistance by 35% when the temperature increases to 200°C however the  $R_{dc}$  base will also increase, and the overall resistance will be quite similar at different temperatures. In toroid cores the outer diameter is larger than the inner therefore you will end up with more layers on the inner radius than on the outer which should be taken into account by for example approximating that half the winding have twice as many layers as the other part. However this should be further investigated.

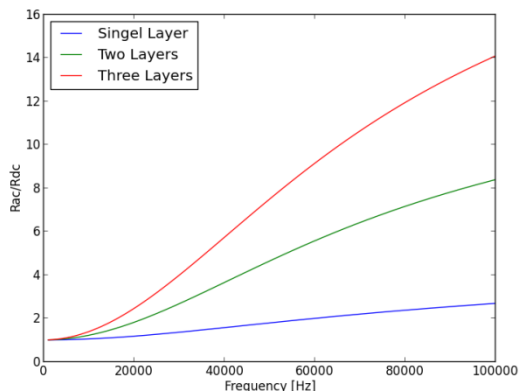


Figure 6-3  $R_{ac}/R_{dc}$  for  $O_d = 1.25$  mm at 25 °C

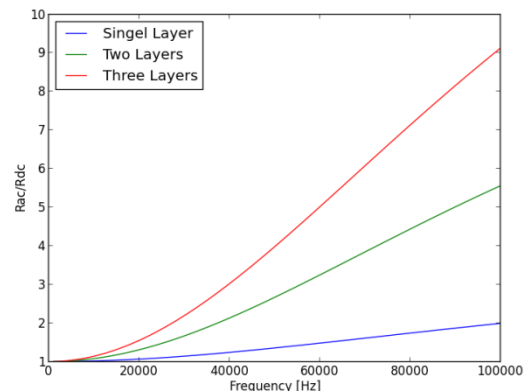


Figure 6-4  $R_{ac}/R_{dc}$  for  $O_d = 1.25$  mm at 200 °C

## 6.2 Litz wire

In high frequency designs multi stranded wires helps avoid the large increase in  $R_{ac}$  but it is not as simple as having some number of parallel wires, they have to be twisted and insulated from each other to gain the high frequency benefits. The increase in area due to insulation will for a fixed outer diameter lead to less space for copper as the number of wires increases and therefore lower fill factor, and thermal conductivity is reduced.

According to [4] the basic Dowel 1-D equation described in Equation 6-2 - Equation 6-6 can seriously underestimate the winding losses in Litz wire and [5] reports an error of 60 % with Dowel. However [5] have developed a simplified equation with an error less than 4% based on 2-D simulations. The large error with Dowel equations is primary in cases where the wire diameter is larger than the penetration depth and therefore only in such cases a modified approach should be considered.

Litz wire for temperatures above 155°C do not seem to exist commercially at least in any manufacturers investigated by me, or by SmartMotor, however [3] reported during a conference that they had Litz wire for 180°C. The temperatures classes normally reported is at 130°C and 155°C which make them the B and F thermal class, more on this in the next chapter.

Litz wire for 200C was necessary to perform the high temperature measurements described in later sections, and therefore a small test with differential scanning calorimetry was performed in cooperation with Assoc. Prof. Frank Maurseth showing that no melting effects appeared in an insulation of a sample of BLOCK CLI 30 x 0.1  $\Phi$  Litz wire in the range from 25°C-200°C. This means that for short term tests this type of Litz wire can be used without much degradation of the insulation however thermal ageing is likely very present.

At operation temperatures outside of the rated, there are high possibilities of turn to turn damage and short circuits due to thermal ageing, therefore the resistance before and after the measurements should be checked. And if these parameters do not change the windings should not have been damaged during the tests. In two experiments carried out the windings was damaged after prolonged exposure to high temperature, and had to be repeated.

Table 6-1 summarizes the advantages and disadvantages for Litz wires, the easy bending of wires is especially advantageous in toroid cores due to the geometry.

Table 6-1 Advantages and disadvantages with Litz wires [2].

Advantages	Disadvantages
Low eddy losses	Low fill factor
Easy to bend	Low thermal conductivity
	High costs

### 6.3 Round wire

Round wires are the most common wires and can be fitted on a magnetic component with either square fitting Figure 6-5 which under ideal conditions reach a fill factor of 0.7854. Or hexagonal fitting see Figure 6-6 which under ideal conditions have a fill factor of 0.9069, under normal conditions you will get a mix between the two [2]. Large round wires have better thermal conductivity than Litz wire due to a lower insulation to copper ratio. See Table 6-2 for the advantages and disadvantages with round windings [2].

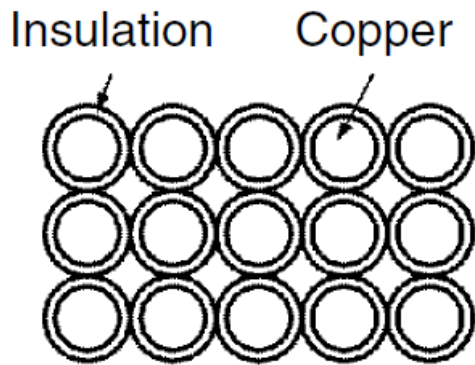


Figure 6-5 Square fitting

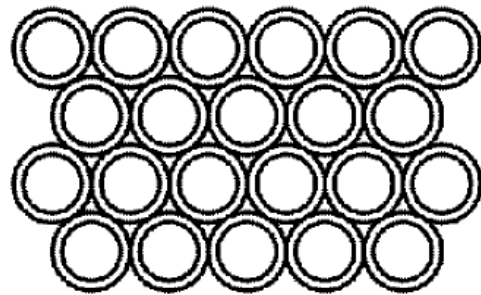


Figure 6-6 Hexagonal fitting

Table 6-2 Advantages and disadvantages with round wires

Advantages	Disadvantages
Low cost	High fill factor
High eddy losses	High thermal conductivity



The insulation which is often used for round wires in magnetic components is enamel however during experimentation at higher temperatures it was discovered that the insulation in all samples (3) using enamel became damaged along the borders, where the wires had been bent. This happened at temperatures below the rated insulation temperature and far below the maximum peak temperature.

Figure 6-7 and Figure 6-8 shows the damaged insulation in two of the samples. In the second picture most of the turns have been removed revealing that there is damage in all layers. This was not investigated in detail and might be solved by having a larger bending diameter putting less stress on the insulation but this will again lead to a looser winding which take more space and have other negative sides The damaged insulation lead to a short circuit in the winding which in one case resulted in a meltdown of most wires behind the component since the high frequency ripple was able to pass through. In the two other cases it was found by measuring the resistance of the coils before and after the damage happened.

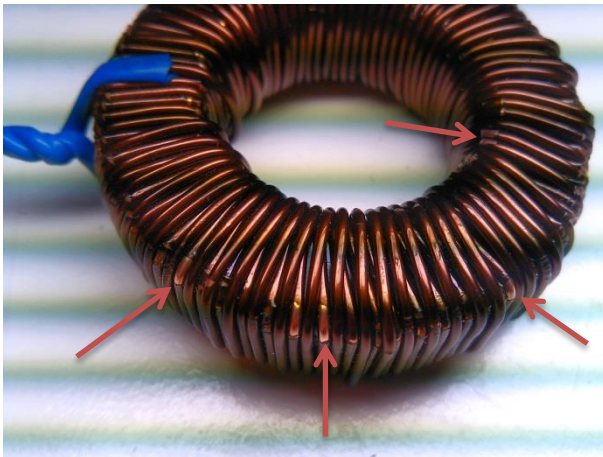


Figure 6-7 Damage to enamel insulation operated at 170 °C

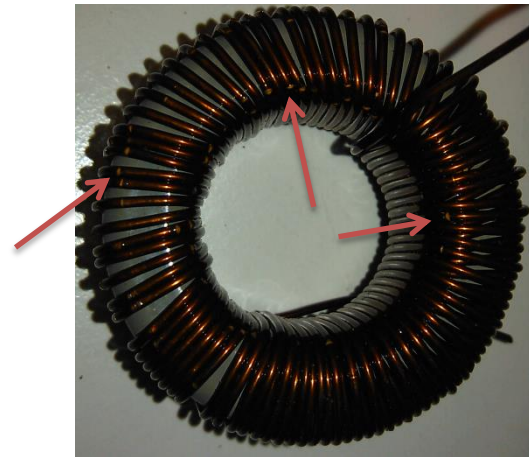


Figure 6-8 Damage to enamel insulation operated at 180.5 °C

## 6.4 Foil winding

Foil windings have very low eddy losses for fields parallel to the foil, and is most commonly used when you need a high copper cross section. Large insulated foils of copper or aluminum is wound around the core providing a very large surface area which leads to the low eddy losses. Leakage flux especially in gapped core can induce large eddy currents and losses in the foils if they are located too close to the gap. To avoid this, the common solution is to move the foil further out from the core. See Table 6-3 for the advantages and disadvantages with foil windings [2].

Table 6-3 Advantages and disadvantages with foil windings

Advantages	Disadvantages
Low costs	Hard to fit
Low eddy losses	
High filling factor	
High thermal conductivity	

## 6.5 Parasitic capacitances

The parasitic capacitances in high frequency magnetic components can have a large effect on the performance of the components and the full system. Leakage capacitance distorts the output waveform, decreases the efficiency of the system and stray capacitance between the turns leads to increased EMI, and ringing. At increasing switching frequency the leakage capacitance have a larger and larger effect. The parasitic capacitance is heavily geometry dependent and can be split into three main factors.

- Capacitances between windings
- Self-capacitance of the winding
- Capacitance between the winding and the core

### Capacitances between windings ( $C_{intra}$ )

In a transformer there will be leakage capacitance between the windings, which is often the cause of common mode current and therefore EMI. The effect of the capacitances between the windings is that when steps in the common mode voltage happen, a charge equal to  $C_{intra}\Delta V$  is injected. The current injected resonates with the leakage inductance causing ringing effects.  $C_{intra}$  can be calculated with Equation 6-7 [2].

$$C_{intra} = \frac{\epsilon_0 \epsilon_r S_{win}}{d_{win}} \quad \text{Equation 6-7}$$

$\epsilon_0$	Permittivity of air
$\epsilon_r$	Relative permittivity
$S_{win}$	Area between the windings
$d_{win}$	Distance between the different windings

Reducing  $C_{intra}$  can be done by increasing the distance between windings, reducing the turns in each winding and reducing  $\epsilon_r$ .

### Self-capacitance of the winding

Self-capacitance results in parallel resonances with leakage or magnetizing inductance, and leads to ringing effects. The self-capacitance can be split into two main components.

#### 1. Layer to layer

In a multilayer winding there will be a parasitic capacitance between the layers, providing shortcuts for high frequency noise.

#### 2. Turn to turn

The parasitic capacitance between turns this results in a network of capacitances, connecting all the turns in a winding.

### Capacitance between the windings and the core

There will be a parasitic capacitance between the core and the windings, which especially in ferrite designs can increase the apparent equivalent intra capacitance [2].

### Equivalent model

The distributed parasitic capacitances can be lumped together to form an equivalent model as seen in Figure 6-9 [6]. Here  $C$  describes the leakage capacitance,  $R$  the resistivity in the component and  $L$  the inductance. The equivalent  $C$  is can be measured se section 10.5.

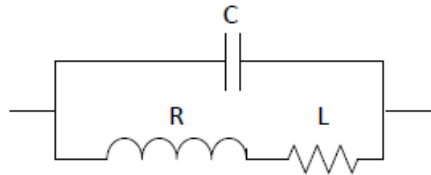


Figure 6-9 Inductor equivalent circuit

Single layer inductors have been shown to have the minimum inductance however this might be impossible to obtain in cases where high inductance or small core size is necessary. Therefore some techniques can be used to decrease the leakage inductance:

1. Bank winding minimizes the voltage difference between layers this is performed by winding both layers at once. First a turn is added to the first layer, and then the next turn is added to the second layer and then a turn on the first layer again. Larger wire diameters complicates this process so for Litz wire it might be a viable option however as the wire diameter increases the process get complicated and expensive.
2. Litz wire should be avoided due to much larger leakage capacitance compared to single strand wires, and in some cases it might be better to have larger winding losses and switch to enamel or similar windings, this also increases the thermal conductivity in the winding.
3. Another possibility is to wind the core with less tension on the wires making a louse winding which will decrease the leakage capacitance, and also increase the thermal conductivity.
4. [8] report that by inserting a air gap between the winding layers the self-capacitance was decreased 8 times this is a quite simple method to decrease the capacitance compared to the method in 1.
5. A newer and more complicated method of decreasing leakage capacitance is to create negative capacitances which are connected to the core which will deliver a negative charge cancelling the injected charge [7] but this depends allot on the circuit topology.
6. Ring cores indirectly leads to larger leakage capacitances due to the inner radius being smaller than the outer, so in a multilayer design if there is two layers on the outer radius it might be 4 on the inner increasing the layer to layer leakage capacitance.

**Leakage capacitance Measurements**

Three C058583A2 cores were wound with different winding methods and measured see section 10.5 and 11.3 for more details and other measurements on leakage capacitance. Strategy one (Figure 6-11) and four (Figure 6-12) was tested and compared to a baseline (Figure 6-10).

**Normal winding**

A core with 50 turns of 120 0.1mm Litz wire was wound on a C058583A2 core to get a basic idea about the leakage capacitance in inductor cores. The impedance plot can be seen in Figure 6-10 and the measured values in Table 6-4. The secondary peak is likely caused by the inductor to earth capacitance.

Table 6-4 Measured values for a normal winding

L [μH]	C [pF]	f <sub>0</sub> [kHz]
247.6	261.2	624.9

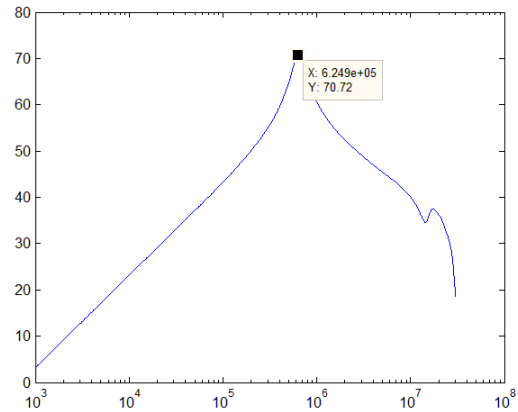


Figure 6-10 Impedance versus frequency for a normally wound core

**Bank winding**

A bank winding was wound on a C058583A2 core this decreased the leakage capacitance by 43 % as can be seen in Table 6-5 and Figure 6-11. The secondary peak has also disappeared or been moved outside the scope of the measurement which was up to 30 MHz.

Table 6-5 Measured values for a Bank winding

L [μH]	C [pF]	f <sub>0</sub> [kHz]
304.4	150	742.6

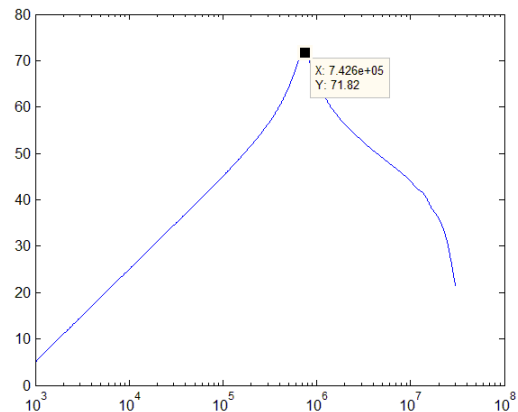


Figure 6-11 Impedance versus frequency for a bank winding

**Air gap between the layers**

A winding with an air gap of 3.4 mm between the layers was wound using a Scotch transparent tape. This resulted in a 38.3 % reduction in leakage capacitance. However due to the 3 mm of tape the inner radius became smaller leading to the windings in the outer layer being packed more together which likely raised the leakage inductance.

Table 6-6 Measured values an inductor with air gap between layers

L [μH]	C [pF]	f <sub>0</sub> [kHz]
254.2	161	785.7

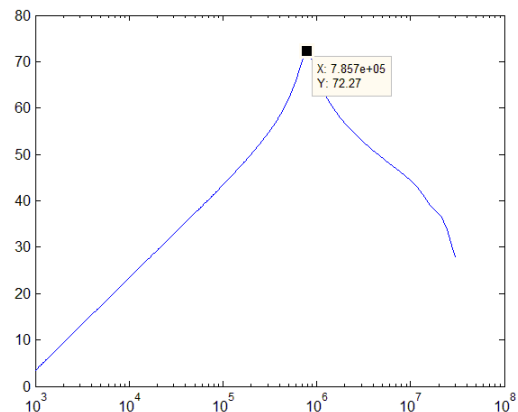


Figure 6-12 Impedance versus frequency for a winding with air gap between the layers

## 6.6 References

- [1] R. Lund Memo "Skin and proximity effect"
- [2] A. Bossche, V. Valchev Inductors and Transformers for Power Electronics 2005
- [3] <http://www.rubadue.com/>
- [4] Wojda, R. P.; Kazimierczuk, M.K., "Winding resistance of litz-wire and multi-strand inductors," *Power Electronics, IET* , vol.5, no.2, pp.257,268, Feb. 2012
- [5] Xi Nan; Sullivan, C.R., "Simplified high-accuracy calculation of eddy-current loss in round-wire windings," *Power Electronics Specialists Conference, 2004. PESC 04. 2004 IEEE 35th Annual* , vol.2, no., pp.873,879 Vol.2, 20-25 June 2004
- [6] Neugebauer, T.C.; Perreault, D.J., "Parasitic capacitance cancellation in filter inductors," *Power Electronics, IEEE Transactions on* , vol.21, no.1, pp.282,288, Jan. 2006
- [7] Hui-Fen Huang; Mao Ye; Shi-Yun Liu, "Equivalent parallel capacitance cancellation of integrated EMI filter using coupled components," *Electromagnetic Compatibility (APEMC), 2012 Asia-Pacific Symposium on* , vol., no., pp.133,136, 21-24 May 2012
- [8] Zdanowski, Mariusz; Rabkowski, J.; Kostov, K.; Peter-Nee, H., "The role of the parasitic capacitance of the inductor in boost converters with normally-on SiC JFETs," *Power Electronics and Motion Control Conference (IPEMC), 2012 7th International* , vol.3, no., pp.1842,1847, 2-5 June 2012

## 7 Thermal Aspects & Models

The losses generated by windings and core losses lead to a temperature increase, and the heat generated are transported to the surroundings by different heat transfer mechanisms: conduction, convection and radiation. Inside the component primary conduction and radiation transports the heat outward, while on the surface radiation and convection cools the core down. The convection can be forced or natural depending on the external cooling system.

The heat generation is according to [3] the main limitation in magnetic components experiencing a heating higher than  $100 \text{ mWcm}^{-3}$ . A high temperature leads to rapid deformation of the winding insulation, and can destroy the lamination in powder cores, or if the temperature is above the curie temperature melt the magnetic material. An accurate analytical model of the temperature rise leads to better optimization of the component. This chapter will cover the basics heat transfer models for magnetic components and create thermal model of toroid's.

### 7.1 Introduction

The theoretical thermal upper limit for magnetic components can be split into several factors:

- The internal temperature limit for the core is governed by hotspots in the magnetic material, which temperature needs to be limited to well below the curie temperature. Powder cores have a high curie temperature compared to ferrites, and in the latter case more attention need to be paid to this limit.
- Core coating and binding agents have a relatively low maximum operation temperature and in powder cores the epoxy coating is limited to  $200^\circ\text{C}$
- Adjacent components thermal limit.

The standard thermal class according to the IEC 317 for inductive modules is listed in Table 7-1 and represents the maximum temperature under rated load [7].

Table 7-1 Thermal classes for inductive modules

Thermal class	Maximum allowed temperature °C
Y	90
A	105
E	120
B	130
F	155
H	180
200	200
220	220
250	250

## 7.2 Thermal modeling

Thermal modeling is important to improve core loss calculations and avoid overheating of the component under operation. The two heat sources are core and winding losses, depending on the design the core losses might be more critical than winding losses. In a large winding design with several winding layers, the core losses are insulated far better from the surroundings than in a single layer design. Therefore a rule of thumb is that as the winding layers increase, the core losses have to decrease to stay below the temperature limit.

## 7.3 COMSOL model

A simple COMSOL model to simulate the heat transfer was created using the conjugate heat transfer module. The purpose of the model is to have a fast way to determine how accurate the results by the analytical program was in terms of heat transfer, and since COMSOL is widely recognized in the industry as an accurate tool for modeling different physic systems, with a finite element models. This should give a good comparison to the developed models.

### Basic model

The first model created was to determine how accurate the convective cooling and radiation equations that will be shown in the next chapters. The model consists of a toroid assumed to be lying flat with the properties of Table 7-2. Meshing and was done by the automatic physics controlled mesh see Figure 7-1, and a finer mesh did not improve the results meaning the model is mesh independent.

The conjugate heat transfer conditions applied was:

- External natural convection with vertical wall on the outer and inner surface.
- External natural convection with horizontal plate, Upside on the upper part.
- External natural convection with horizontal plate, downside on the lower part.
- Surface to ambient radiation on all surfaces.

Table 7-2 COMSOL Model inputs

Property	Value
Outer Diameter	51.7 mm
Inner Diameter	30.9 mm
Height	14.4 mm
Power generated	10 W
Material	Copper
Mesh	Normal

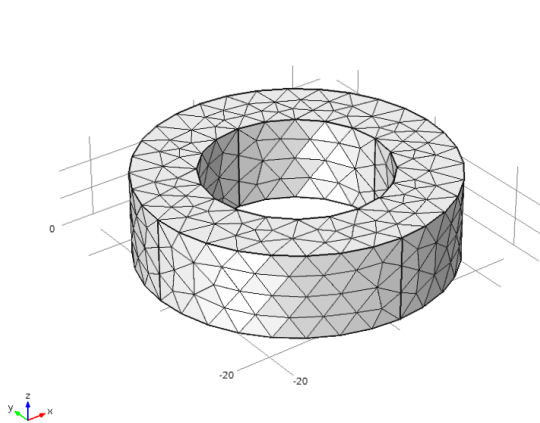


Figure 7-1 Toroid mesh

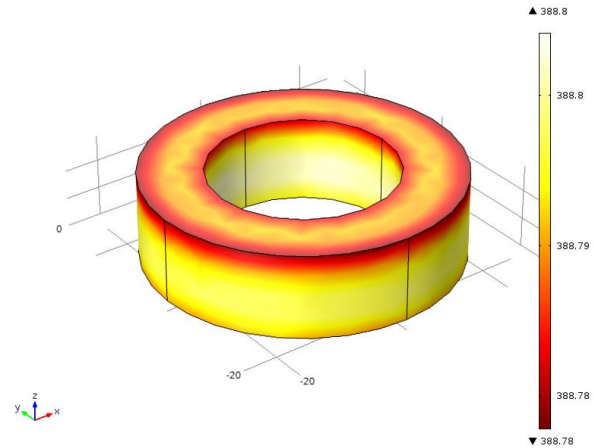


Figure 7-2 Simulation results.

## 7.4 Heat transfer by conduction

Conduction is the transfer of energy by interactions between atoms, and electrons which transfer kinetic energy among each other to obtain a steady state. This kind of heat transfer can be modeled by a temperature gradient  $\Delta T$  and the material property, thermal conductivity  $\lambda$  [1] see Equation 7-1.

$$\dot{q} = -\lambda_{th} \cdot \frac{\partial T}{\partial x} \quad \text{Equation 7-1}$$

$\dot{q}$  Heat flux  
 $\lambda_{th}$  Thermal conductivity

According to [5] conduction is independent of temperature for most materials. It is difficult to determine the thermal conductivity on interfaces between surfaces, which means experiments are necessary to find these values. The thermal conductivity of some materials likely to be found in magnetic components is listed in Table 7-3.

Table 7-3 Thermal conductivity for some materials [7]

Material	Temperature	Conductivity $\lambda$ [ $\text{Wm}^{-1}\text{°C}$ ]
Aluminum	(T = 100°C)	206
Ferrites (MnZn,NiZn)	(T = 100°C)	3.8
Copper	(T = 100°C)	379
Epoxy resin(unfilled)	(T = 100°C)	0.78
Epoxy resin(filled)	(T = 100°C)	0.25
Transformer oil	(T = 100°C)	0.12
Cardboard	(T = 100°C)	0.04
Water (T = 20°C)	(T = 20°C)	0.6
Air (T = 30°C)	(T = 30°C)	0.026
Air(T = 70°C)	(T = 70°C)	0.030
MPP, KoolM $\mu$ , High Flux, Xflux	-	8



## 7.5 Heat transfer by convection

Heat transport by convection refers to the superposition of conductive heat transport and energy transport due to macroscopic movements of the fluid [1]. The temperature profile out from a solid object and into a liquid will follow an exponential decreasing curve called the boundary layer see Figure 7-3 and Figure 7-4. The thickness of the boundary layer is approximately  $\lambda/\alpha$  where  $\alpha$  is the heat transfer coefficient which depends on the fluid, process and geometrical configuration. The heat flux can be calculated by Equation 7-2 [1]. In order to achieve high power density in the component active or forced cooling is preferred see the next section.

$$\dot{q} = \alpha_{th}(T_{th,s} - T_{th,\infty}) \quad \text{Equation 7-2}$$

$\alpha_{th}$  Mean convection heat transfer coefficient.  
 $T_{th,s}$  Surface temperature  
 $T_{th,\infty}$  Flow temperature

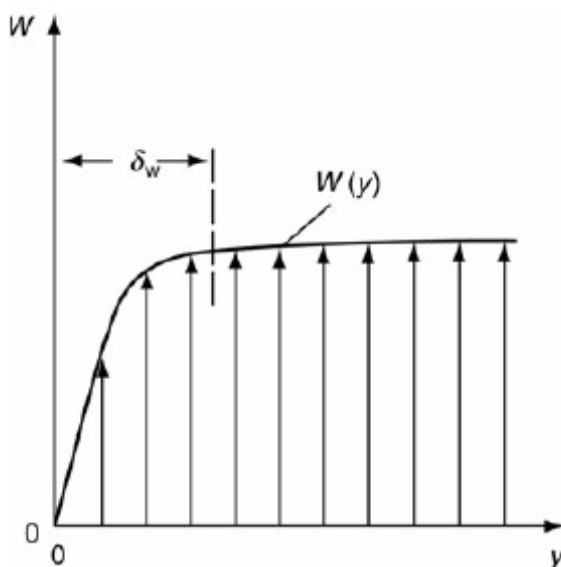


Figure 7-3 Boundary layer fluid velocity profile perpendicular to a wall

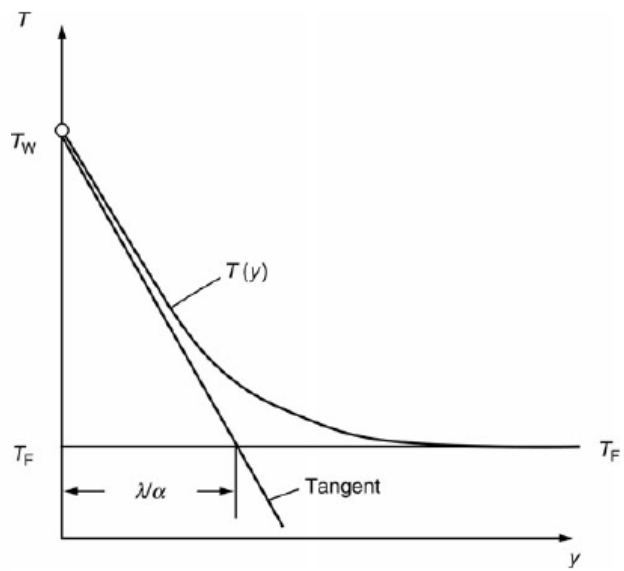


Figure 7-4 Boundary layer Temperature profile perpendicular to a wall

## 7.6 Natural convection and forced convection

A convection process which is not influenced by any outside factors are called natural convection, and only density gradients near the surfaces exchange heat, if an external factor like a fan or similar leads to a fluid flow it is called forced convection.

Forced convection reduces the surface to ambient resistance but do not affect the internal resistance on the other hand, increasing the forced convection to high values will create a high temperature gradient inside the component. This will lead to high thermal stress which could break ferrites and reduce the lifetime of insulation [7].

According to [9] the complicated flow separation process which happened along the boundary layer, it is impossible to analytically express the heat transfer coefficients for forced convection, but based on experimental data the flow across cylinders can be calculated by Equation 7-3.

$$\alpha_{th} = \frac{C\lambda}{d} \left( \frac{U_\infty d}{\nu} \right)^n P_{rf}^{\frac{1}{3}} \tag{Equation 7-3}$$

- $\alpha_{th}$  Mean convection heat transfer coefficient.
- $d$  Height of the magnetic component
- $\lambda$  Thermal conductivity
- $n, C$  Constants which depends on geometry found in [7]
- $U_\infty$  Velocity of the flow
- $\nu$  Kinematic viscosity
- $P_{rf}$  The prandtl number at the film temperature

**Main limitations**

- The constants n and C is only available for limited number of configurations
- Do not consider all temperature dependent effects

For forced convection in atmospheric pressure in air Equation 7-3 can be simplified to Equation 7-4 which is valid up to  $U_\infty = 12$  m/s [7] and it combines both forced and natural convection.

$$\alpha_{th} = (3.33 + 4.8U_\infty^{0.8})L_t^{-0.288} \tag{Equation 7-4}$$

$L_t$  Total distance of the boundary layer

The total distance of the boundary layer ( $L_t$ ) can be found by approximating the distance of the boundary layer see Figure 7-5.

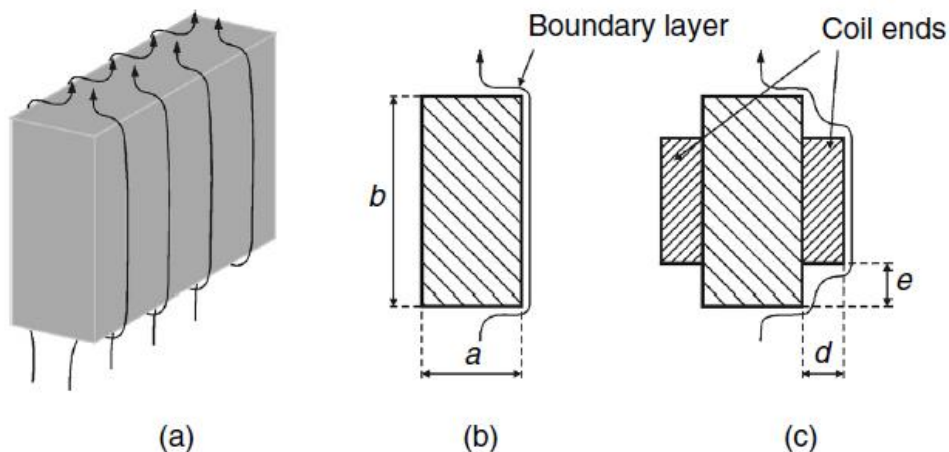


Figure 7-5 The total distance of the boundary layer  $L_t = a + b + 2(d^2 + e^2)^{0.5}$

Natural convection can be expressed by Equation 7-5 [7].

$$\alpha_{th} = C \left( \frac{P}{P_{ref}} \right)^{0.477} \left( \frac{T_a}{T_{a,ref}} \right)^{-0.218} \frac{\Delta T^{0.225}}{L^{0.285}} \quad \text{Equation 7-5}$$

### Main limitations

- The constants n and C is only available for limited number of configurations

The previous recommended models are not valid for temperatures above 400 K therefore a high temperature model needs to be developed from scratch. The basic equations will is described in the following equations see [1] for a more details.

The heat transfer models for natural convection that have been developed for circular toroid's are based on the general expression of convective heat transfer from isothermal three dimensional bodies see Equation 7-11.

$$v = \frac{\mu_{th}}{\rho_{th}} \quad \text{Equation 7-6}$$

$v$  Kinematic viscosity  
 $\rho_{th}$  Density of the cooling fluid  
 $\mu_{th}$  Dynamic viscosity

The prandtl number describes the ratio of momentum diffusivity to thermal diffusivity see Equation 7-7.

$$Pr = \frac{v \rho_{th} C_p}{\lambda} \quad \text{Equation 7-7}$$

$Pr$  Prandtl number  
 $v$  Kinematic viscosity  
 $C_p$  The constant pressure specific heat capacity  
 $\lambda$  Thermal conductivity of the fluid

$$\kappa = \frac{\lambda}{\rho_{th} C_p} \quad \text{Equation 7-8}$$

$\kappa$  The thermal diffusivity

### Natural Convection

Convection by natural sources can be described by the Grashof number Equation 7-9 which describes the ratio of internal driving force to a viscous force acting on the flow, this relationship is valid up to  $Gr = 10^9$  and the flow is turbulent for larger values.

$$Gr = \frac{L^3 g \beta_{th} \Delta T}{\nu^2} \quad \text{Equation 7-9}$$

$Gr$  Grashof number  
 $L$  The characteristic length  
 $g$  Gravity constant

$\beta_{th}$  The thermal volume expansion coefficient  
 $\Delta T$  Difference between wall and bulk fluid temperature

The Rayleigh number Equation 7-10 is a dimensionless number associated with the heat transfer within the fluid in natural convection.

$$Ra = GrPr \quad \text{Equation 7-10}$$

Ra Rayleigh number

### Natural Convection on Vertical Surfaces

The Nusselt number describes the improvement of heat transfer compared to a hypothetical static fluid. The Nusselt number can be found by Equation 7-11 and Equation 7-12.

Vertical cylinders natural convection:

$$Nu = \left( 0.825 + 0.387[Raf_1(pr)]^{\frac{1}{6}} \right)^2 \quad \text{Equation 7-11}$$

$f_1$  function  
 $Nu$  Nusselt number

$$f_1(Pr) = \left[ 1 + \left( \frac{0.492}{Pr} \right)^{\frac{9}{16}} \right]^{-\frac{16}{9}} \quad \text{Equation 7-12}$$

Horizontal cylinders natural convection:

$$Nu = \left( 0.6 + 0.387[Raf_2(pr)]^{\frac{1}{6}} \right)^2 \quad \text{Equation 7-13}$$

$$f_2(Pr) = \left[ 1 + \left( \frac{0.559}{Pr} \right)^{\frac{9}{16}} \right]^{-\frac{16}{9}} \quad \text{Equation 7-14}$$

$$\alpha_{th} = \frac{Nu\lambda}{L} \quad \text{Equation 7-15}$$

Examples of the expected thermal conductivity in smaller toroids can be seen in Table 7-4 it can be seen that the ambient temperature only has a minimal influence on the thermal conductivity, however it has a small negative influence. This is possible due to the density of the air is decreasing.

Table 7-4 Thermal conductivity examples

Core	$Ta = 25$ $P = 10W$	$Ta = 150$ $P = 10W$
C058583A2	$\alpha_v = 13.62$ $\alpha_h = 12.42$ $\Delta T = 86$	$\alpha_v = 13$ $\alpha_h = 11.72$ $\Delta T = 88$
C055089A2	$\alpha_v = 10.98$ $\alpha_h = 10.31$ $\Delta T = 91$	$\alpha_v = 10.23$ $\alpha_h = 9.54$ $\Delta T = 93$
0077715A7	$\alpha_v = 11.23$ $\alpha_h = 10.02$ $\Delta T = 86.92$	$\alpha_v = 10.47$ $\alpha_h = 9.2$ $\Delta T = 88$
Core	$Ta = 25$ $P = 3W$	$Ta = 150$ $P = 3W$
C058583A2	$\alpha_v = 11.38$ $\alpha_h = 10.3$ $\Delta T = 51$	$\alpha_v = 10.84$ $\alpha_h = 9.73$ $\Delta T = 52$
C055089A2	$\alpha_v = 9.0$ $\alpha_h = 8.44$ $\Delta T = 33$	$\alpha_v = 8.45$ $\alpha_h = 7.85$ $\Delta T = 34$
0077715A7	$\alpha_v = 9.24$ $\alpha_h = 8.2$ $\Delta T = 31$	$\alpha_v = 8.69$ $\alpha_h = 7.57$ $\Delta T = 32.6$

### Forced Convection

Forced convection happens when there is an external source of fluid flow that can be described by Equation 7-17. This equation relates forced convection to Rayleigh number which is used instead of the Nusselt number in Equation 7-15. The characteristic length  $L$  is different than in natural convection since, this is the boundary the fluid moves along on its path around the component, and has to be calculated based on the actual fluid movement.

$$Re = \frac{wL}{\nu} \quad \text{Equation 7-16}$$

$Re$  Reynolds number  
 $w$  Fluid velocity

$$Ra = RePr \quad \text{Equation 7-17}$$

$Ra$  Rayleigh number

The previous equations require experimental data which have been found and are located in Table 7-5 for air and oil,  $T$  is evaluated at the point halfway between ambient and surface temperature.

Table 7-5 Thermal properties of Air and Oil [8]  $T$  in Celsius

Air	$\rho_{th}$	$1.225 \cdot 273 / (T + 258)$	$[Kg \cdot m^{-3}]$
	$\beta_{th}$	$1 / (T + 273)$	$[K^{-1}]$
	$\mu_{th}$	$16.8 \cdot 10^{-6} + 52 \cdot 10^{-9} \cdot T$	$[Kg \cdot m^{-1} \cdot s^{-1}]$
	$\lambda$	$0.0242 + 6.2 \cdot 10^{-5} \cdot T$	$[W \cdot m^{-1} \cdot K^{-1}]$
	$C_p$	1000	$[J \cdot kg^{-1} \cdot K^{-1}]$
Oil	$\rho_{th}$	$887 - 0.659 \cdot T$	$[Kg \cdot m^{-3}]$
	$\beta_{th}$	$8.6 \cdot 10^{-4}$	$[K^{-1}]$
	$\mu_{th}$	$0.13573 \cdot 10^{-5} \exp(2797.3 / (T + 273))$	$[Kg \cdot m^{-1} \cdot s^{-1}]$
	$\lambda$	$0.124 - 1.525 \cdot 10^{-4} \cdot T$	$[W \cdot m^{-1} \cdot K^{-1}]$
	$C_p$	$1960 + 4.005 \cdot T$	$[J \cdot kg^{-1} \cdot K^{-1}]$

## 7.7 Heat transfer by radiation

The energy transmitted to the surroundings by electromagnetic waves is called radiation, and is both small compared to other mechanisms and demanding to model [5]. The heat transfer by radiation can be estimated by Stefan-Boltzmann's law see Equation 7-18 [4].  $P_{rad}$  is the radiated power,  $\epsilon$  is emissivity of the surface,  $T_s$  is the surface temperature,  $T_a$  the ambient temperature and  $A$  is the effective surface area.

$$P_{rad} = 5.7 \cdot 10^{-8} \cdot \epsilon \cdot A_{eff} (T_{th,s}^4 - T_{th,a}^4) \quad \text{Equation 7-18}$$

$\epsilon$  Emissivity  
 $A_{eff}$  Effective core area

The emissivity of some surfaces have been investigated and listed in Table 7-6 these values can be used to calculate the thermal dissipation from radiation. Using the value for ferrites the radiated power for some temperatures are given in Table 7-7., it can be seen that at the extreme case with the ambient temperature of 250°C and  $\Delta T$  of 100°C the power dissipation ability has increase nearly fivefold.

Table 7-6 Emissivity of some surfaces [7]

Material	Temperature	Emissivity [-]
Aluminium polished	(T = 100°C)	0.04
Ferrites	(T = 100°C)	0.95
Copper polished	(T = 100°C)	0.052
Isolation paper	(T = 100°C)	0.9
Enamel	(T = 100°C)	0.9
Enamel Copper	(T = 100°C)	0.9
Typical Transformer	Na	0.58 [9]

Table 7-7 Radiation at different temperatures

Case	$\epsilon$	$T_a$	$T_s$	$P_{rad}$	$R_\theta$
Close to normal temperature	0.9	293	393	845.6·A	0.118/ $A_{eff}$
Elevated temperature	0.9	418	518	2245.5·A	0.045/ $A_{eff}$
Extreme temperature	0.9	518	618	4000·A	0.025/ $A_{eff}$

The heat transfer from radiation depends on the surface area which is able to radiate energy away from the component. This means that the effective surface (enveloped surface) is smaller than the real surface area, the enveloped surface includes all vertical parts but in areas where the radiation from two surfaces will interact with each other the radiation will be lower than the sum of the surfaces and this can be approximated by the Pythagorean theorem.

The effective surface area for toroid's can be calculated with Equation 7-19 and Equation 7-20 [10]

$$F = \frac{H_w}{D_{iw}} \left( \left( \sqrt{\frac{H_w^2}{D_{iw}^2} + 1} \right) - \frac{H_w}{D_{iw}} \right) \quad \text{Equation 7-19}$$

$F$  View factor

$D_{ow}$	Core outer diameter including wire
$D_{iw}$	Core inner diameter including wire
$H_w$	Core height including wire

$$A_{eff} = 0.5\pi(D_{ow}^2 - D_{iw}^2) + \pi D_{ow}H_w + F\pi D_{iw}H_w \quad \text{Equation 7-20}$$

The equations describing the heat transfer from radiation is not easy to experimentally verify due to convective heat transfer, but a COMSOL model was created based on the KoolM $\mu$  sample described in Table 10-1 with 10 W of internal power generated and an emissive coefficient of 0.5 to compare the different ways to calculate the effective surface area. COMSOL do not use the effective surface area Equation 7-20. The deviation in surface area between the two formulas for the mentioned model is only 6.71 %.

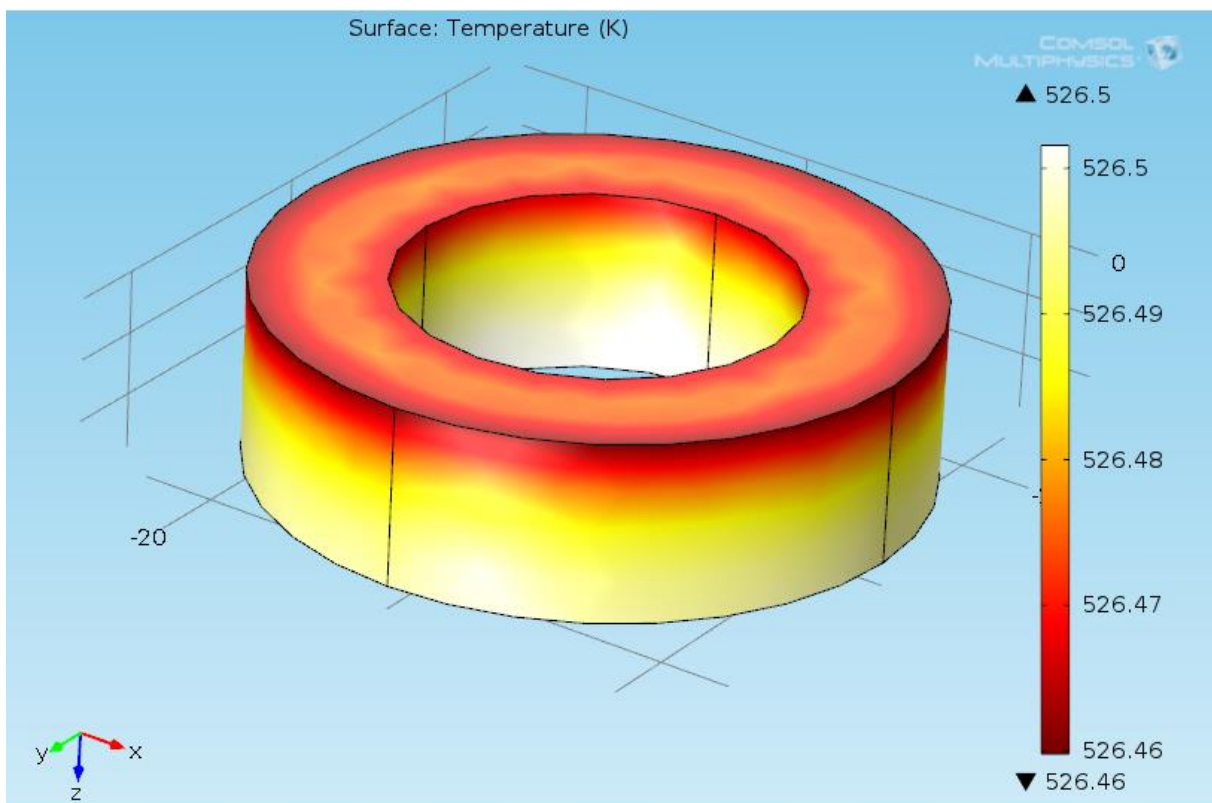


Figure 7-6 COMSOL model of a core including only radiation

## 7.8 Mounting

There are primarily 6 different ways a toroid core can be mounted to a PCB and located in space and this can have a lot to say for the cooling efficiency, however the cooling options might be limited due to space issues. The different options are:

- Vertical mounted core on a vertical PCB this option lets air pass through the component increasing cooling and more space

- Horizontal mounted core on a vertical PCB this do not let air pass through the core reducing the cooling efficiency, however a small air gap can be created between the PCB and core to increase the cooling.
- The two previous options under the PCB.
- The two first options just on a vertical PCB. It is likely that this have the overall best cooling efficiency.

Depending on previous described cases the characteristic length changes and have to be calculated for each case, and which surfaces that a vertical and horizontal changes which have to be taken into account in any model. In Figure 7-7 vertical and horizontal mounted cores are shown.

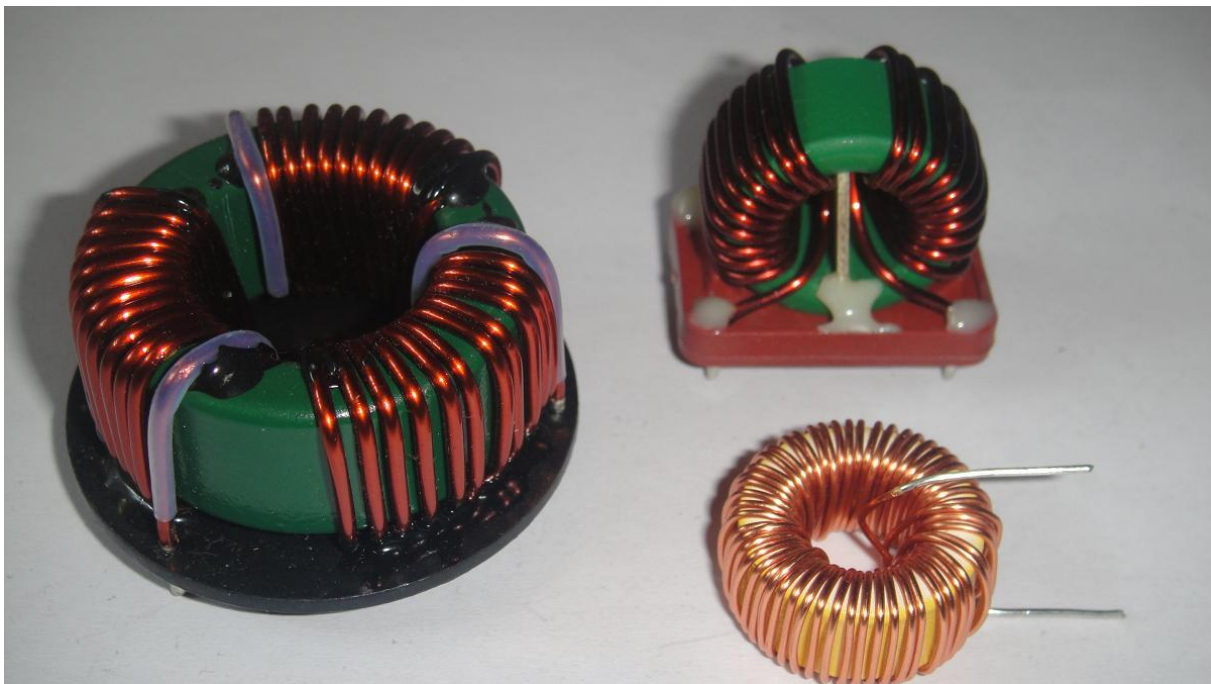


Figure 7-7 Horizontal and vertical mounted cores

## 7.9 Empirical thermal model

The temperature rise of an inductor core can be estimated by a best fit curve based on empirical data [6] which has been shown to have an error of less than five percent [2]. This approach is recommended from several magnetic core manufactures but do not take into account other cooling options than natural convection with air.

$$T_{increase} = \left( \frac{P}{10S} \right)^{0.833} \quad \text{Equation 7-21}$$

$P$  Power loss W  
 $S$  Surface area including the windings  $m^2$



### Main limitations

- Do not consider ambient temperature
- Do not consider forced convection or heat sinks
- Do not consider geometry or how the core is mounted
- Only available for air

## 7.10 Model comparison

The different thermal models have been compared to a COMSOL model of the same core in

Table 7-9. The model includes that all surface areas radiates energy, and natural convection is in effect. The model data can be seen in Table 7-8. The measured values were performed by driving a large 50 Hz current through a core with 16 turns of Litz wire. The COMSOL model do not take into account the increase of surface area due to the windings, while empirical model assumes that the whole surface area is covered which means that it would overestimate the temperature by a small bit, if the core was fully covered in turns. It can be observed that analytical model overestimates the temperature by a large factor and therefore the empirical model should be used. This problem was not discovered due to some parameters which was wrong leading to very good results in the tested cases. The problem is most likely related to the calculation of surface area since both the COMSOL model and analytical model have problems.

Table 7-8 COMSOL model data for C058583A2

Variable	Value	Unit	Description
Od	51.7	[mm]	Outer diameter
Id	30.9	[mm]	Inner diameter
Ht	14.4	[mm]	Height
$\epsilon$	0.58	[-]	Emissivity

Table 7-9 Comparison of temperature increase in C058583A2 for natural convection

Power [W]	COMSOL [°C]	Analytical [°C]	Empirical [°C]	Measured Values [°C]
10	95.65	98	42.83	56.7
3	36.10	22	15.71	21.3
1	14.41	17.3	6.29	9.6

A second sample was prepared with 106 turns of Litz wire on a C058583A2 to see how the models perform on a core with windings, it can be seen that the COMSOL model is do not manage to predict the losses accurate in the way it is designed. However as the temperature increases the analytical model outperforms the empirical model.

Table 7-10 C058583A2 including windings

Variable	Value	Unit	Description
Od	39	[mm]	Outer diameter
Id	11	[mm]	Inner diameter
Ht	16	[mm]	Height
$\epsilon$	0.58	[-]	Emissivity

Table 7-11 Temperature comparison in C058548A2 with 106 turns of 120 x 0.1 Litz wires with natural convection cooling

Power [W]	COMSOL [°C]	Analytical [°C]	Empirical [°C]	Measured Values [°C]
10	121	117	83.71	91
3	46.7	48	30.7	30
1	18	12.57	12.29	17.35

The 106 turns C058583A2 test was repeated at 100 °C ambient temperature, and the results can be seen in Table 7-12. However to keep a stable ambient temperature at 100 °C is complicated especially since forced convection is necessary to increase the temperature in the heating chamber, and very low accuracy in the measured values is to be expected. It can be seen that the core increases in temperature in comparison to the ambient for the COMSOL model this could be due to convective cooling is reduced at higher temperature, due to lower air density or other factors.

Table 7-12 Temperature comparison in C058548A2 with 106 turns of 120 x 0.1 Litz wires with natural convection cooling at 100 °C ambient temperature

Power [W]	COMSOL [°C]	Analytical [°C]	Empirical [°C]	Measured Values [°C]
10	197.04	164	183.71	157.87
10	197.04	164	183.71	148.5
3	156.18	139	130.7	112.5
3	156.18	139	130.7	117

### 7.11 Winding thermal resistance

The thermal resistance of a single layer winding is according to [11] in the range from 0.6 to 1.5 Wm<sup>-1</sup>K<sup>-1</sup> at a fill factor of 0.5. In a multilayer design like a Litz wire COMSOL modeling of the problem shows that the thermal conductivity for multilayer design is close to that of a single layer. By varying the copper area and insulation the thermal conductivity at different fill factors was obtained [11] see Figure 7-12.

This model do not consider the heat generation within the windings therefore the model in [11] was replicated in COMSOL with 50% of the heat loss in the windings and 50% in the core see Table 7-13. Rearranging Equation 7-1 yields Equation 7-22 to calculate the thermal conductivity.

$$\lambda = \frac{Pl}{\Delta Twd}$$

Equation 7-22

- l* Length from the heat source to the boundary
- w* Width of material
- d* Depth of material

Table 7-13 COMSOL model data for the windings

Variable	Value	Unit	Description
$\lambda_{cu}$	401	[Wm <sup>-1</sup> K <sup>-1</sup> ]	Thermal conduction in copper
$\lambda_{insulation}$	0.5	[Wm <sup>-1</sup> K <sup>-1</sup> ]	Thermal conduction in insulation
$\lambda_{air}$	0.03	[Wm <sup>-1</sup> K <sup>-1</sup> ]	Thermal conduction in air
$P_{core}$	5	[W]	Heat source in the core
$P_{Cu}$	5	[W]	Heat source distributed evenly in the layers
$d_{ins}$	2·10 <sup>-4</sup>	[m]	Insulation thickness
$A_{cu}$	2·10 <sup>-6</sup>	[m <sup>2</sup> ]	Copper wire cross section in each layer
Fill factor	0.5	[-]	

The Thermal conductivity in the cases where the losses in the windings equals those in the core increases  $\lambda$  to 0.76 Wm<sup>-1</sup>K<sup>-1</sup>. However with two layers  $\lambda$  decreases to 0.727, three layers 0.6816 and 10 layers 0.699 see Figure 7-8 - Figure 7-11. In practice it is nearly impossible especially in toroid's to have a perfect winding pattern so these values should be used as a maximum for the thermal coefficient. A simulation with-non ideal winding configuration can be seen in Figure 7-13 decreasing  $\lambda$  from 0.6816 to 0.273, somewhere between these values is the likely true heat conductivity for a three layer design.

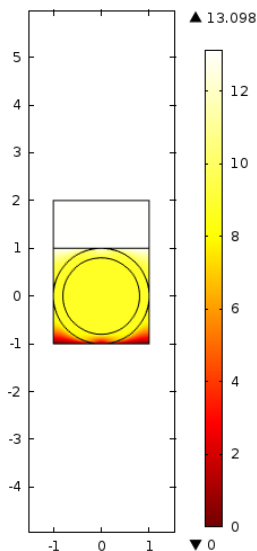


Figure 7-8 Heat conduction in a single layer

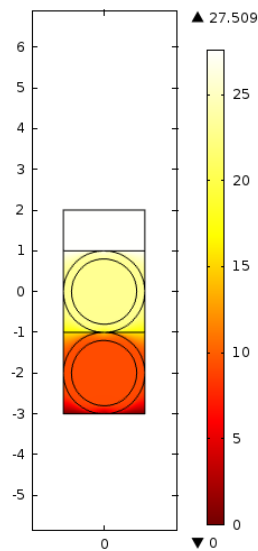


Figure 7-9 Heat Conduction in two layers

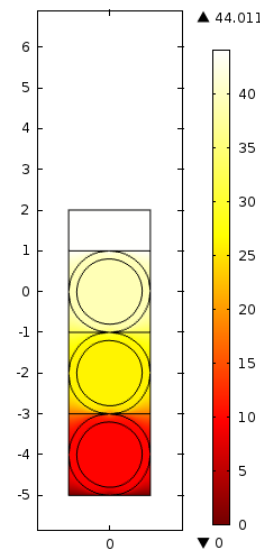


Figure 7-10 Heat conduction in three layers

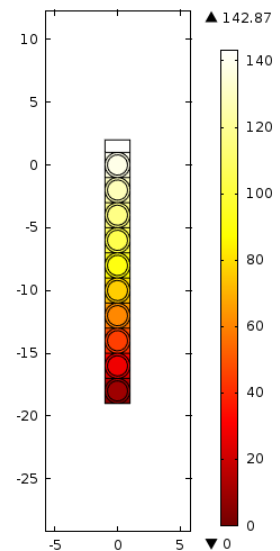


Figure 7-11 Heat conduction in ten layers

The fill factor in the winding section also affects the thermal conductivity and lower fill factor means that more of the winding area is isolation and air, this have been plotted in Figure 7-12 for a single layer.

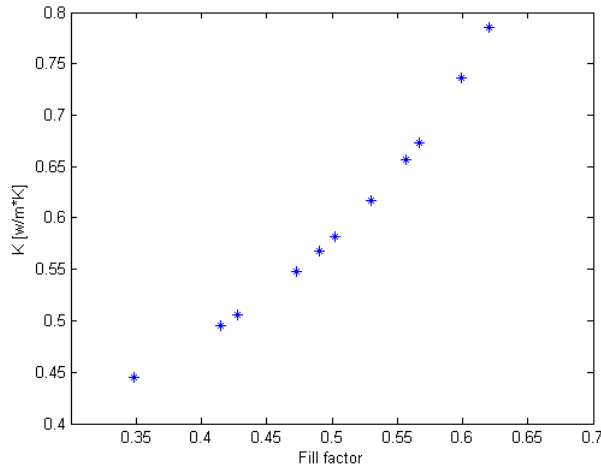


Figure 7-12 Thermal conductivity for different fill factors [11]

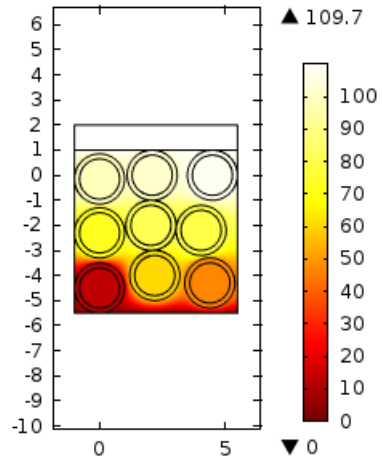


Figure 7-13 Heat conduction for non-ideal windings

In Table 7-15 values for the thermal conductivity in 9 different cases have been listed depending on where the loss is located and layers. These values will in the next chapter be used as a part of a thermal model of magnetic components.

Table 7-14 Thermal conductivity for different configurations with 50 % fill factor

Layers	Core loss 25%	Core loss 50%	Core loss 75%
1	0.91	0.76	0.65
2	0.9	0.75	0.64
3	0.82	0.681	0.58
10	0.84	0.7	0.6

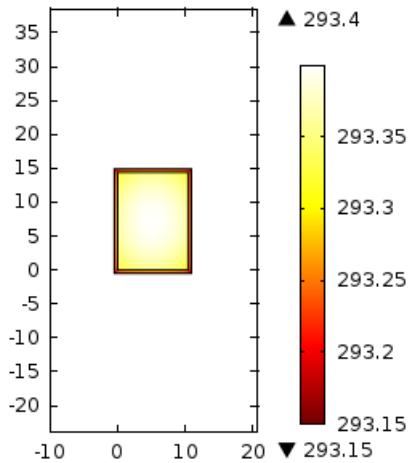
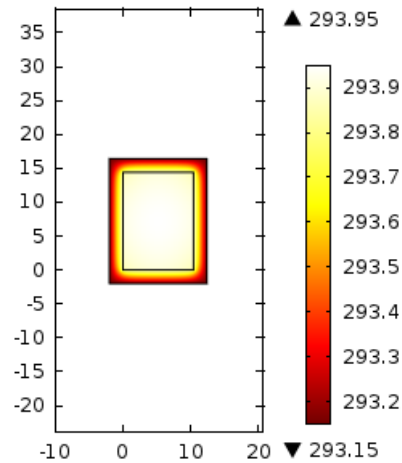
### 7.12 Core thermal resistance

The thermal conductivity of different magnetic materials is listed in Table 4-1 - Table 4-2 and can be used to calculate the thermal resistance of the core. For an uncoated core this resistance is close to zero and can be neglected, however in the case of powder cores, the epoxy coating have a much lower thermal conductivity. An approximate value for this can be found in Table 7-3 where epoxy resins have a thermal conductivity of  $0.25 \text{ K}\cdot\text{W}^{-1}$ . A simple Comsol model reveals that the core thermal resistance can still be neglected see Figure 7-14 and Figure 7-15.

The model was created by a 2D equivalent of the core with  $293.15^\circ\text{C}$  boundary condition on the outer surfaces, and a heat source covering the inner area see Table 7-15 for the other constraints.

Table 7-15 COMSOL model data for core thermal resistance

Variable	Value	Unit	Description
$O_d$	51.7	[mm]	Outer diameter
$I_d$	30.9	[mm]	Inner diameter
$H_t$	14.4	[mm]	Height
$\lambda_{core}$	8	$[\text{Wm}^{-1}\text{K}^{-1}]$	Thermal conduction in the core
$\lambda_{insulation}$	0.25	$[\text{Wm}^{-1}\text{K}^{-1}]$	Thermal conduction in epoxy
$P_{core}$	5	[W]	Heat source in the core
$d_{ins}$	0.5	[mm]	Insulation thickness

Figure 7-14 Heat conduction in the core with  $d_{ins} = 0.5$  mmFigure 7-15 Heat conduction in the core with  $d_{ins} = 2$  mm

### 7.13 Thermal model for toroid magnetic components

The temperature increase of an inductor can be modeled by an analytical model which depends on the actual configuration of the magnetic material. The designs which implanted into the magnetic design software are toroid cores and other cores with the windings fully exposed to the environment, in cores with very high fill factor this is not correct however the model will be developed for the general case. This lays the foundations for the model, and an equivalent circuit based analogy can be made further explained in literature [4].

The thermal resistance between the maximum core temperature and the ambient can in an inductor is split into these components:

**Core thermal resistance ( $R_{th,c}$ )** is the thermal resistance between the core and windings, it is hard to quantify due to that the thermal sources are evenly distributed through the magnetic material and therefore depends greatly on geometry [3] however as shown in section 7.12 this resistance is so low that it can be ignored for powder cores and ferrites due to the semi high thermal conductivity of the material.

**Winding thermal resistance ( $R_{th,w}$ )** is the thermal resistance from the core and to the surface of the windings. The heat generated by the windings is distributed from the core and to the surface inside each turn. Copper have a very low thermal resistance but due to the insulation  $R_{th,w}$  is much higher [3] see section 7.11.

**External forced convection resistance  $R_{th,forced}$**  this resistance describes the cooling from forced convection on the surfaces facing the cooling stream, see section 7.6 for further details.

**External natural convection for vertical surfaces resistance  $R_{th,cond,v}$**  describes the cooling by natural sources on vertical surfaces (section 7.6).

**External natural convection for horizontal surfaces resistance  $R_{th,cond,h}$**  describes the cooling by natural sources on horizontal surfaces.

**Sink or PCB resistance**  $R_{th,sink}$  describes the heat transfer to the board the core is mounted on or to other sources like a heat sink (section 7.6).

**Radiation resistance**  $R_{th,rad}$  describes the cooling done by radiation (section 7.7).

The complete equivalent circuit for a toroid can be seen in Figure 7-16  $P_c$  describes core losses and  $P_w$  the winding losses however since  $R_{th,c}$  is very low the winding and core losses can be put as a single source simplifying the model.

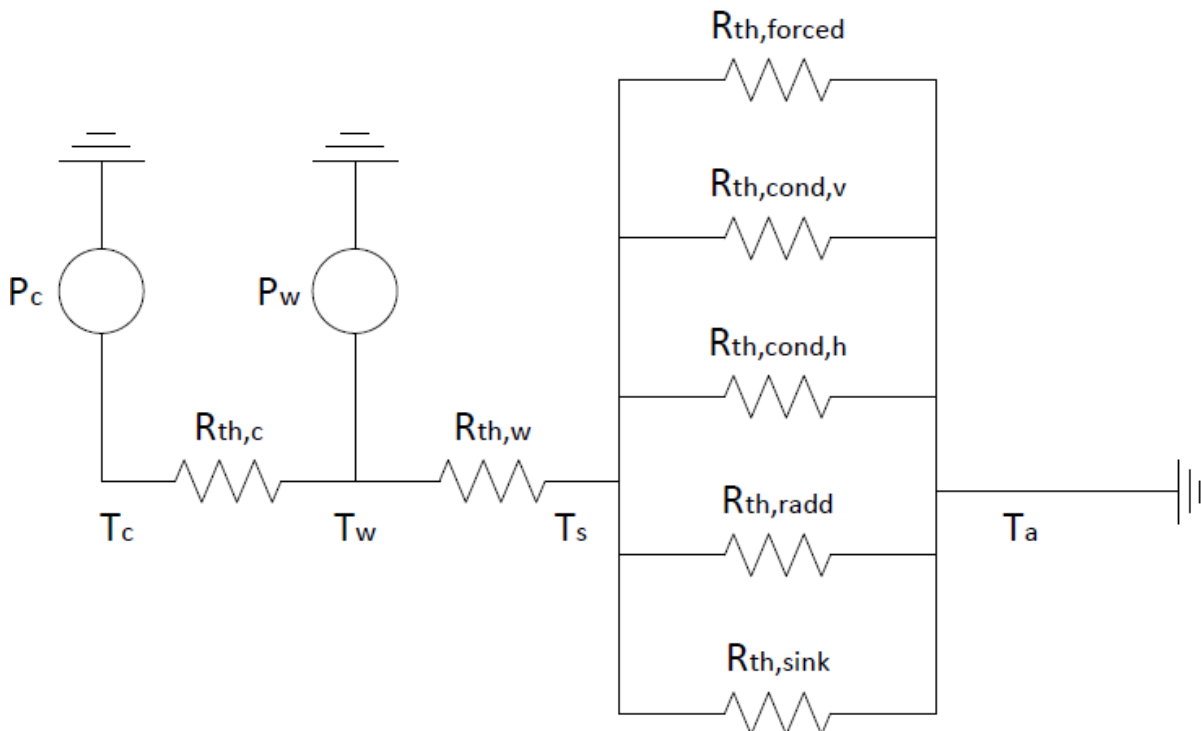


Figure 7-16 Equivalent thermal circuit

#### Assumptions for the model

- Toroid or similar shape
- The core is fully covered with windings
- The emissivity for the whole component is assumed to be 0.58 from Table 7-6
- The windings thickness increases twice as much on the inner diameter compared to the outer.
- Pressure is not taken into account

## 7.14 External thermal resistance

The external thermal resistance describes how easily the windings are cooled down.

### Natural Convection

The external thermal resistance for natural convection is described by Equation 7-23 and Equation 7-24 see Appendix G for the derivation.

$$R_{\theta,cond_h} = \frac{T_{th,s} - T_{th,a}}{\left(0.6 + 0.387 \left[ \frac{L^3 g \beta_{th} (T_{th,s} - T_{th,a}) Pr}{\nu^2} \left[ 1 + \left( \frac{0.559}{Pr} \right)^{\frac{9}{16}} \right]^{-\frac{16}{9}} \right)^{\frac{1}{6}} \right)^2 \frac{\lambda S_h (T_{th,s} - T_{th,a})}{L}} \quad \text{Equation 7-23}$$

$$R_{\theta,cond_v} = \frac{T_{th,s} - T_{th,a}}{\left(0.825 + 0.387 \left[ \frac{L^3 g \beta_{th} (T_{th,s} - T_{th,a}) Pr}{\nu^2} \left[ 1 + \left( \frac{0.492}{Pr} \right)^{\frac{9}{16}} \right]^{-\frac{16}{9}} \right)^{\frac{1}{6}} \right)^2 \frac{\lambda S_v (T_{th,s} - T_{th,a})}{L}} \quad \text{Equation 7-24}$$

### Radiation

$$R_{\theta,rad} = \frac{T_{th,s} - T_{th,a}}{5.7 \cdot 10^{-8} \cdot E \cdot A_{eff} (T_{th,s}^4 - T_{th,a}^4)} \quad \text{Equation 7-25}$$

Inserting Equation 7-19, Equation 7-20 into Equation 7-18 gives the total heat loss from radiation based on the dimensions of the core including the windings. However this results in a nonlinear equation and is best to be solved by a computer. See Appendix G for example of the basic calculation with some simplifications.

## 7.15 References

- [1] VDI Heat Atlas, Springer-Verlag Berlin 2010
- [2] Zientarski, J.R.R.; Pinheiro, J.R.; Hey, H.L.; Beltrame, R.C.; Candido, D.B.; , "A design methodology for boost inductor applied to PFC converters considering the core temperature rise and the conducted EMI noise," *Power Electronics and Applications, 2009. EPE '09. 13th European Conference on* , vol., no., pp.1-10, 8-10 Sept. 2009
- [3] Lloyd H. Dixon "Magnetic Design Handbook" Texas Instruments 2001
- [4] N. Mohan and T. M. Undeland, Power Electroncis Converters, Applications, and Design: John Wiley & sons, 2003.
- [5] Jonas Muhlethaler "Optimal Design of inductive components Based on Accurate Loss and Thermal Models" 2012
- [6] Magnetics® Technical Bulleting "Powder Core Catalog" 2011
- [7] A. Bossche, V. Valchev Inductors and Transformers for Power Electronics 2005
- [8] Villar, I.; Viscarret, U.; Etxeberria-Otadui, I.; Rufer, A.; , "Transient thermal model of a medium frequency power transformer," *Industrial Electronics, 2008. IECON 2008. 34th Annual Conference of IEEE* , vol., no., pp.1033-1038, 10-13 Nov. 2008
- [9] Coonrod, Neil R., "Transformer Computer Design Aid for Higher Frequency Switching Power Supplies," *Power Electronics, IEEE Transactions on* , vol.PE-1, no.4, pp.248,256, Oct. 1986
- [10] Refai-Ahmed, G.; Yovanovich, M.M.; Cooper, D., "Heat transfer modeling of toroidal inductors: Effect of orientations," *Thermal and Thermomechanical Phenomena in Electronic Systems, 1998. ITherm '98. The Sixth Intersociety Conference on* , vol., no., pp.417,423, 27-30 May 1998
- [11] T. Nilsen and R. Lund memo "Calculation of thermal conductivity in a Litz wire bunch with COMSOL multiphysics" 2006



## 8 Inductor Software

### 8.1 Short introduction

Designing inductors for 200°C applications requires design software, deep knowledge in the subject or it can be done with a tedious iterative process. No such software which can be customized for higher temperatures, new loss models or several cooling options was found. Therefore new software was developed from scratch with a modified approach magnetic approach aimed at powder cores [3] which is also close to the method described in [1] and was later extended to soft ferrite materials.

The main initial parameters are dc-bias, temperature, inductance, current, frequency, limits and how much of the current that are harmonics. The current up to the fundamental frequency is treated as dc and only the components at the switching frequency and upwards will be treated as ac. General guidelines says this is usually up to 10% [3]. The software optimizes the volume of the inductors with an iterative algorithm adjusting for temperature and permeability until an acceptable solution is obtained.

### 8.2 Limitations

The main goal of the program is to decrease the initial pool of core configurations and materials to a smaller amount that is possible to model more accurately with more advance software like COMSOL.

The software uses the analytical approach to magnetic design which means it is impossible to get completely accurate results however the aim of the software is to be in the close proximity of the real values in the range of 80 – 90 percent. The materials shipped from the manufactures have a permeability which is only within +/- 8 % of the real value meaning the software has some lower accuracy due to this.

#### Main Simplifications

- The program have a simplified air gap model which assumes that the leakage flux do not interact with the windings creating additionally losses. It also assumes perfect windings
- The temperature models are only checked up to 200°C for powder cores and 130°C for ferrites.
- The software does not consider real wire sizes, but uses optimal wire cross section.

See more in appendix B.

### 8.3 Input parameters

The graphical interface (GUI) shown in Figure 8-1 was made so that it is simple to design inductors and customize the input parameters. The software was primary created for ac inductors however at a later time modified to also be able to predict inductors for dc designs.

The screenshot shows the 'Inductor Calculator - [Preview]' window. It is divided into several sections for parameter input:

- Parameters:** Includes fields for Dc Bias (0 [A]), Ambient Temperature (50 [°C]), Temperature limit (210 [°C]), Peak Inductance (0.001431 [H]), Current Peak Value (5 [A]), Average output Current (4.71 [A]), Ripple current (10 [%]), Fundamental Frequency (50 [Hz]), Switching frequency (100000 [Hz]), Current Density (200 [A/cm<sup>2</sup>]), Maximum Fill Factor (0.7 [-]), Number of results (2 [-]), Minimum iterations (20 [-]), Number of stacked cores (1 [-]), Temperature deviation (0.01 [K]), Max winding layers (10 [-]), and a checked 'Core' option with value 0077715A7.
- Physical Dimensions:** Includes Maximum core height (0 [mm]), Maximum core diameter (0 [mm]), Maximum air gap (2 [mm]), Forced Convection (0 [m/s]), Heat Sink (0 [K/W]), and Thermal conductivity of the winding (0 [W/m<sup>2</sup>C]).
- Litz Wire:** Includes a checked 'Litz Wire' option, Number of strands in the bundle (120 [-]), Strand diameter (0.1 [mm]), and Bundle diameter (1.1 [mm]).
- Material:** Includes checked 'Powder Core' and unchecked 'Ferrites' options.
- Options:** Includes an unchecked 'Fast Thermal' option.

A 'Run' button is located at the bottom left of the parameter section.

Figure 8-1 GUI of the Inductor designer

**Input parameters:****1. Dc Bias**

Permeability has to be adjusted according to the magnetizing forces which mean value is raised by the product of dc current and windings.

**2. Ambient Temperature**

This parameter is to adjust for the temperature of the surroundings which is used in permeability calculations, thermal calculations and as a part of the temperature limit.

**3. Temperature limit**

Maximum temperature is the limiting value for core and winding losses and the inductor have to stay below this limit. This value depends on what materials that is used and the temperature limit of surrounding components. The included database has a temperature limit of 200 degrees, but due to the simplifications in the analytical models the maximum temperature should be used a guideline and not an absolute limit.

**4. Peak Inductance**

The inductance wanted at peak fundamental current adjusted for frequency, temperature, current peak and dc bias.

**5. Ripple peak value**

The ripple peak current value which is used in the loss calculations.

**6. Current Peak Value**

The output current peak value which is used in the peak permeability calculations for a high frequency filter with a fundamental current this would be the peak of the fundamental not including dc bias.

**7. Average output current**

The average output current which is used to determine the losses.

**8. Ripple Current**

The percent ripple experienced at the switching frequency, a good approximation is at around 10%, this is calculated from the current peak value.

**9. Fundamental Frequency**

This value should be set to the fundamental frequency of the load.

**10. Switching Frequency**

The high frequency losses are assumed to be around the switching frequency so this value should be set to the switching frequency of converter / inverter.

**11. Current Density**

The current density in the windings can be set with this option for a high frequency design this is often in the order of  $200 \text{ Acm}^{-2}$ .

**12. Maximum Fill Factor**

The maximum copper fill factor is the product of windings and cross section of each conductor divided by the window area. The recommended value is around 0.4 but in Litz wire designs or for other reasons the fill factor can be raised.

**13. Number Of Results**

The results are sorted based on minimum volume and this option makes it possible to obtain several different cores which satisfy the input parameters starting with the smallest core.

**14. Minimum Number of Iterations**

The minimum number of iterations is used to make sure that the design has actually reached convergence and not just found a minor stable area. This value should be kept above 20.

**15. Number Of Stacked Cores**

In some cases it would be beneficial to stack several cores on top of each other resulting in a smaller design this option give that possibility. All the relevant input core data is simply multiplied with this factor.

**16. Maximum Temperature Deviation**

The large number of temperature dependent variables can lead to long computing time however this option set how small the temperature deviation between iterations have to be before the result is considered correct, however putting a very low value can lead to the program getting stuck. To counter act this, a hard limit of 500 iterations was hardcoded which will result in the core being ignored.

### **17. Maximum Number Of Winding Layers**

Depending on how many turns the core needs to obtain the necessary inductance the software approximates how many turns can fit into each winding layer this option put a limit to how many layers there can be. The number of winding layers greatly affects the ac resistance see section 6.1 and parasitic capacitances see section 6.5.

### **18. Maximum core height**

In many designs the space is limited and this option will lead to all cores with a height larger than the input is ignored, however this only for the core material and with windings the inductor can become larger.

### **19. Maximum core diameter**

In many designs the space is limited and this option will lead to all cores with a diameter larger than the input is ignored, however this only for the core material and with windings the inductor can become larger.

### **20. Maximum air gap**

Ferrite materials needs an air gap store energy and to limit the flux however an increasing air gap leads to larger fringing flux which can induce currents in the windings or generate other problems. This option will set a limit to the length of the air gap.

### **21. Forced Convection**

Natural convection is assumed for the thermal calculations if this option is not checked, if a value is entered this will describe the mean flow over the component.

### **22. Heat Sink**

The unknown nature of the heat sink, pcb board or similar is impossible to predict generally therefore it is assumed that the thermal resistance to these elements are infinite however this option can be used to enter this resistance.

### **23. Thermal conductivity of the winding**

The winding configuration can be too complicated to calculate the conductivity accurate especially in the case of Litz wire. The software approximate this value based on the number of layers and fill factor if no value is given see section 7.11 for more information and values.

### **24. Litz wire**

In a high frequency design Litz wire may be necessary to reduce the winding losses see section 6.1 and 0. The initial program setup assumes normal windings so choosing this option leads the thermal calculations to use approximations to the heat transfer in Litz wire however the maximum fill factor has to be adjusted by the user. This option could also be used in cases where the wire size is known by setting strands to 1 and having strand diameter and bundle diameter equal to the wire size.

### **25. Number of strands in the bundle**

Litz wire is built up by smaller wires here called strands this number is used to determine wire losses by increasing the layer variable by the number of layers there would be in a bundle.

**26. Strand diameter**

The diameter of the strand is used to determine the  $x$  coefficient in section 6.1 which describes the radius to skin depth.

**27. Bundle diameter**

The diameter of the bundle is used to calculate different parameters which are affected by the size of the windings.

**28. Fast Thermal**

The thermal calculations use a nonlinear solver which in some cases can increase the computing time. Choosing this option leads to a faster thermal calculations based on section 7.9 and will not consider forced convection, temperature or any other thermal related inputs.

**29. Ferrite or Powder Cores**

The program and its databases are built up around ferrites and powder cores. This check box is used to either choose ferrite materials or powder cores. The option to run both in same run was not implanted.

**30. Core**

In the cases where it would be beneficial to do calculations on a specific core, the part number can be entered here.

**31. Run**

This runs the program based on the input and outputs possible core sizes and configurations in a excel file called Log.csv this file is located in the same folder as the software.

## 8.4 Output parameters

The results from running the program can be found in the files named Results\_Powder.txt or Results\_Ferrite.txt in the programs folder. The output information provided can be viewed in Table 8-1.

Table 8-1 Output Parameters

Parameter	Value	
<b>Core Data</b>	[-]	All information provided by the manufacturer is provided here.
<b>H</b>	[ATcm <sup>-1</sup> ]	Magnetizing field used to calculate permeability and inductance.
<b>Bpeak Ripple</b>	[T]	Peak value of the magnetic flux density.
<b>Al</b>	[nH·N <sup>-2</sup> ]	Core nominal inductance adjusted for temperature, dc-bias, and frequency.
<b>Turns</b>	[-]	Number of turns necessary to obtain required inductance.
<b>Wire D</b>	[m]	The diameter required of the wire.
<b>Copper loss</b>	[W]	Losses in the wire.
<b>Core Loss</b>	[W]	Losses in the magnetic material.
<b>Total Loss</b>	[W]	The losses including core and copper loss
<b>Loss per volume</b>	[mWcm <sup>-3</sup> ]	The loss per volume in cases where this is above 100 mW cm <sup>-3</sup> the design is likely loss limited.
<b>Core Temperature</b>	[°C]	The surface temperature of the core due to losses.
<b>Temperature</b>	[°C]	The total temperature of the core in Celsius.
<b>Wire-Area</b>	[m <sup>2</sup> ]	Copper area in each wire.
<b>Current Density</b>	[Acm <sup>-2</sup> ]	Current density provided by the input parameters.
<b>Core</b>	[-]	The power loss per unit volume.
<b>My Correction</b>	[-]	The roll off in permeability.
<b>Fill factor</b>	[-]	How much of the cross section of the core is filled with wires.
<b>Peak L</b>	[H]	The calculated inductance on the peak value of the fundamental waveform.
<b>Average L</b>	[H]	The calculated inductance at zero crossing for the fundamental waveform.
<b>Volume</b>	[mm <sup>-3</sup> ]	The volume of the core.
<b>Inverter Frequency</b>	[kHz]	The switching frequency.
<b>Surface</b>	[m <sup>2</sup> ]	The surface area of the component used to calculate the temperature gain.
<b>Winding Layers</b>	[-]	The calculated number of layers in the design
<b>Al from leakage</b>	[nHN <sup>-2</sup> ]	Primary the added nominal inductance from leakage fields.
<b>Gap length</b>	[cm]	In ferrite designs this describes the length of the gap.
<b>Fr ripple</b>	[-]	This is the dowel factor $R_{ac}/R_{dc}$
<b>Winding length</b>	[m]	The analytical length of the wire

## 8.5 Experimental results

The software described in the previous sections was used to create 4 different samples where the Temperature, permeability, turns, fill factor, and loss was compared to the analytical values see chapter 10 for the lab setup and 11.2.1 for the results. Generally it was a good correlation between the analytical values and the measured except for temperature.

## 8.6 References

- [1] Lloyd H. Dixon "Magnetic Design Handbook" Texas Instruments 2001
- [2] Magnetics® Technical Bulletin "Powder Core Catalog" 2011
- [3] Dr. Richard Lund SmartMotor email correspondence 31.09.2012

## 9 Filter Dimensions

The most common way to control a switch mode power supply is with pulse width modulation where constant switching frequency is used, output voltage is controlled by adjusting the duty cycle. The resulting output waveform need to be filtered so that components are put under lower stress.

### 9.1 Filter for a Buck converter

The output voltage straight out from a buck converter Figure 9-1 have large dv/dt effects and at times the instantaneous voltage will either be zero or as much as the input side, by using elements which stores energy like inductors and capacitors the waveform will smoothen out. In the periods where the switch is on the inductive elements charges due to a positive voltage, while in the off periods the inductive element releases its energy while they discharges see Figure 9-2[1].

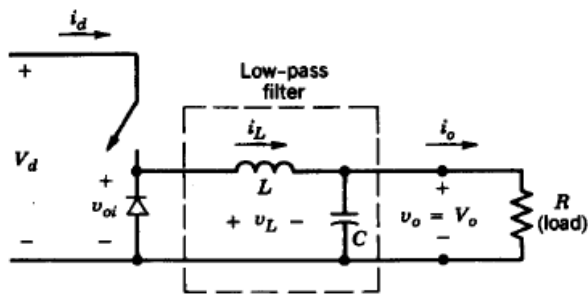


Figure 9-1 Buck converter [1]

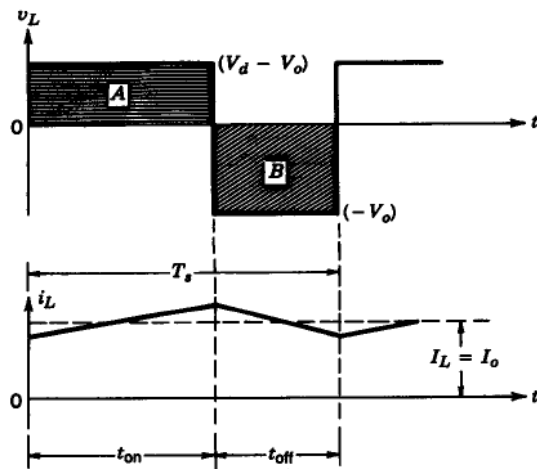


Figure 9-2 Buck converter in continues mode [1]

The buck converter can operate in continues mode which means that over a period not all the energy from the inductive element is released leading to a waveform as show in Figure 9-2 or discontinues mode which means that all the energy is discharged in the off period, and there will be some time where the voltage in the circuit will be zero. The ripple in continues mode is reduced by larger inductive elements or by using higher frequency, the voltage ripple is not improved directly by the inductive elements but by capacitive.

The most basic equation for an inductor Equation 9-1 can be rearranged into Equation 9-2, which can be used inductance for a maximum ripple current.

$$V_o = L \frac{dI_L}{dt} \tag{Equation 9-1}$$

- L Inductance
- V<sub>o</sub> Output voltage
- ΔI<sub>L</sub> Current ripple

$$L = \frac{V_o t_{off}}{\Delta I_L} \tag{Equation 9-2}$$

- t<sub>off</sub> Time period the switch is off



Assuming that the ripple component of  $I_l$  flows in to the capacitor C. The capacitor delivers charge when the ripple current is below average and the necessary capacitance can be calculated by Equation 9-3 [2].

$$C = \frac{T_s^2(1-D)V_o}{8L\Delta V_o} \quad \text{Equation 9-3}$$

$T_s$       Switching period  
C          Capacitance

The filter capacitor will also lead to a voltage drop across the equivalent series resistor (ESR) and therefore the ESR should be kept low [2]. The buck converter will be used to determine the accuracy of the inductor software and in Table 9-1 filter specifications for some cases can be viewed see more information in Appendix D section V where the filters are calculated, designed with the inductor software and tested.

Table 9-1 Buck filter specifications

Buck filter specification						
$V_o$ [V]	F [kHz]	D	$\Delta I_l$ [A]	$\Delta V_o$ [V]	L [mH]	C [ $\mu$ F]
30	10	0.5	1.2	0.4545	1.25	33
100	10	0.5	4	1.5152	1.25	33
30	10	0.5	0.6	0.2273	2.5	33
100	10	0.5	2	0.7576	2.5	33
30	10	0.5	0.4286	0.1623	3.5	33
100	10	0.5	1.428	0.54	3.5	33
30	5	0.5	0.66	0.5	4.5	33
100	5	0.5	2.22	1.68	4.5	33

## 9.2 Sinus and dv/dt Filter

A sinus and dv/dt filter will be calculated for a SiC inverter based on the case information given in the introduction repeated in Table 9-2. It is assumed the inverter uses PWM switching technique with maximum modulation index of one.

Table 9-2 Drive specification

Drive Specification	
$V_{dc}$	600 V
$S$	3000 Va
$f_{sw}$	Up to 100 kHz
$T_{amb}$	150 °C
$\frac{dv}{dt} \max$	1 kV/ $\mu$ s
Where	$V_{dc}$ is the Dc-link voltage $S$ is the apparant power delivered $f_{sw}$ is the switching frequency $T_{amb}$ is the downhole ambient temperature

The maximum line to line voltage can be found using Equation 9-4,  $m_a$  is the modulation index which in this case will be set to 1, the worst case scenario before going into over modulation.

$$V_{ll,rms} = 0.612m_aV_d \quad \text{Equation 9-4}$$

### 9.2.1 RLC Dv/dt Filter

A dv/dt filter for silicon carbide drives need to limit the dv/dt to minimum 1 kV/ $\mu$ s, how this is done is closer explained in chapter 3. A simulation model of the circuit was developed in section 3.6 and the filter values was calculated based on the equations in Table 3-3.

Table 9-3 Dv/dt filter values

Parameter	Value
Phase Voltage	$V_{ll,rms}$ 367.2 V
Phase Current	$I_{rms}$ 4.71 A
Resonance frequency	$f_0$ 377 658
Filter inductance	$L_f$ 15.9 $\mu$ H
Filter capacitance	$C_f$ 201 nF
Filter resistance	$R_f$ 35.58 $\Omega$

The filter parameters was simulated with the RLC PSCAD model due to limitations with software only a single 1 meter section of the cable could be simulated. see Figure 9-3 to Figure 9-7 for the circuit topology and the waveforms recorded before and after the filter. From the simulation results the three phase sinus filter improves the voltage and current waveform and keep the rise time in the order of around 2  $\mu$ s. The effect of leakage capacitance have not been included however this will lead to more oscilations in the circuit.

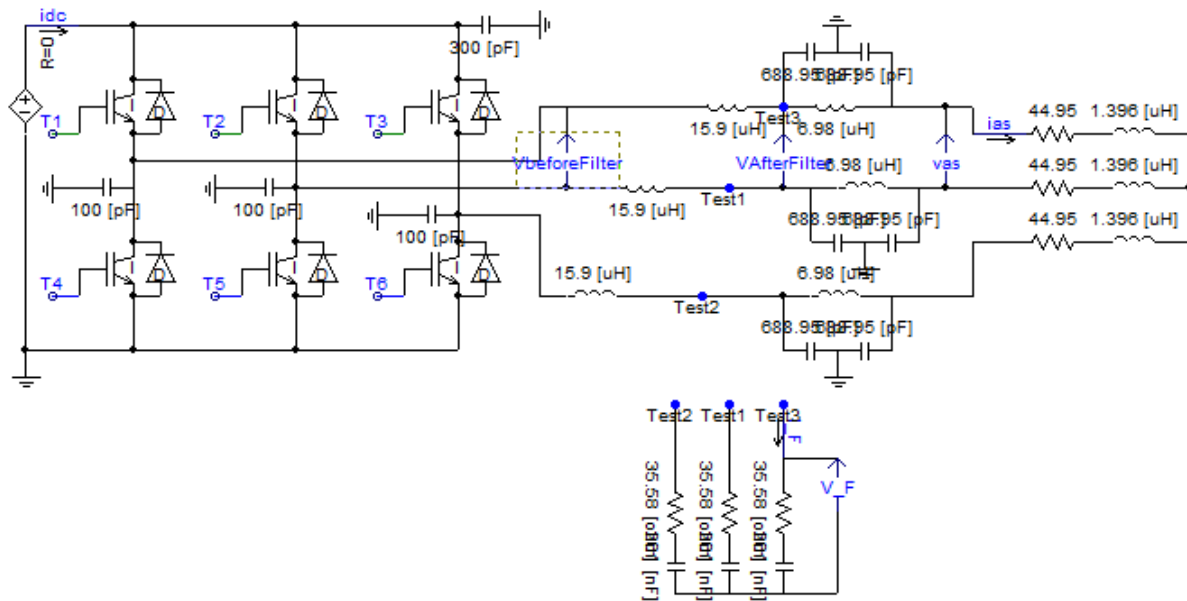


Figure 9-3 Circuit topology of the RLC filter model

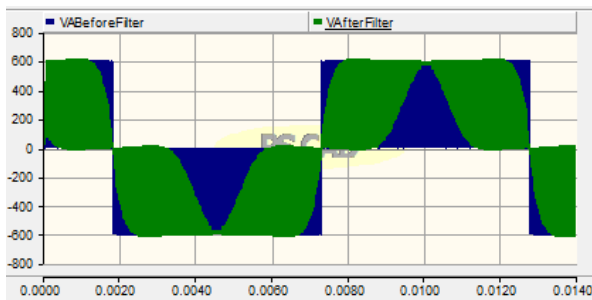


Figure 9-4 The voltage waveform before and after the filter

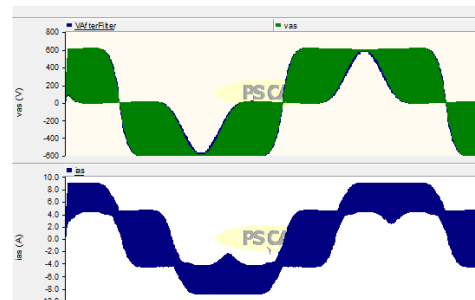


Figure 9-5 The voltage and current waveform before the load

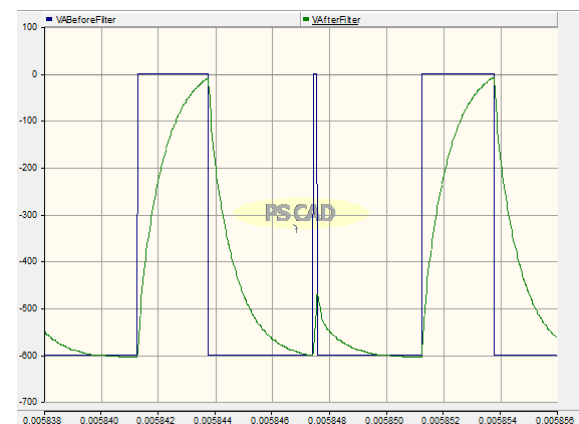


Figure 9-6 Zoomed in view of the voltage before and after the filter

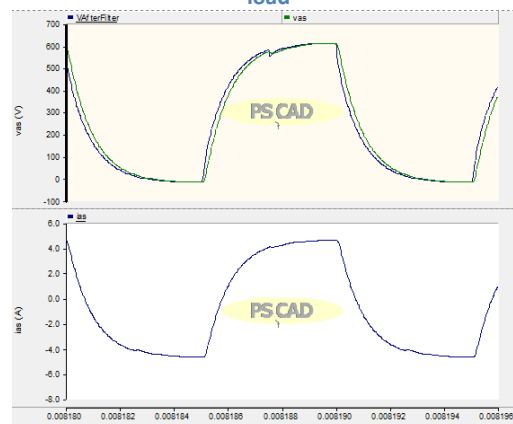


Figure 9-7 Zoomed in view of the voltage and current at the load

### 9.2.2 Sinus Filter

The purpose of a sinus filter is to create a nearly sinusoidal output waveform from the filter. The calculations are performed in the appendix D sections VII, and the results for the sinus filter are summarized in Table 9-4. The design process follows the equations in chapter 2 and using the recommended starting value for  $L_f$  at 1% Pu with a switching frequency at 100 k[Hz]. The dampening factor was set at 2.

Table 9-4 Sinus filter values

	Parameter	Value
Phase Voltage	$V_{ll,rms}$	367.2 V
Phase Current	$I_{rms}$	4.71 A
Base impedance	$Z_{Base}$	44.95 $\Omega$
Base inductance	$L_{base}$	0.143 H
Resonance frequency	$f_0$	33 333
Filter inductance	$L_f$	1.43 mH
Filter capacitance	$C_f$	15,9 nF

The filter parameters was simulated using the pscad model, however due to limitations with software only a single 1 meter section of the cable could be simulated. From the simulation results the three phase sinus filter improves the voltage and current waveform to nearly sinusoidal.

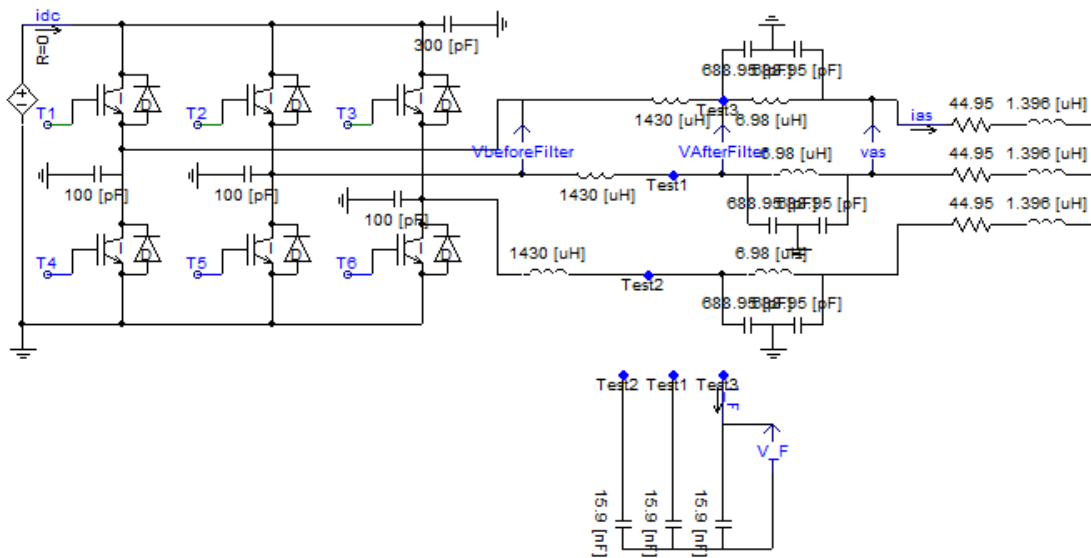


Figure 9-8 Circuit topology of the Sinus filter model

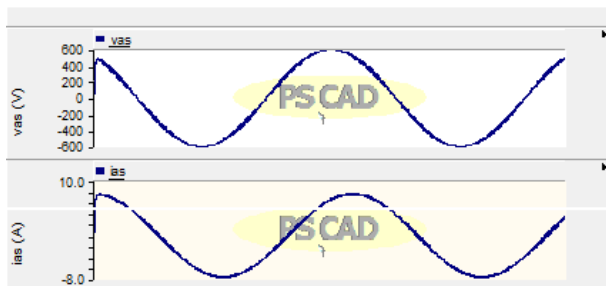


Figure 9-9 The voltage at the load and current

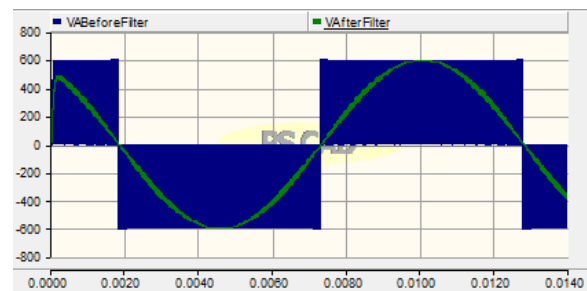


Figure 9-10 Filtered and unfiltered line to line voltage

### 9.3 Filter comparison

The RLC and Sinus filter, both improves the waveforms so this section will compare the size of the two filters. The inductors were designed by the software in chapter 8 with the input parameters that can be viewed in Table 9-5. The smallest volume inductor which can be used are shown in Table 9-6 however this do not include any volume increase due to the windings.

The temperature factor was disregarded due to the cores being so small that it is likely the temperature models do not model them correctly and the software have not been verified on so small cores. However if the component do keep this high temperature it can be solved by using a heat sink or removing heat by the pcb board.

It can be seen that the RLC filter inductor can be made very small compared to the sinus filter, this is both due to a much smaller inductance and smaller reduction in permeability due the few turns which is necessary. The Sinus filter inductor will also have a much larger volume due to the windings. Parallel connection and stacking several cores on top of each other were considered but did not lead to a smaller design.

Table 9-5 Input parameters

	Inductor 1	Inductor 2
Dc Bias	0 A	0 A
Ambient temp.	25°C	25°C
Peak inductance	1.43 mH	15.9 μH
Current Peak	6.66 A	6.66A
Average output Current	4.71 A	4.71 A
Ripple current	10 %	10 %
Fundamental frequency	1	1
Switching frequency	100 000 Hz	100 000 Hz
Current Density	200	200
Number of strands in bundle	120	120
Strand diameter	0.1 mm	0.1 mm
Bundle diameter	1.55 mm	1.55 mm

Table 9-6 Software recommendations

Inductor 1	Analytical prediction		Inductor 2	Analytical prediction	
Core Data	C055306A2		Core Data	C058128A2	
Linital	7.21	mH	Linital	2.37	μH
Lpeak	1.44	mH	Lpeak	1.62	μH
Turns	133	-	Turns	17	-
Copper loss	0.07	W	Copperloss	0.0027	W
CoreLoss	11.28	W	CoreLoss	0.103	W
Total Loss	11.35	W	Total Loss	0.106	W
Temperature	152	°C	Temperature	33.94	°C
MyCorrection	0.205	-	MyCorrection	0.68	-
Fill factor	0.82	-	Fill factor	0.54	-
Volume	1800	mm <sup>3</sup>	Volume	244	mm <sup>3</sup>

## 9.4 References

- [1] N. Mohan and T. M. Undeland, Power Electronics Converters, Applications, and Design: John Wiley & sons, 2003.
- [2] Øyvind Holm Sneffjellå, "Silicon Carbide Technologies for High Temperature Motor Drives", Master thesis, June 2011.

## 10 Laboratory Setup

This chapter describes how the laboratory setups were done, what equipment that has been used and some initial measurements and comparisons.

There were four different setups:

- Core characterization with a BROCHAUS MPG 100D steel tester. The measurements which was performed was core loss in powder and ferrite cores, in the frequency range from 5 kHz to 10 kHz at 20°C, 108°C, and 180.5°C.
- Core loss with a waveform generator and an amplifier at 5 kHz, 20 kHz 50 kHz and 100 kHz, at 20°C and 180°C.
- Inductor characterization with a buck converter.
- Impedance measurements with a network analyzer.

### 10.1 Samples

The magnetic material which was possible to acquire for the tests, and that can be used in high temperature designs are listed in Table 10-1. These include four different powder cores and two ferrites, everything is from Magnetics® except the N27 which is produced by Siemens.

Table 10-1 Core materials

	$\mu$	B [T]	Al [nH/N <sup>2</sup> ]	Ve [mm <sup>3</sup> ]	Ae [mm <sup>2</sup> ]	le [mm]	H [mm]	Material
<b>C058583A2</b>	160	1.5	101	4150	46.4	89.5	9.78	High Flux
<b>C058548A2</b>	125	1.5	127	5340	65.6	81.4	11.5	High Flux
<b>C055089A2</b>	125	0.75	178	15600	134	116	16.1	MPP
<b>0077715A7</b>	125	1.05	152	15900	125	127	14.4	KoolM $\mu$
<b>ZR44916TC</b>	2300	0.47	2710	15010	118	127	15.9	R
<b>N27</b>	2000	0.5	5100	166250	625	308	25	N27

### 10.2 Core loss characterization

The analytical data on core parameters are usually only available for a limited temperature ranges, and is also not necessary accurate, therefore core loss characterization was performed, at three different temperatures 20°C, 108°C and 180.5°C.

#### 10.2.1 Measurement setup BROCHAUS MPG

The core characterization was performed with a BROCHAUS MPG 100D which is used to define the magnetic qualities of electric sheets, and other magnetic materials. The rated measurement range is from 3 Hz to 10 kHz [2] for toroid geometries with an inner diameter larger than 26 mm [2]. U core geometries are not directly supported but can be transformed into an equivalent toroid core [3].

The measurements are performed electrically by a primary winding which creates a magnetic field based on the input parameters. Voltage is measured over a precision resistor (shunt) in the secondary winding which is unaffected by temperature and induced fields. Two separate systems measure the values of B and H simultaneous avoiding errors due to phase differences [2], however during the characterization of powder cores it was discovered that phase problems still might apply

for long wires or different lengths of the primary and secondary winding. A flow chart over the system can be seen in Figure 10-1.

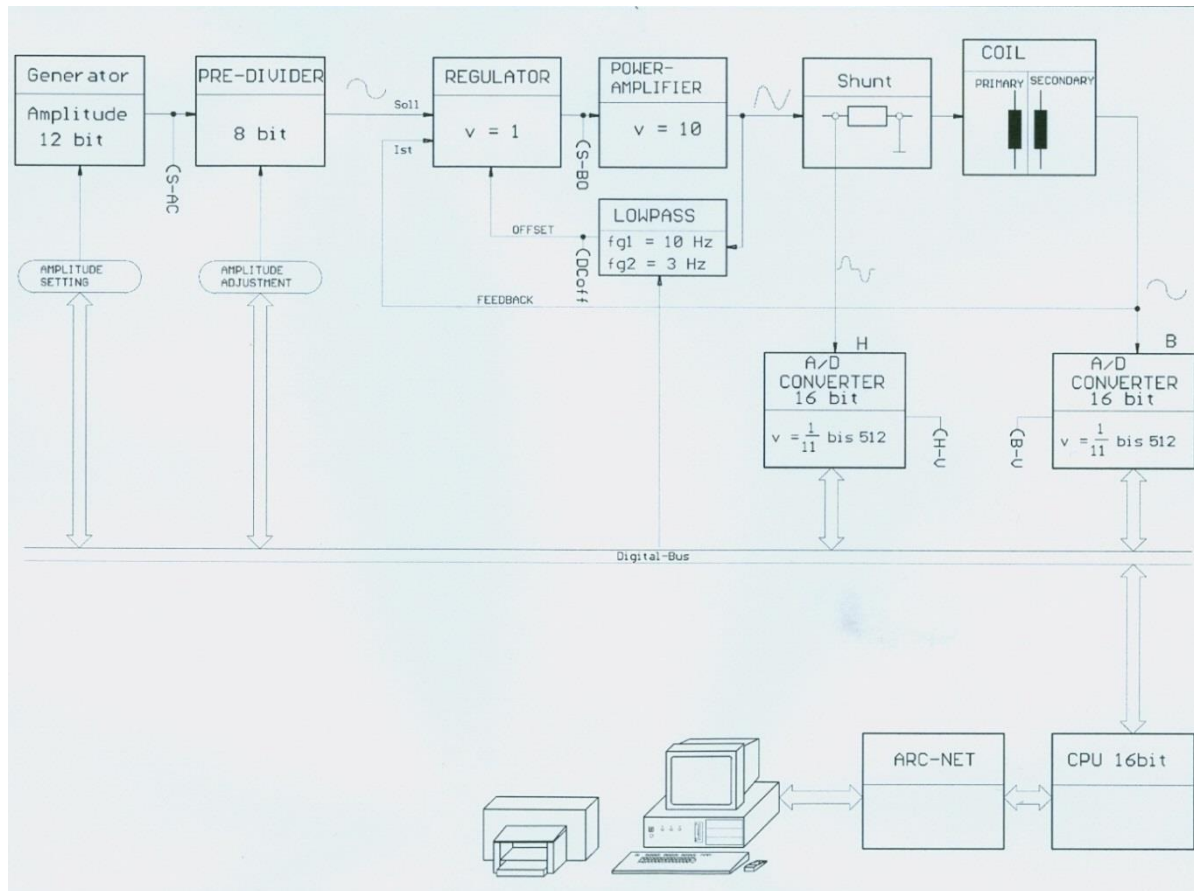


Figure 10-1 Control principle for electric sheet measuring instrument [2]

The high temperature measurements were performed by increasing the ambient temperature to the desired value with a heating chamber see Figure 10-2. It was assumed that the low losses induced in the materials from the measurements would not significantly alter the core temperature, and the heating chamber was set at forced convection meaning that if the core should increase in temperature, it would be rapidly cooled down. The samples were heated up to the required temperature for a minimum of four hours before the measurements began, which for materials with thermal conductivity of 8 (see Table 4-2) is more than enough to get a uniform temperature in the material. The secondary and primary winding was connected to BROCHAUS MPG by having 30 cm long wires going out of the heating chamber and into, the plugin system see Figure 10-3. The equipment that was used can be viewed in Table 10-2.

Table 10-2 Lab equipment

Application	Equipment	Product number
Temperature measurements	Temp. measurer	FLUKE 51:2
Adjusting the ambient temperature	Heating chamber	TERMAKS TS 8056



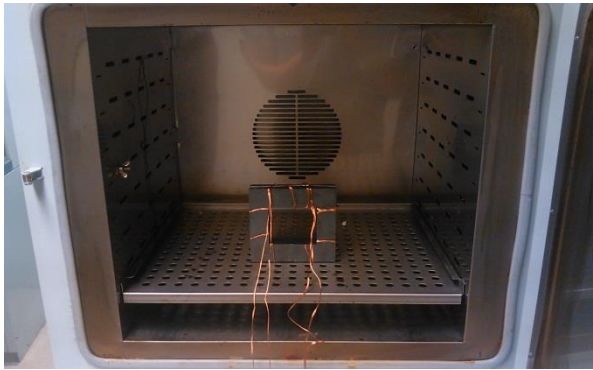


Figure 10-2 The heating chamber rated for 0°C to 200°C





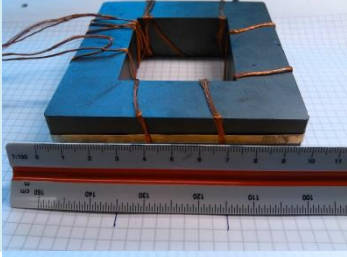
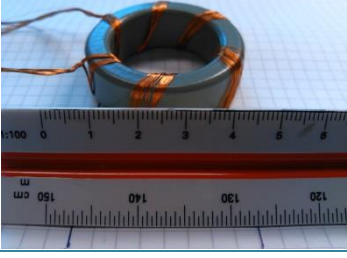
Figure 10-3 The plugin system for ring cores in BROCHAUS MPG 100D

### Samples

Details on the samples prepared for the core characterization can be found in Table 10-3. A primary winding with 8 turns is used to magnetize the core in the range from 4 mT to 106 mT for powder cores. This low range was chosen due to constraints in the Brochause measurement setup, however the ripple flux which will be inducing the core losses in real applications are not likely to be much larger. The secondary winding is set to be 8 turns with the same length as the primary to avoid phase problems. [2] recommends five turns on both primary and secondary this was disregarded due to the small increase in windings raised the induced flux to a more appropriate level and [2] is most likely a recommendation for high permeability materials. The heating chambers maximum temperature was measured to 180.5 °C when the settings was set to 200 °C and 108 °C with settings at 120 °C.

Table 10-3 Core loss samples

Picture	Primary windings	Secondary windings	Description
	8	8	<p>A single <b>0077715A7</b> core wound with 8 turns of 120 x 0.1 mm Litz wire with a theoretical peak flux of 98 mT at 10 A.</p> <p><b>The purpose:</b> of this sample is to test the core losses in koolMμ materials</p>
	8	8	<p>A single <b>C058583A2</b> core wound with 8 turns of 120 x 0.1 mm Litz wire with a theoretical peak flux of 179 mT at 10 A.</p> <p><b>The purpose:</b> of this sample is to test the core losses in HighFlux materials</p>

	8	8	<b>A single C058548A2</b> core wound with 8 turns of 120 x 0.1 mm Litz wire with a theoretical peak flux of 154 mT at 10 A. <b>The purpose:</b> of this sample is to test the core losses in HighFlux materials
	8	8	<b>A single C055089A2</b> core wound with 8 turns of 120 x 0.1 mm Litz wire with a theoretical peak flux of 108 mT at 10 A. <b>The purpose:</b> of this sample is to test the core losses in MPP materials
	6	6	<b>A single ZR44916TC</b> core wound with 6 turns of 30 x 0.1 mm Litz wire with a theoretical peak flux of 1360 mT at 10 A. <b>The purpose:</b> of this sample is to test the core losses for an R material ferrite with no air gap.
	8	4	<b>A double N27 U core</b> core wound with 8 turns of 30 x 0.1 mm Litz wire with a theoretical peak flux of 650 mT at 10 [A]. <b>The purpose:</b> of this sample is to test the core losses for a N27 material ferrite with no air gap.

### 10.2.2 Core characterisation at 180.5°C

The Litz wire used in the measurements are rated for 130°C but as shown in section 0 deterioration is not expected at 200°C for short term exposure, however in the case of short circuit in the winding, a change in resistivity is to be expected. Therefore the resistance in both the primary and the secondary winding was measured before and after the high temperature tests. This can be viewed in Table 10-4. There were no large deviations in the measured results meaning it is highly unlikely that any damage happened. However two samples not shown here had to be redone due to winding failure.

Table 10-4 Winding resistance before and after the high temperature tests

Sample number	Material	Rel. Perm.	Primary winding 20°C	Secondary winding 20°C	Primary winding after 180.5°C	Secondary winding after 180.5°C
1	High Flux	160	16.74 mΩ	16.68 mΩ	16.75 mΩ	16.70 mΩ
2	High Flux	125	18.01 mΩ	18.10 mΩ	18.02 mΩ	18.16 mΩ
3	KoolMμ	125	18.10 mΩ	18.21 mΩ	18.16 mΩ	18.29 mΩ
4	MPP	125	21.36 mΩ	19.80 mΩ	20.28 mΩ	19.94 mΩ
5	N27	2000	27.60 mΩ	27.87 mΩ	27.82 mΩ	27.14 mΩ
6	R	2300	09.60 mΩ	18.90 mΩ	09.56 mΩ	18.76 mΩ

### 10.3 100 kHz measurements

The BROCHAUSE steel tester had a secondary system for measurements above 10 kHz however it was not possible to get this operational within the time frame of this master thesis. Therefore another setup was made by using a signal generator which could create high frequency, non-sinusoidal and fundamental. The problem with using a function generator is that it can only supply low current, and therefore a 100 kHz amplifier was connected in series amplifying the signal to a maximum of 7.5 A<sub>rms</sub> with maximum voltage output of 40 V<sub>pp</sub>. An Oscilloscope was connected over the test object measuring voltage and current while a power analyzer module automatically calculated the power using all available data points (2500). At measurements lower than 20 kHz a high accuracy power meter was connected to the system see Table 10-5 for the complete equipment list. This setup is consistent with the setup used in [5].

Table 10-5 Lab equipment for 100 kHz

Application	Equipment	Product number
Signal generation	Signal generator	WAVETEK 187
Signal amplification up to 7.5 A 100 kHz	4-quadrant amplifier	Toellner TOE 7610-20
Current measurement	Current probe	TEKTRONIX P6021
Voltage measurement	Voltage probe	TEKTRONIX P5200A
Power measurements < 20 kHz	Power meter	YOKOGAWA 2533E43
Power measurements	Oscilloscope	TEKTRONIX TPS 2014
Oscilloscope power application	Power application	TEKTRONIX TPS2OWR1
Signal summation	Custom made	-
50 Hz signal 12 V <sub>Rms</sub>	Custom made	-
Temperature measurements	Data logger	AGILENT 34972A

#### 10.3.1 Core Loss measurements

The core losses was measured up to 100 kHz with the amplifier setup, however it is not likely these results is as accurate as the loss measurements from the Brochause. The current probe was calibrated until the error was less than 0.5 % at 5 kHz and the voltage probe to 1 %, however due to the large inductive load, the error in the measurements can be significantly higher and it was not possible to calibrate the probes for higher frequencies.

The flux density in the core material was found by measuring the voltage in a secondary winding and using Equation 10-1 see Table 10-6 for the relevant waveforms.

$$B = \frac{1}{NA_e} \int_0^t V(t) dt \quad \text{Equation 10-1}$$

Table 10-6 Equations to calculate the flux density in the core

Waveform	Equation
Sinus wave	$B_{peak} = \frac{V_{rms}}{4.44NA_e f}$
Square wave	$B_{peak} = \frac{V_{rms}}{4NA_e f}$
Triangular wave	$B_{peak} = \frac{V_{rms}}{4.619NA_e f}$

The secondary winding has a small voltage drop, but very low current flow in these wires. To avoid phase angle problems the winding length was set to the same length as the primary. The wire losses was minimized by using Litz wire of  $240 \times \Phi 0.1$  which is several times smaller than the penetration depth at 100 kHz which means that the winding losses should be very close to the dc value.

Therefore the dc losses in the windings was measured and subtracted from the measured values at higher frequencies, this is a small source of error but should not influence the overall results.

The amplifiers low output voltage for 100 kHz tests was counteracted by maximizing the flux density in the core by lowering the number of turns, and keeping the output current at around  $7.5 A_{rms}$ , with the voltage at  $20 V_{peak}$  see below for an example with 0077715A7 (KoolM $\mu$ ) at 100 kHz. This shows that the maximum flux density that can be tested at 100 kHz is 52 mT with 4 turns. This might seem like a small number but in a real application the ripple wave should normally not very large.

$$V_{peak} = I_{peak} \cdot j\omega L$$

$$L = \frac{20}{\sqrt{2} \cdot 7.5 \cdot 2\pi \cdot 100000} = 3 \cdot 10^{-6} \text{ [H]}$$

$$L = N^2 A_l \cdot 10^{-9}$$

$$N = \sqrt{\frac{L}{A_l \cdot 10^{-9}}} = 4.44 \text{ turns}$$

$$B_{peak} = \frac{NI_{peak}\mu}{l_e} = 4\sqrt{2} \cdot 7.5 \cdot 125\mu_0 = 52 \text{ [mT]}$$

To validate the setup, values from the Brochaue were compared to the measurements with the amplifier see Figure 10-4 and Figure 10-5. It can be seen that the accuracy of the amplifier measurements is not very compared to the Brochaue however at 5 kHz the winding losses equals around 90 - 95 % of the measured loss meaning a very small measurement error would yield results that deviate strongly from the expected result. At higher frequency this error decreases since most of the losses is located in the core. The test frequency was set to 5 kHz due to large deviations in the measurements in the Brochaue for frequencies near 10 kHz.

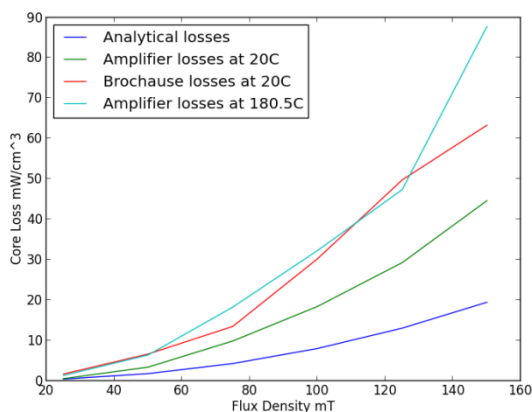


Figure 10-4 Measured loss in High Flux at 5 kHz

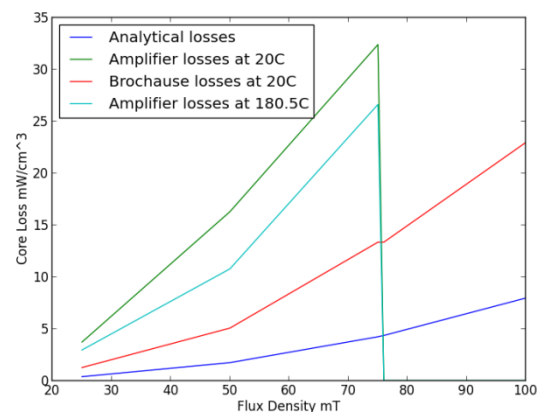


Figure 10-5 Measured loss in KoolM $\mu$  at 5 kHz

For the measurements between 5 kHz and 20 kHz a high accuracy power meter was also used however due to the very inductive load it is likely these measurements is not as accurate as the scope measurements. The accuracy of oscilloscope measurements at 100 kHz need to be very exact due to in for example a 90 VA coil operating at 100 kHz with 4 W of losses and a necessary accuracy of 0.4W would require an angle accuracy of 0.00444 rad. This translates to a time accuracy of 7.06 ns.

The TEKTRONIX TPS 2014 have a time accuracy of 5 ns and therefore the error is 0.00629 rad at 100 kHz which translates into 0.62 W at 100 VA. This is the maximum error that can happen since measured cores had smaller VA than this at 100 kHz.

At high frequencies the Brochause or the accurate power meter could not be used to compare the measured values, due to this as extra security a temperature sensor was connected to the core. The temperature gain of the core is primary dependent on geometry, therefore by measuring the temperature and loss at 100 kHz and comparing it to a core with the same dc loss, it is possible to verify the results within a reasonable frame if the values are correct, however as seen in chapter 7.11 a bit lower temperature is to be expected in the dc measurements due to all loss is located in the windings which is better cooled than the core. Calometric measurements would have been better but due to the limited time it was not possible to set up.

### 10.3.2 Fundamental waveform with a high frequency ripple

The current waveform experienced by filters is normally a fundamental with a high frequency ripple see chapter 3 and 5. The losses, temperature and inductance in a inductor experiencing such a waveform was investigated by summing the signals from a signal generator and a secondary waveform, taken directly from the grid due to voltage limitations with the signal generator which could only generator 20V<sub>pp</sub> while the amplifier which was connected in series needed 35 V<sub>pp</sub> to operate at maximum.

### 10.3.3 Non-sinusoidal losses

Chapter 5 describes non-sinusoidal losses and by using the signal generator and amplifier this problem was planned to be investigated, however the error in the measurements was too large to draw any concrete conclusions.

## 10.4 Measurements with a Buck Converter

The inductors designed in the previous chapters should be tested in real applications to determine the leakage inductance, saturation and performance. A buck converter operating in continues mode was set up in the lab see Figure 9-1 Buck converter [1] for the circuit topology and Table 10-7 for the equipment that was used.

Table 10-7 Lab equipment Buck converter

Application	Equipment	Product number
Signal generation	Signal generator	WAVETEK 187
Adjustable input voltage	3-phase variac	LUBECKE 3R54-22-H
Dc voltage generation	Dc-Link	GOSSEN
Buck converter switch	Converter	Custom by NTNU
Adjustable resistance	Resistance	RUSHTRAT
Filter	Capacitor 33μ	B25832-A4336-K009
Filter	Inductor	Custom
Power measurements	Power meter	YOKOGAWA 2533E43
Power measurements	Oscilloscope	TEKTRONIX TPS 2014
Oscilloscope power application	Power application	TEKTRONIX TPS20WR1
Voltage measurement	Voltage probe	TEKTRONIX P5200A
Current measurement	Current probe	FLUKE 80i-110s
Temperature measurements	Data logger	AGILENT 34972A

A Variac was connected to the main supply to give a variable voltage to the dc-link which feed the converter. The core under testing was mounted horizontal thereby reducing the heat loss in one direction. A capacitor of 33 $\mu$  was connected from the inductor to the negative voltage of the converter, and the resistive load connected from the inductor to the negative side.

The power losses voltage and current waveform was measured by an oscilloscope and a power meter. Surface temperature was measured by a nonmagnetic thermocouple of T-type. The sensor was attached by covering it with a bit of the winding, so this could lead to a small error however the sensor itself had a tolerance of around 0.5°C up to 125°C.

Inductors was designed based on the four cases described in the buck filter section see section 9.1 and Table 9-1. See section 11.2 for the results and more details can be found in appendix D section V.

**Table 10-8 Inductance and resistivity measurements in some inductors**

Sample Nr.	Material	Rel. Permeability	Turns		Resistance m $\Omega$		Inductance mH	
			Primary	Secondary	Primary	Secondary	Primary	Secondary
	KoolM $\mu$	125	50	50	50.44	57.16	0.421	0.45
	HighFlux	160	85	85	56	77.35	0.804	0.8
	HighFlux	160	110	110	138.25	138.7	1.47	1.38
	HighFlux	125	106	-	97.54	-	1.909	
	HighFlux	160	50	-	37.78	-	0.355	
	HighFlux	160	50	-	39.49	-	0.387	

## 10.5 Leakage capacitance

The leakage capacitance of the magnetic cores was measured in cooperation with Amir Hayati Soloot and the equipment in Table 10-9 which measures the impedance from 4 Hz to 30 MHz. This was then used to calculate the leakage capacitance.

**Table 10-9 Lab equipment for Leakage capacitance**

Application	Equipment	Product number
Impedance measurement	Network analyzer	AGILENT E5061B

The leakage capacitance can be calculated by Equation 10-2 when the self-resonance frequency and inductance is known.

$$\omega^2 = \frac{1}{LC} \quad \text{Equation 10-2}$$

The inductance in powder cores is not constant above a few hundred kilohertz therefore the inductance at the resonance frequency is different from values measured at low frequency. This is a problem since it was hard to measure the inductance at higher frequency with the available equipment. Therefore the inductance measured at 10 kHz was adjusted by the analytical data provided by the manufacturer, however this lowers the accuracy of the results. No better solution was found in time and most of the larger cores have a low self-resonance frequency. The analytical

data that was used can be viewed in [6], and some initial measurements can be viewed in Table 10-10 and Figure 10-6 - Figure 10-9, while the main results will be covered in the next chapter.

Table 10-10 Leakage capacitance and SRF in some different inductors

Turns	Type	Inductance at 10 kHz	Self-resonance frequency	Adjusted Inductance	Leakage capacitance
165	KoolMμ Litz 120 strand	5.5 mH	97.14 kHz	5.5 mH	488 pF
136	High Flux 160μ Enamel	3.0 mH	280 kHz	2.94 mH	107.6 pF
41	KoolMμ Litz 120 strand	0.242 mH	670 kHz	0.235 mH	240 pF
16	KoolMμ Litz 240 strand	35 μH	2.29 MHz	31.5 μH	153 pF

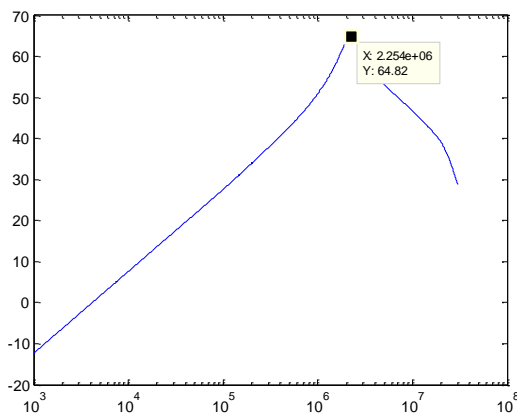


Figure 10-6 Impedance plot for 16 Turns Litz wire 240 strands

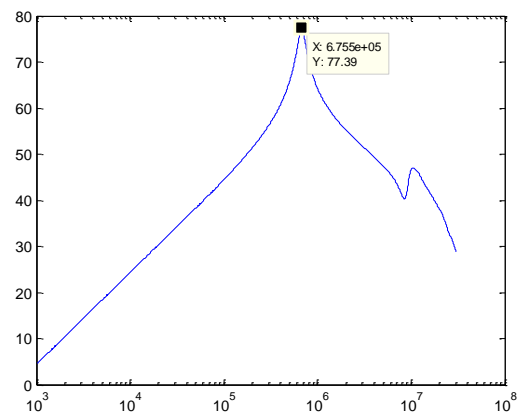


Figure 10-7 Impedance plot for KoolMμ 41 Turns Litz wire 120 strands

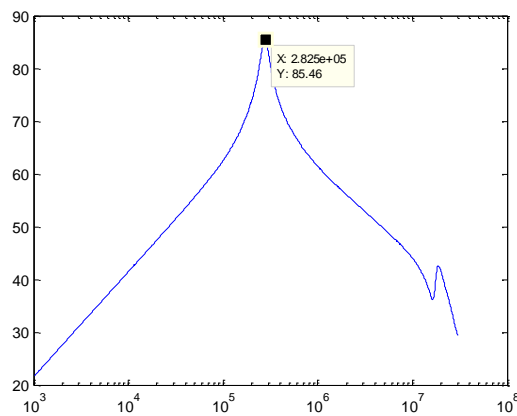


Figure 10-8 Impedance plot for 136 Turns enamel

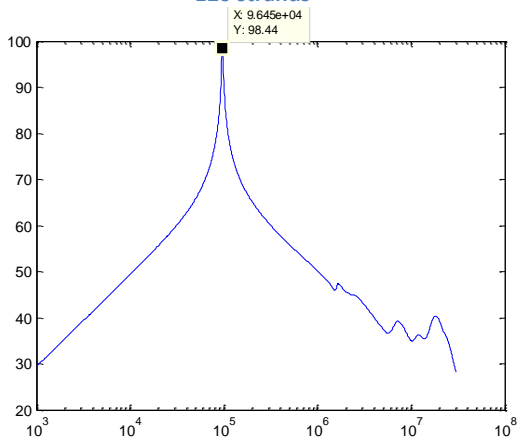


Figure 10-9 Impedance plot for 165 Turns Litz 120 strands



## 10.6 References

- [1] N. Mohan and T. M. Undeland, "Power Electronic Converters, Applications, and Design": John Wiley & sons, 2003.
- [2] "BROCHAUS MPG100 USER MANUAL" 2001
- [3] Discussion with Arne Nysveen
- [4] Discussion with Edris Agheb
- [5] Christopher G. Oliver "Measurement and Modeling of Core Loss in Powder Core Materials Core Loss in Powder Core Materials" 2012
- [6] Magnetics® Technical Bulletin "Powder Core Catalog" 2012



## 11 Measurements and Discussion

In the previous chapter the main points of the measurement setup and error sources was discussed, in this chapter the focus will be on the results. The raw data from the measurements is located in appendix D however the Brochause data was too large to be included and can be found in the DAIM database.

### 11.1 Core loss

The core loss in N27, R-ferrite, High Flux, MPP, and KoolM $\mu$  was measured at different temperature levels 20°C 108°C and 180.5°C for the frequencies 3 kHz, 5 kHz, 7 kHz and 9 kHz with a Brochause steel tester. An amplifier was used to measure core losses at 5 kHz, 20 kHz, 50 kHz, and 100 kHz for the temperatures 22°C and 180°C. From core loss theory the losses is not expected to abruptly change several magnitudes however this is the case in some of the Brochause measurements, the cause is likely an automatic system in the measurement equipment which changed the control method between controlling H and B.

The analytical loss data was provided by the manufacturer [1] for the powder cores see Equation 11-1- Equation 11-4. Based on this the lowest losses is expected in MPP and the largest in High Flux 160, it can also be seen that the losses nearly double by using High Flux 160 over High Flux 125. Note that the losses increase with higher permeability should not be used as a rule since in other materials the losses can decrease by increasing the permeability.

$$\text{MPP } 125\mu \quad P_v = 53.05f^{2.06}\hat{B}^{1.56} \quad \text{Equation 11-1}$$

$$\text{HighFlux } 125 \quad P_v = 246f^{2.23}\hat{B}^{1.47} \quad \text{Equation 11-2}$$

$$\text{High Flux } 160 \quad P_v = 447.6f^{2.3}\hat{B}^{1.41} \quad \text{Equation 11-3}$$

$$\text{KoolM}\mu \text{ } 125 \quad P_v = 91.58f^{2.2}\hat{B}^{1.63} \quad \text{Equation 11-4}$$

#### 11.1.1 Core loss in KoolM $\mu$ 5 kHz – 9 kHz

The core loss measured in KoolM $\mu$  with the Brochause setup can be viewed in Figure 11-1 - Figure 11-4.

The analytical data underestimates the core losses severely at all frequencies. One explanation for this could be the large variation between the samples since the manufacturer only promises that each core is within 8% of the promised permeability value.

A sample with 8% lower permeability than the rated should consist of 8% more air/binder and

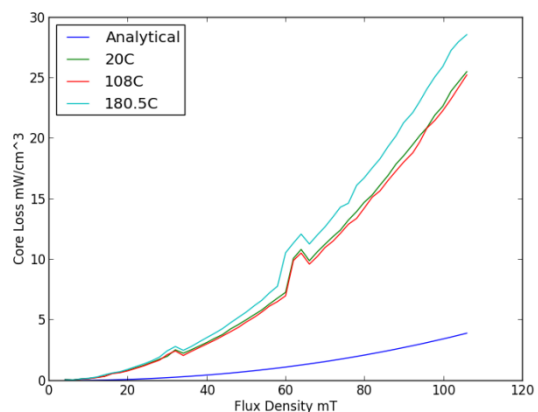


Figure 11-1 Measured loss in KoolM $\mu$  at 3 kHz

therefore might have different losses. To test this idea the permeability was measured which resulted in a relative permeability of 143, this could explain a bit of the large difference.

No analytical data for higher permeability KoolM $\mu$  cores were available, however lower permeability cores have nearly twice as high losses as the 125 $\mu$  core at 5 kHz and 100mT.

Another possibility would be that the loss measurements are wrong or performed in a different manner than the background data for the analytical data, and the analytical data is based on the Steinmetz equation which in some cases can underestimate or overestimate the losses.

However as it can be seen in Figure 11-5 where the losses have been measured with the amplifier setup there is not a large deviation between the two setups.

The losses measured at 7 kHz is most likely only valid up to 70 mT and the 10 kHz measurements do not seem to have become stable even if the data is the mean of several measurements.

The temperature do not affect the losses in any great extent up to 180°C however a 5 -10 % increase in loss is indicated which primarily happens in the temperature range from 108°C to 180°C. For temperatures below 108°C there is no significant deviation due to temperature.

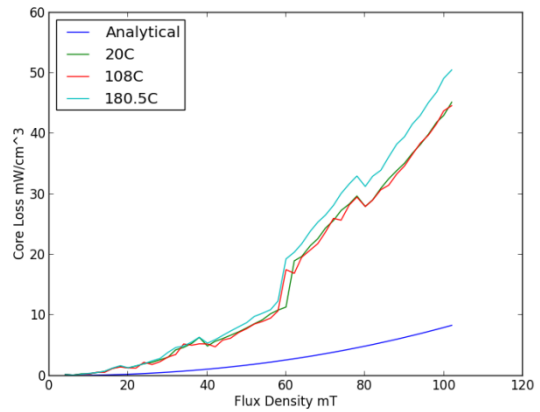


Figure 11-2 Measured loss in KoolM $\mu$  at 5 kHz

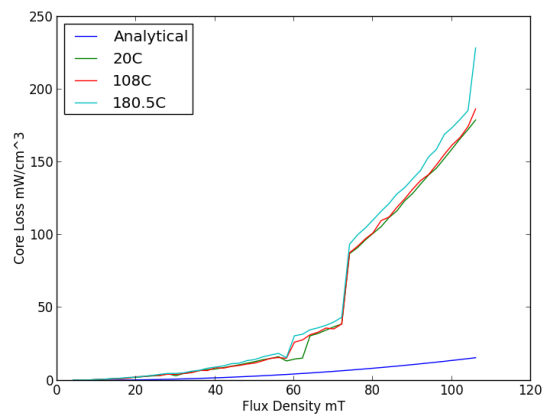


Figure 11-3 Measured loss in KoolM $\mu$  at 7 kHz

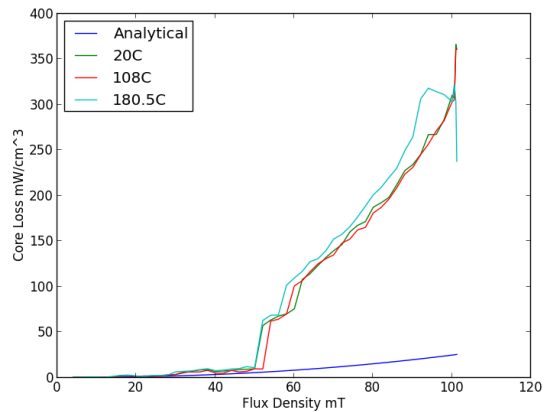


Figure 11-4 Measured loss in KoolM $\mu$  at 10 kHz

**11.1.2 Core loss in KoolM $\mu$  5 kHz – 100 kHz**

The losses in KoolM $\mu$  between 5 kHz and 100 kHz were found using the amplifier setup described in the previous chapter see Figure 11-5 to Figure 11-8 for the graphical representation of loss versus flux density. The correlation between the Brochause and the amplifier at 5 kHz is good bellow 50 mT but the amplifier measurers somewhat lower losses at 75 mT. This is to be expected since it can be seen in Figure 11-2 that there have been a discontinues jump in losses at 60 mT. The measurements was performed twice, however in the cases where there was a large variation between the two measurements more measurements was performed. Initially 5 measurements at each point were planned but due to the very low variation between the samples this did not seem necessary especially due to long time each measurement took.

The analytical data underestimates the losses for all frequencies measured with a factor of 200 – 300 %. The temperature has a similar influence at 100 kHz as at 5 kHz.

The measurements at 50 and 100 kHz was not possible to perform in the full flux density range due to constraints in the equipment, and the losses at 100 kHz is so low that the error from measuring the angle between real losses and reactive losses might seriously influence the values, therefore the 100 kHz losses should not be trusted.

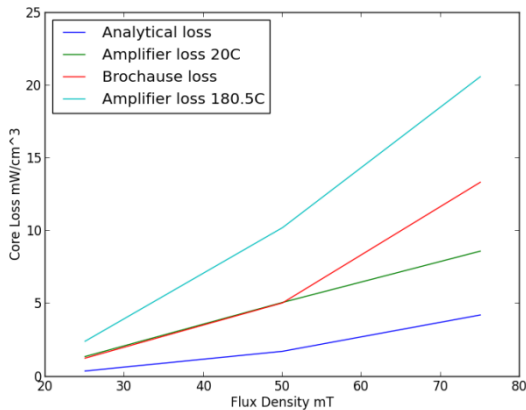


Figure 11-5 Measured loss in KoolM $\mu$  at 5 kHz

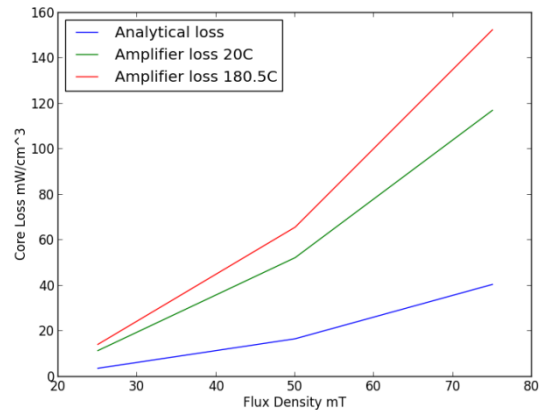


Figure 11-6 Measured loss in KoolM $\mu$  at 20 kHz

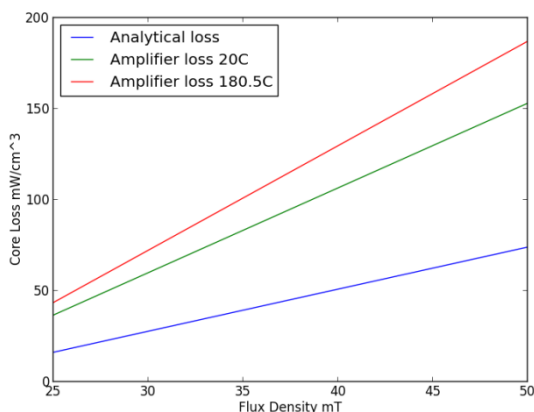


Figure 11-7 Measured loss in KoolM $\mu$  at 50 kHz

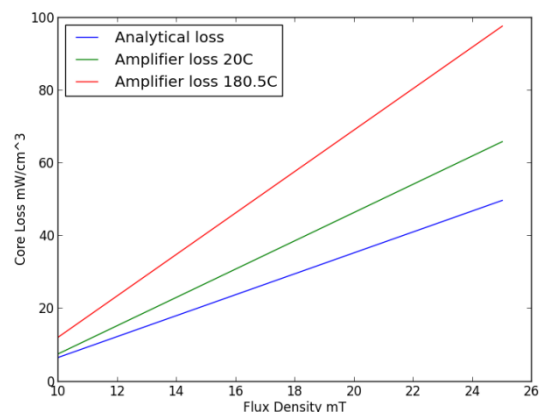


Figure 11-8 Measured loss in KoolM $\mu$  at 100 kHz

The measured values can be used to calculate new values for the Steinmetz equation which determines the analytical data see Table 11-2. The new parameters have been plotted in Figure 11-9 and Figure 11-10. It can be seen that the accuracy of the Steinmetz equation can be increased by measuring some points in the area of interest, however the values should not be extrapolated. In a high temperature design this should be done close to the operation temperature.

Table 11-1 KoolM $\mu$  new Steinmetz parameters

Range	k	$\alpha$	$\beta$
5 kHz – 20 kHz 0.025 mT – 0.075 mT	31.73	1.8822	1.6731
20 kHz – 50 kHz 0.025 mT – 0.05mT	1135	1.17	2.2001

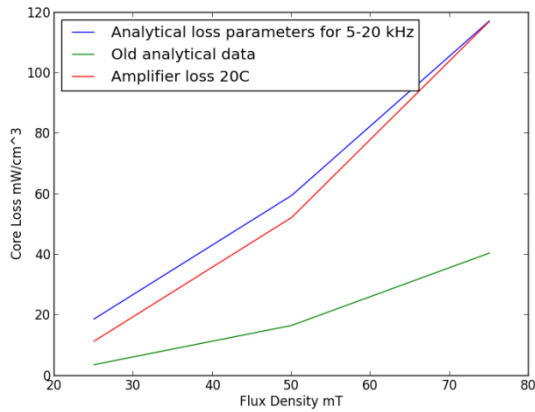


Figure 11-9 Comparison of new Steinmetz parameters for 5 - 20 kHz at 20 kHz

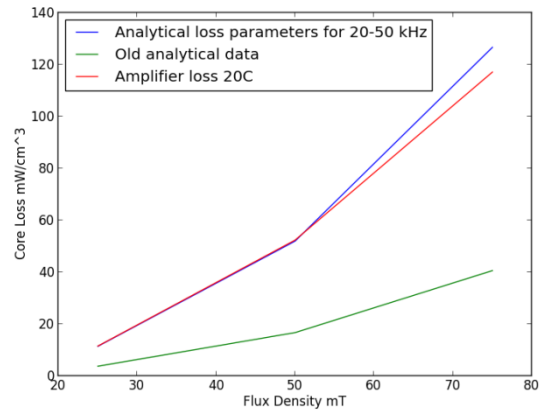


Figure 11-10 Comparison of new Steinmetz parameters for 20 - 50 kHz at 20 kHz

**11.1.3 Core loss in High Flux 160 5 kHz – 9.9 kHz**

The core loss measured with the Brochause setup can be seen in Figure 11-11 to Figure 11-14. There is less discontinues data with the Brochause measurement equipment in testing the High Flux materials compared to the KoolMμ, this could be due to the material properties which make measurements easier to perform. However there is still some control problems which leads to discontinues data in some case especially at 9.9 kHz but this is very close to the maximum rating of the equipment.

The relative permeability of the materials was measured to 150 which mean some loss differences are to be expected, however as in the previous section the losses are very much larger than what should be expected in the magnitude of up to 600 %.

The temperature does not affect the losses in any significant way up to 180°C except a loss reduction of some percent.

The measurement sample was quite small physically which means there is a larger expected error than in the other samples.

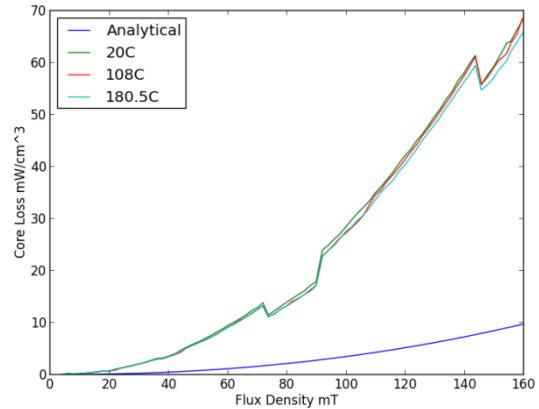


Figure 11-11 Measured loss in HighFlux 160 at 3 kHz

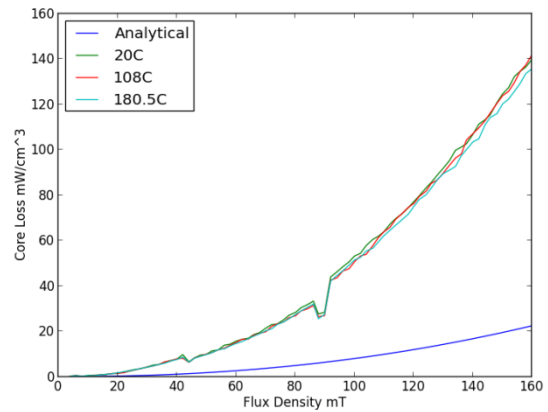


Figure 11-12 Measured loss in HighFlux 160 at 5 kHz

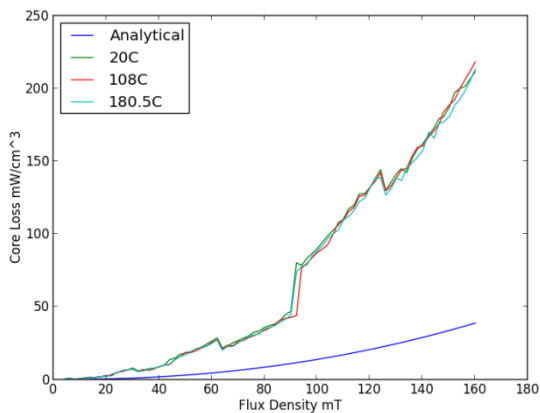


Figure 11-13 Measured loss in HighFlux 160 at 7 kHz

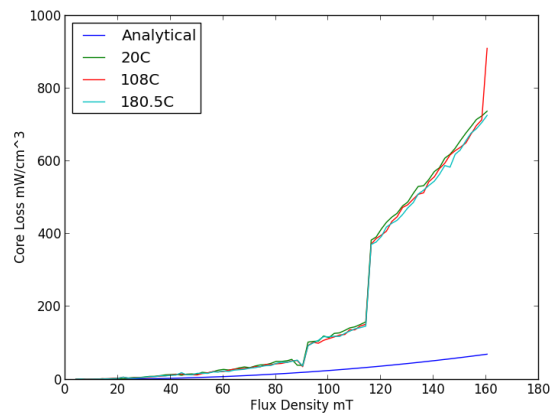


Figure 11-14 Measured loss in HighFlux 160 at 9.9 kHz

**11.1.4 Core loss in High Flux 160 5 kHz – 100 kHz**

The high frequency measurements can be viewed in Figure 11-15 - Figure 11-18 it can be seen that the analytical data match the measured values in a large extent up to 100 kHz. However there is a large deviation between the values measured with the Brochause setup compared to the amplifier this might indicate that the Brochause steel tester is not suited for measuring low permeability cores with high accuracy, since the amplifier results is built upon 48 separate measurements making it highly unlikely that so many point would fit the analytical data if measurement setup was not somewhat accurate. The high flux material could be measured up to a larger flux density than the previous and the losses are higher which increases the accuracy.

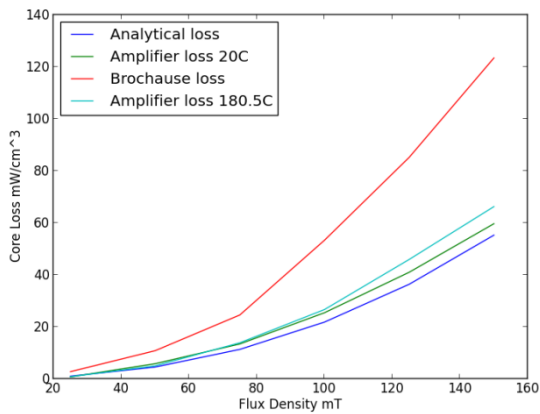


Figure 11-15 Measured loss in High Flux at 5 kHz

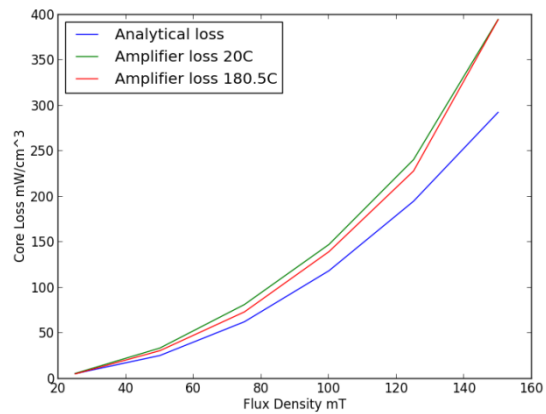


Figure 11-16 Measured loss in High Flux at 20 kHz

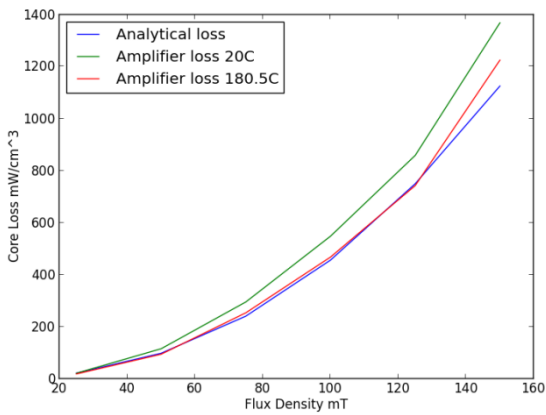


Figure 11-17 Measured loss in High Flux at 50 kHz

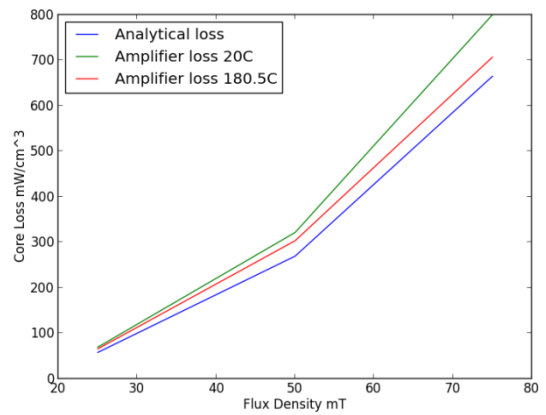


Figure 11-18 Measured loss in High Flux at 100 kHz

**11.1.5 Core loss in High Flux 125 5 kHz- 9.9 kHz**

The losses in High Flux 125 $\mu$  material can be viewed in Figure 11-19 to Figure 11-22 however the losses above 80 mT should not be trusted since it can be seen that there is a discontinuity in the data, as previously explained this is likely due to a change in the control system. The same relationships between the temperature and losses as with High Flux 160 is present which results in a small negative temperature coefficient in the losses with increasing temperature, at least up to 180°C.

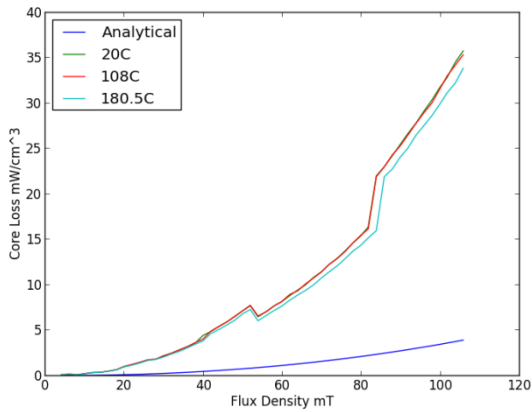


Figure 11-19 Measured loss in HighFlux 125 at 3 kHz

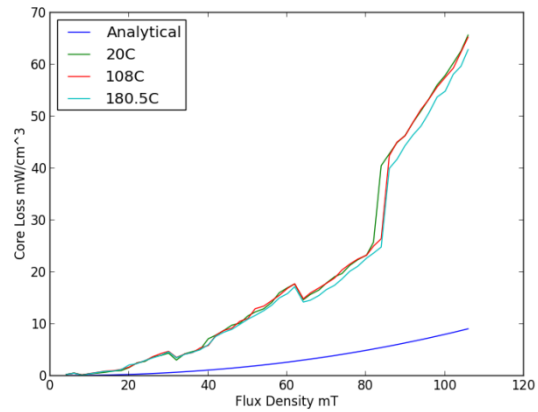


Figure 11-20 Measured loss in HighFlux 125 at 5 kHz

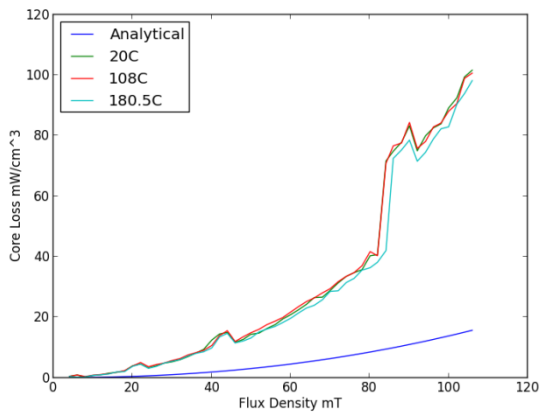


Figure 11-21 Measured loss in HighFlux 125 at 7 kHz

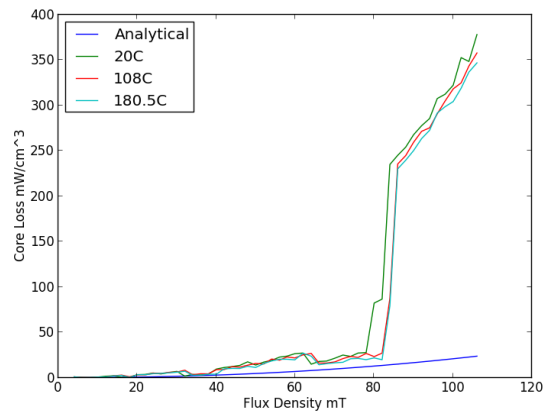


Figure 11-22 Measured loss in HighFlux 125 at 9.9 kHz

**11.1.6 Core loss in MPP 5 kHz- 9 kHz**

The MPP losses were complicated to measure and the Brochouse were not able to get results above 5 kHz at 180°C see figure Figure 11-23 - Figure 11-26 for the measured values. It can be seen that in MPP the losses are several magnitudes higher than the analytical data even if the relative permeability is very close to the rated value of 125. The previous measurements and this one indicated there are large differences among the cores in the magnitude of core loss in the same way that the manufacturer does only guarantee that the permeability is within +/- 8 %. In the measurements there is no relevant increase in core loss by temperature from 3 kHz to 5 kHz however there seem to be some problem in measuring loss at high temperature for higher frequencies but this is likely to be related to the measurement equipment.

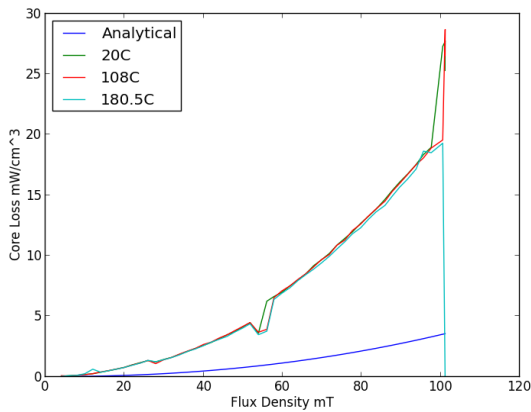


Figure 11-23 Measured loss in MPP 125 at 3 kHz

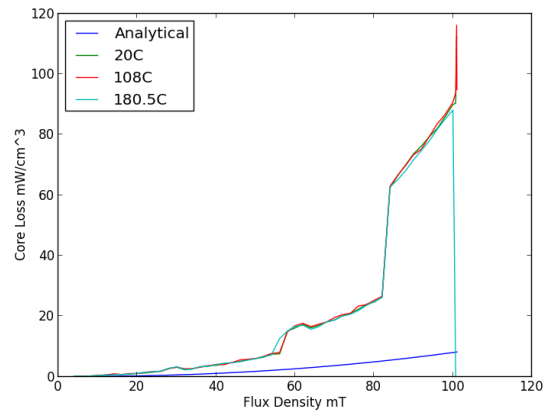


Figure 11-24 Measured loss in MPP 125 at 5 kHz

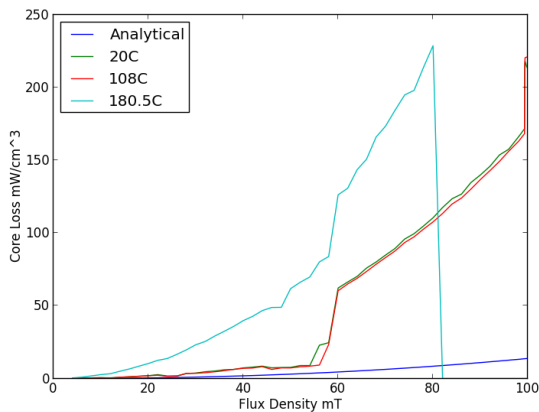


Figure 11-25 Measured loss in MPP 125 160 at 7 kHz

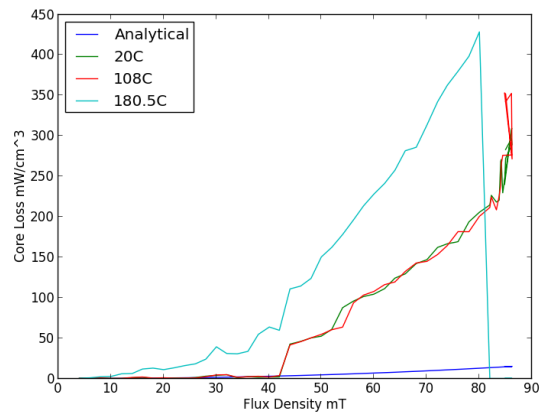


Figure 11-26 Measured loss in MPP 125 at 9.9 kHz

**11.1.7 Core loss in MPP 5 kHz- 100 kHz**

The loss in MPP was measured up to 100 kHz using the amplifier setup. However the loss which was measured is not very large giving possibility of a large error. The low core loss means that the angle between real loss and reactive loss become very important which was shown in section 10.3.1. This should primarily be the case at 100 kHz but at 50 kHz the losses are allot lower meaning the error is large in this case also. Some small relationships can however be found, that there is some close to no increase in core losses with temperature.



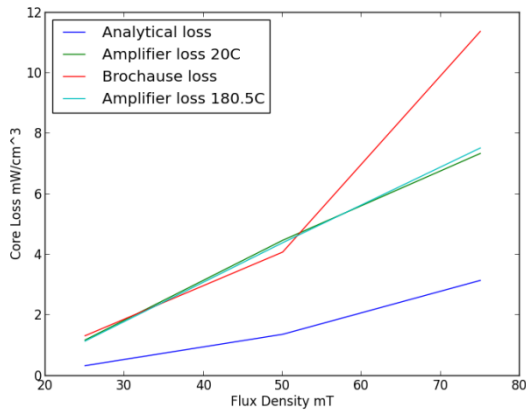


Figure 11-27 Measured loss in MPP at 5 kHz

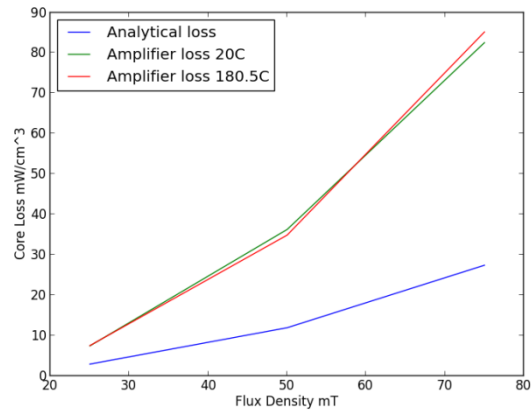


Figure 11-28 Measured loss in MPP at 20 kHz

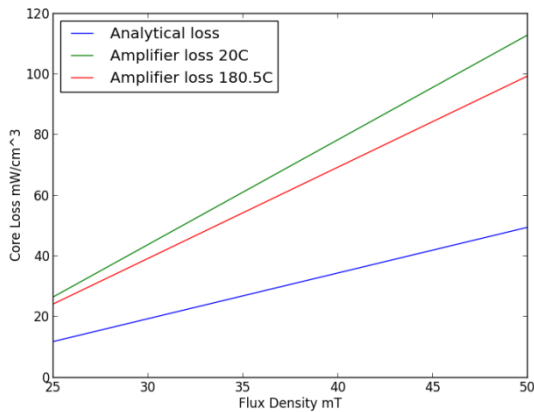


Figure 11-29 Measured loss in MPP at 50 kHz

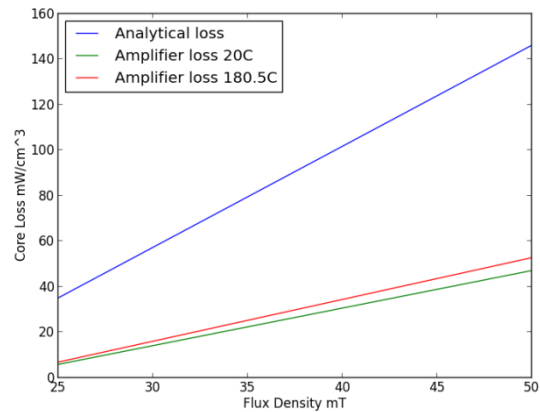


Figure 11-30 Measured loss in MPP at 100 kHz

The measured values can be used to calculate new values for the Steinmetz equation which determines the analytical data see Table 11-2. The new parameters have been plotted in Figure 11-31 and Figure 11-32. The MPP loss should be further investigated with a more accurate loss setup, possible involving calorimetric measurements.

Table 11-2 MPP new Steinmetz parameters

Range	k	$\alpha$	$\beta$
5 kHz – 20 kHz 0.025 mT – 0.075 mT	33.24	1.74	1.66
20 kHz – 50 kHz 0.025 mT – 0.05mT	861.76	1.24	2.3

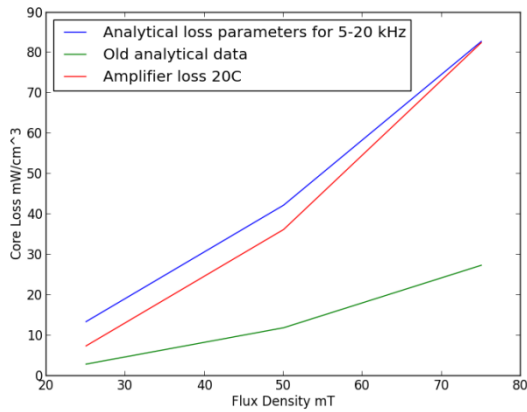


Figure 11-31 Comparison of new Steinmetz parameters for 5 - 20 kHz at 20 kHz

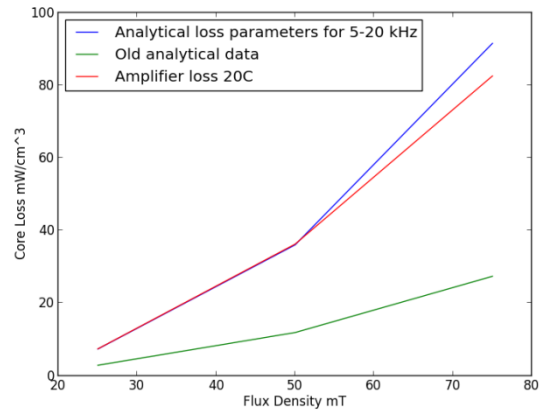


Figure 11-32 Comparison of new Steinmetz parameters for 20 - 50 kHz at 20 kHz

### 11.1.8 Core loss in N27 Ferrite

A N27 ferrite core from EPCOS was measured with the Brochause steel tester, and the sample was quite large compared to all other measured cores with a weight that was around 6 – 7 times higher than any other samples. This reduces the measurement error, however it was a double U core which was transferred to the equivalent toroid shape.

The measurement fit the analytical data very well, but the measured loss is lower than the producer’s analytical data. This could be because the analytical data is for another temperature point than the measurement values. The temperature decreases the losses up to a minimum in the vicinity of 130°C while at 180°C it has increased back to the initial value. This is an expected relationship due to normally ferrites are created with a minimum around the operation temperature which decreases the chances of thermal runaway. The curie temperature of N27 is < 220°C so larger loss was expected at 180°C than the measured values. The 7 kHz and 9 kHz measurements had so large deviations and errors that they were not included, this was caused by instability in the Brochause control system.

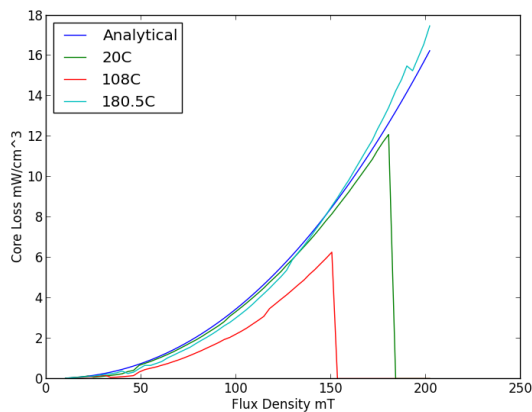


Figure 11-33 Measured loss in N27 at 3 kHz

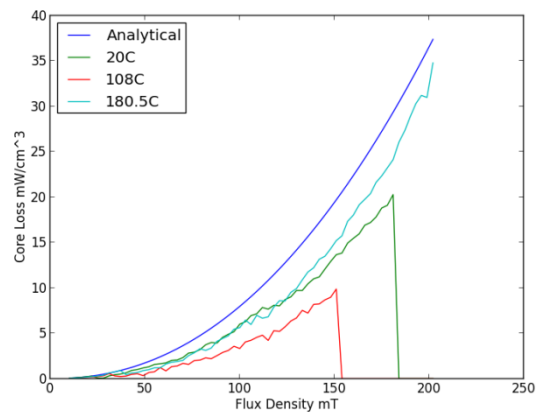


Figure 11-34 Measured loss in N27 at 5 kHz

**11.1.9 Core loss in R Ferrite**

The core loss measured in magnetics® R ferrite (ZR44916TC) can be viewed in Figure 11-35 - Figure 11-38. According to the measurements the analytical data provided from the manufacturer fits close to the measured data. However it is likely the analytical data is for another temperature point than what have been tested. It can be seen that the material have a loss minimum at around 130 °C which is expected, since its normal to create such a minimum to avoid thermal runaway.

The measurements was performed from 10 mT until the core went into saturation, this explains the large increase in loss close to the maximum flux density which is decreasing with temperature. The data around the border of saturation should not be trusted.

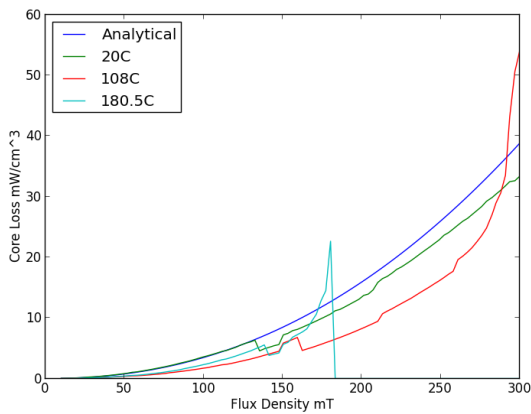


Figure 11-35 Measured loss in R ferrite at 3 kHz

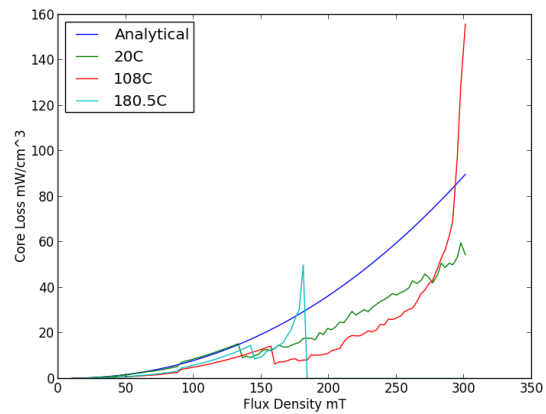


Figure 11-36 Measured loss in R ferrite at 5 kHz

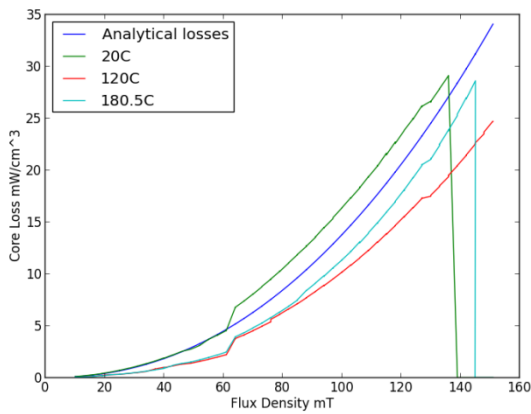


Figure 11-37 Measured loss in R ferrite at 7 kHz

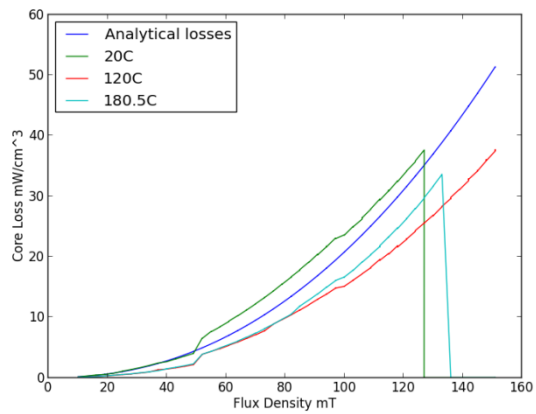


Figure 11-38 Measured loss in R ferrite at 9 kHz

## 11.2 Buck converter

### 11.2.1 Inductor measurements and comparison

Three different buck filters was created, based on the theory in section 9.1 and designed with the inductor software that has been developed. The purpose of the measurements is to determine how close to the real values the analytical approach is. The basic properties of the filter can be seen in Table 11-3 however see appendix D section V for more details.

Table 11-3 Buck filter properties

Nr	$V_o$ [V]	F [kHz]	D	$\Delta I_l$ [A]	$\Delta V_o$ [V]	L [mH]	$I_{dc}$ [A]	C [ $\mu$ F]
1	30	10	0.5	1.2	0.4545	1.25	3	33
2	30	10	0.5	0.6	0.2273	2.5	2	33
3	30	5	0.5	3	2.27	1	5	33

The results from the testing can be viewed in Table 11-4 and Table 11-5. It can be seen that there is a close correlation between the measurements and the analytical data, however it is clearly shown that the 8 % variation in permeability given by the manufacturer need to be taken into account. The losses correlate closely in inductor 2 however lower accuracy is present in the KoolM $\mu$  sample this could be explained by the data in the section 11.1.1 and 11.1.2 which showed that the analytical data underestimates the core losses by a big factor. The temperature is overestimated in all samples however the temperature of the cores is so low that low accuracy was to be expected. The thermal model was evaluated against measurements with large losses in section 7.10 which indicated that it is accurate. The analytical software estimates the fill factor with high accuracy in the samples.

Table 11-4 Comparison of analytical design and measured values for inductors

Inductor 1	Analytical prediction	Measured values		Inductor 2	Analytical prediction	Measured values	
Core Data	125M $\mu$ 0077715A7			Core Data	160 High Flux C058583A2		
Linital	1.52	1.646	mH	Linital	2.91 mH	2.57	mH
Lpeak	1.31	1.035	mH	Lpeak	2.53 mH	1.68	mH
I peak	0.6	0.72	A	I peak	0.3	0.444	A
Turns	98	100	-	Turns	169	170	-
Copper loss	0.52810	-	W	Copperloss	0.276112	-	W
CoreLoss	0.13924	--	W	CoreLoss	0.233555	-	W
Total Loss	0.66734	1.2	W	Total Loss	0.509667	0.494	W
Temperature	4.1312	12	°C	Temperature	4.834313	10	°C
MyCorrection	0.85940	0.628	-	MyCorrection	0.868757	0.653	-
Fill factor	0.24658	0.25	-	Fill factor	0.80201	0.83	-

Table 11-5 Comparison of analytical design and measured values for inductors

Inductor 3	Analytical prediction	Measured values	
Core Data	125 HighFlux C058548A2		
L <sub>initial</sub>	1.77 mH	2.01	mH
L <sub>peak</sub>	1.0 mH	0.993	mH
I <sub>peak</sub>	1.5	1.46	A
Turns	118	120	-
Copper loss	2.83		W
CoreLoss	0.076		W
Total Loss	3.19	4.2	W
Temperature	38	24	°C
MyCorrection	0.56	0.49	-
Fill factor	0.34		-

### 11.2.2 Paralleling of inductors

Parallel connection of inductors might be a viable option to reduce toroid powder core components when a component experiences a dc-bias which reduces the effective permeability see more information in section 4.4. The laboratory setup was the buck converter with volt meters connected in series with each core. A high flux 160 was compared to two high flux 160 connected in parallel with a higher number of turns the values was 40 turns 151.7  $\mu$ H and the parallel connection had 2 x 50 turns on separate cores and a parallel inductance of 151.4  $\mu$ H. The second test was a KoolM $\mu$  with 70 turns and 691  $\mu$ H while the parallel connected cores had 2 x 100 turns on separate cores and a parallel inductance of 718  $\mu$ H. The results can be viewed in Figure 11-39 and Figure 11-40. See appendix D section VIII for the data. Analytical the permeability provided by the manufacturer [1] show a close correlation to the measured values however in the high flux sample there is some deviation and the analytical data underestimates the permeability change. Overall the same conclusion can be taken, that in some cases parallel connection might be beneficial especially in limited space designs. It might be easier to locate several inductors instead of a larger piece and since magnetic cores comes in standard sizes in the area between one size and the next parallel confection might be good.

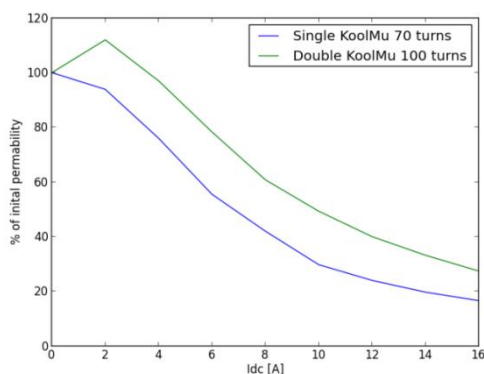


Figure 11-39 Measured permeability with increasing dc current in 0077715A7 (KoolM $\mu$ )

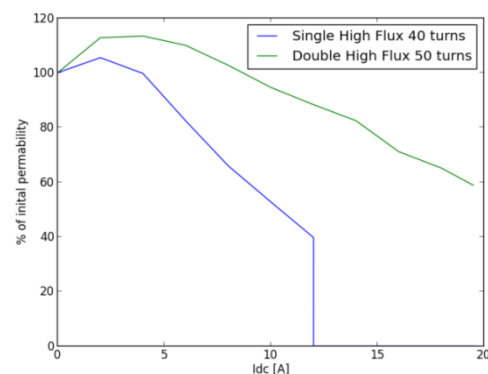


Figure 11-40 Measured permeability with increasing dc current C058583A2 (High Flux 160)

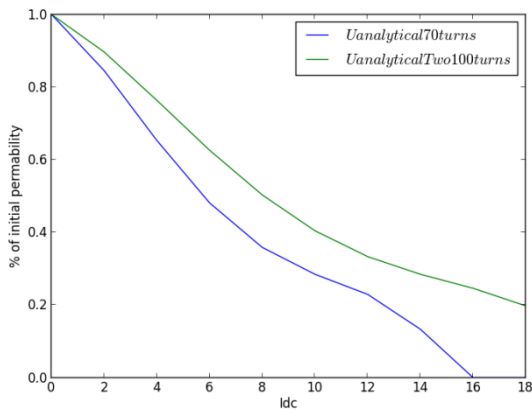


Figure 11-41 Analytical permeability with increasing dc current in 0077715A7 (KoolM $\mu$ )

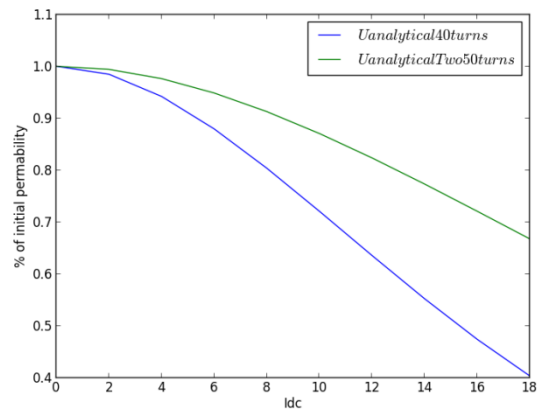


Figure 11-42 Analytical permeability with increasing dc current in C058583A2 (High Flux 160)

### 11.3 Leakage capacitance

#### 11.3.1 Reducing the leakage capacitance

Three C058583A2 cores were wound with different winding methods and measured see section 10.5 and 11.3 for more details. Strategy one (Figure 6-11) and four (Figure 6-12) was tested and compared to a baseline (Figure 6-10).

##### Normal winding

A core with 50 turns of 120 x 0.1mm Litz wire was wound on a C058583A2 core to get a basic idea about the leakage capacitance in inductor cores. The impedance plot can be seen in Figure 6-10, and the measured values in Table 6-4. The secondary peak is likely caused by the inductor to earth capacitance.

Table 11-6 Measured values for a normal winding

L [ $\mu$ H]	C [pF]	$f_0$ [kHz]
247.6	261.2	624.9

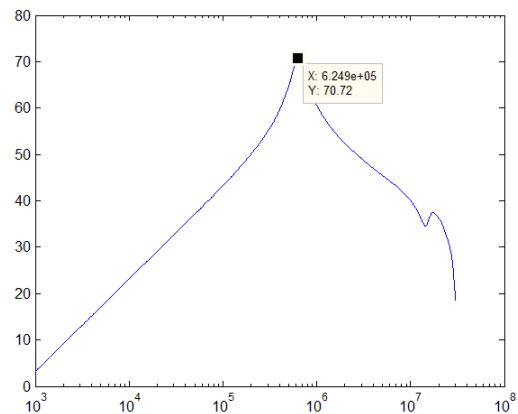


Figure 11-43 Impedance versus frequency for a normally wound core

##### Bank winding

A bank winding was wound on a C058583A2 core, this decreased the leakage capacitance by 43 % as can be seen in Table 6-5 and Figure 6-11. The secondary peak has also disappeared or been moved outside the scope of the measurement which was up to 30 MHz.

Table 11-7 Measured values for a Bank winding

L [ $\mu$ H]	C [pF]	$f_0$ [kHz]
304.4	150	742.6

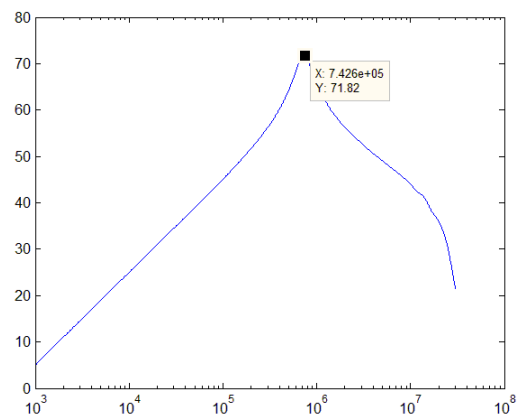


Figure 11-44 Impedance versus frequency for a bank

**Air gap between the layers**

A winding with an air gap of 3.4 mm between the layers was wound using tape. This resulted in a 38.3 % reduction in leakage capacitance. However due to the 3 mm of tape the inner radius became smaller leading to the windings in the outer layer being packed more together which likely raised the leakage inductance a bit.

Table 11-8 Measured values an inductor with air gap between layers

L [μH]	C [pF]	f <sub>0</sub> [kHz]
254.2	161	785.7

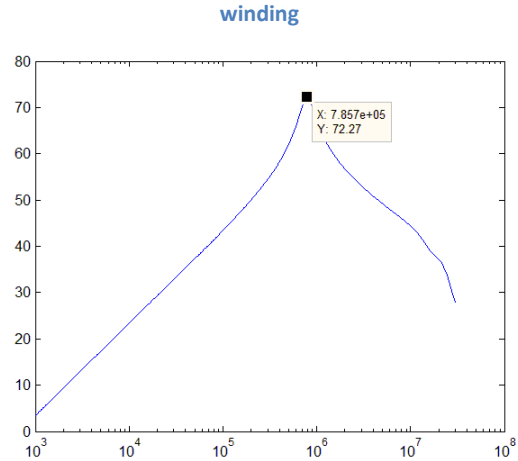


Figure 11-45 Impedance versus frequency for a winding with air gap between the layers

The results indicate that instead of winding the core with a complicated bank winding an air gap could be inserted with nearly the same effect on leakage capacitance however this would also increase the winding size and the size of the component but lead to better cooling with a cheaper/simpler winding technique.

**11.3.2 Parallel connection between two inductors**

Two KoolMμ 0077715A7 was paralleled to see if the effect on the leakage capacitance would agree with general capacitance theory (which might not be the case). In a parallel it is expected that the capacitance add up and inductance decreases. Therefore the capacitance of two 675 pF inductors in parallel (see Figure 11-46 and Table 13-4) is expected to be 1350 pF as it can be seen of Figure 11-47 and Table 11-10 this agrees with the basic theory however the values are higher.

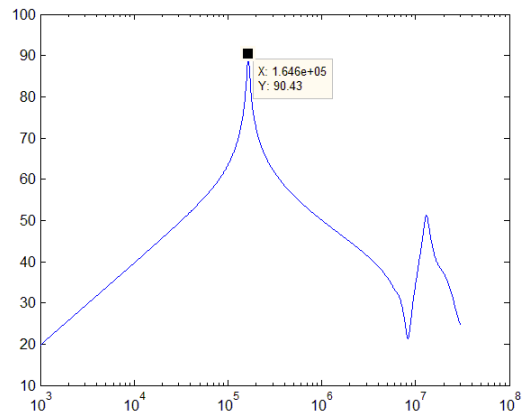


Figure 11-46 A single 100 turn KoolMμ core

Table 11-9 Parameters of a single 100 turn KoolMμ core

L [μH]	C [pF]	f <sub>0</sub> [kHz]
1385	675	164.6

Table 11-10 Parameters of a parallel connection of two 100 turn KoolMμ core

L [μH]	C [pF]	f <sub>0</sub> [kHz]
718	1540	151.3

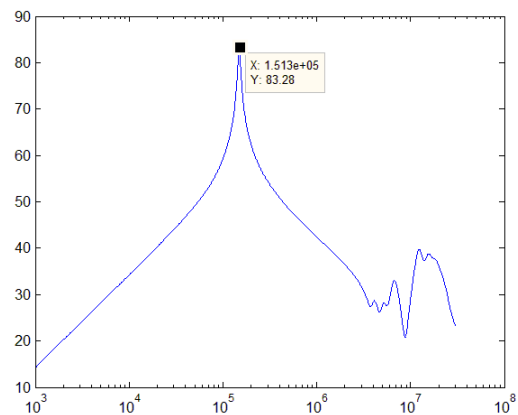


Figure 11-47 Parallel connection of two 100 turn KoolMμ core

**11.3.3 Minimum leakage capacitance**

In a winding each turn could be modelled as a single inductor on the same core which means as long as the mutual capacitances do not increase. General capacitor theory should be valid, since the leakage capacitance is in series adding more turns to the inductor will actually reduce the leakage capacitance up to some point where the mutual capacitances start having a large effect.

**Single Turn**

The first core tested was a 0077715A7 with 1 turn. Table 11-11 show the leakage capacitance, SRF and inductance. It can be seen that with Litz wire and KoolMμ SRF have a maximum of 16.3 MHz. However the inductance was measured at low frequency and the inductance is allot lower which means the leakage capacitance is higher than the estimate number.

Table 11-11 Parameters for a 1 turn KoolMμ core

L [μH]	C [pF]	f <sub>0</sub> [kHz]
1.82	53	16 330

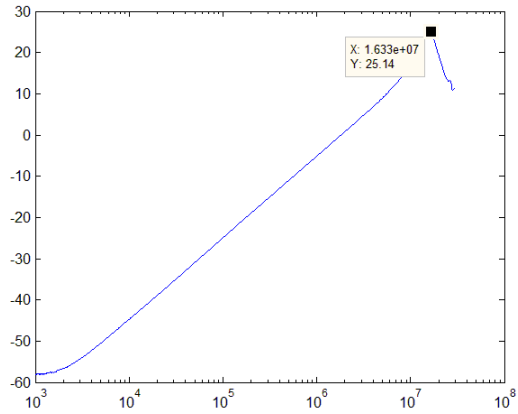


Figure 11-48 A 1 turn Litz wire on a KoolMμ core NB add 20 db to the amplitude

**5 Turns**

The second measurement with a 0077715A7 core with 5 turns of Litz wire can be seen in Table 11-2 however the inductance is likely smaller which increases C.

Table 11-12 Parameters for a 5 turn KoolMμ core

L [μH]	C [pF]	f <sub>0</sub> [kHz]
5.13	41	10970

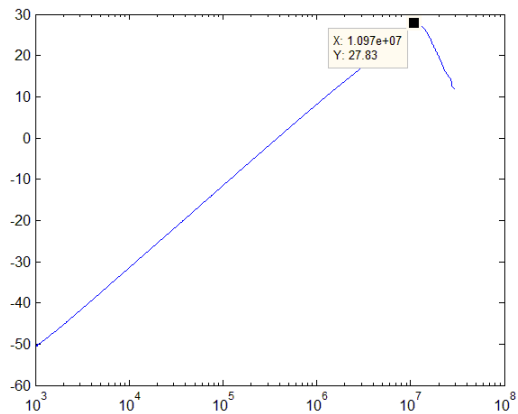


Figure 11-49 A 5 turn KoolMμ core NB add 20 db to the amplitude

**8 Turns**

The third measurement with a 0077715A7 core with 8 turns of Litz wire can be seen in Table 11-13 however the inductance is likely smaller which increases C, however there was no data available to adjust the inductance, but this do not change SRF

Table 11-13 Parameters for a 5 turn KoolMμ core

L [μH]	C [pF]	f <sub>0</sub> [kHz]
11.6	36.6	7721

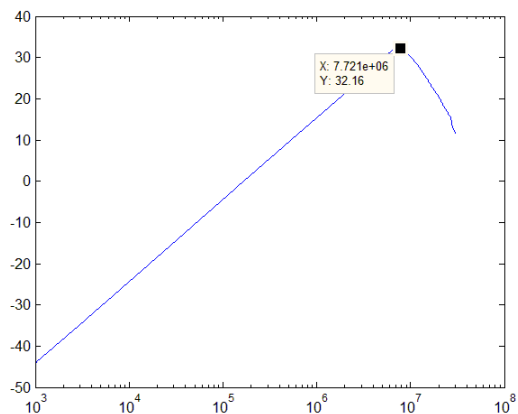


Figure 11-50 A 8 turn KoolMμ core NB add 20 db to the amplitude



**11 Turns**

The fourth measurement was done with a 0077715A7 core with 11 turns of Litz wire. The data can be seen in Table 11-14.

Table 11-14 Parameters for a 5 turn KoolM $\mu$  core

L [ $\mu$ H]	C [pF]	$f_0$ [kHz]
14.904 <sup>1</sup>	57 <sup>2</sup>	5462

<sup>1</sup>Adjusted from 20.7 mH <sup>2</sup>41 pF before adjustment

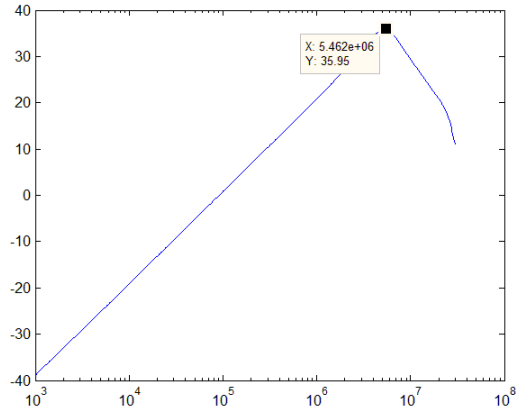


Figure 11-51 A 11 turn KoolM $\mu$  core NB add 20 db to the amplitude

The measurement has large sources of error but based on the data there is a trend pointing towards a minimum of inductance at x turns, which means that if you want minimum leakage capacitance you might want to have a higher inductance than necessary.

**11.3.4 Enamel windings**

The previous tests were performed with Litz wire windings which due to the large insulation to cobber factor is expected to have quite high leakage capacitance. To get an idea about how large the difference between enamel windings and Litz wire a 100 turn Litz wire was compared to a 136 turn high flux core with enamel winding see Figure 11-52 and Figure 11-53. The measurements show a very large reduction leakage capacitance for enamel windings see Table 11-15. The Litz wire has fewer turns on a larger core than the enamel, and still has 3 x more leakage capacitance. Therefore by using enamel windings the leakage capacitance is severely reduced by a factor of around 4.8.

Table 11-15 Litz wire and enamel comparison

Core	L [ $\mu$ H]	C [pF]	$f_0$ [kHz]
100 turn Litz wire	1693	552	188
136 turn enamel	2158	159	267

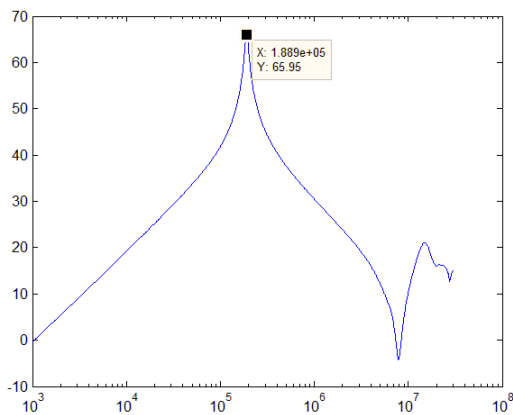


Figure 11-52 A 100 turn koolM $\mu$  core with 100 turns of Litz wire 120 x 0.1mm

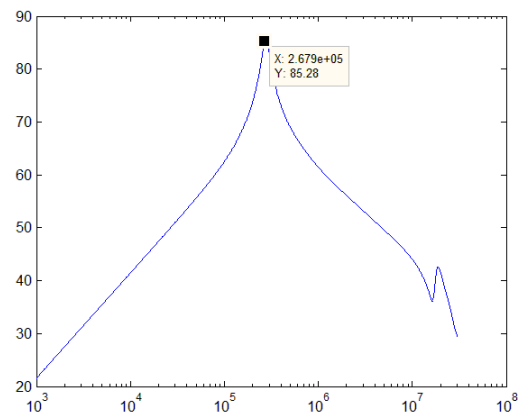


Figure 11-53 A 136 turns high flux 160 core with 136 turns of enamel wire 1 x 1.15 mm

**11.3.5 Leakage capacitance in a hybrid winding of enamel and Litz wire**

It was shown in previous sections that when windings is put in series the leakage capacitance is reduced, therefore by winding a part of a winding with enamel the leakage capacitance should be decreased. A 0077715A7 core was wound with 100 turns of Litz wire and 10 turns of enamel the result reduced the leakage capacitance by 25 % and increased the inductance by 16 %. This configuration could be used in cases where the leakage capacitance is higher than the limit and only a small increase in loss can be tolerated. However it is likely the winding configuration can be improved by further investigation.

Table 11-16 100 Litz wire versus hybrid winding of 100 turn Litz with 10 turns enamel

Core	L [ $\mu$ H]	C [pF]	$f_0$ [kHz]
100 turn Litz wire	1693	552	188
100 turn Litz 10 enamel	1967	411	177

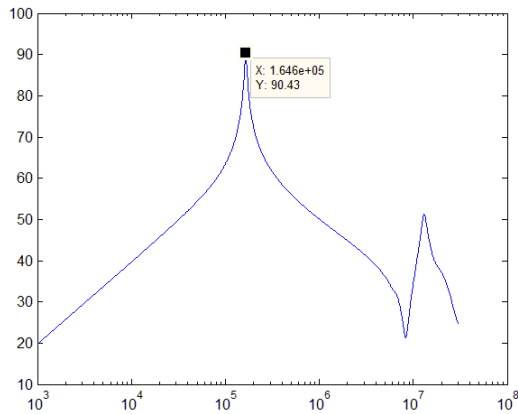


Figure 11-54 A 100 turn KoolM $\mu$  core with 100 turns of Litz wire 120 x 0.1mm

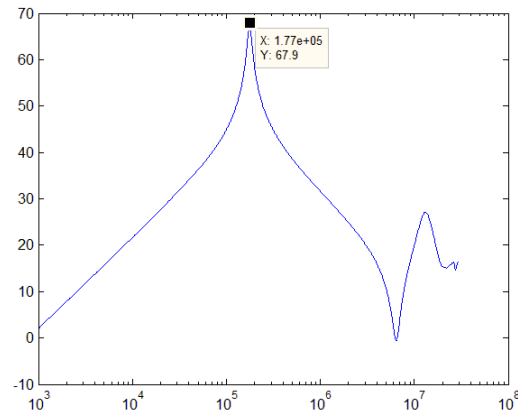


Figure 11-55 A 100 turn KoolM $\mu$  core with 100 turns of Litz wire 120 x 0.1mm and 10 turns of enamel 1 x 1.15 mm 20 db need to be added to the vertical axis

**11.3.6 Temperature and Leakage capacitance**

The leakage capacitance was measured at 22°C and at 118°C for two different windings, to determine if there is any temperature effect on leakage capacitance. It can be seen in Table 11-17 that there is a large reduction in leakage capacitance compared to the initial values. The leakage capacitance at 22°C was measured after the high temperature exposure showing that this was a permanent reduction. A possible explanation could be that the insulation should be easy to bend and fit onto the component, and therefore not fully hardened coming from the manufacturer. Under operation the temperature of the component will rise and finish the hardening process and thereby changing the leakage capacitance. This means that in any leakage capacitance tests of the component should be performed after the component have been heated and the initial values might overestimate the leakage capacitance, but this should be further investigated.

Table 11-17 Leakage capacitance comparison at elevated temperatures

Core	L [ $\mu$ H]	C [pF]	$f_0$ [kHz]
100 turn Litz 22°C	1693	552.23	164
100 turn Litz 118°C	1693	425.58	187
136 turn enamel 22°C	2158	159.12	269
136 turn enamel 118°C	2158	103.29	337

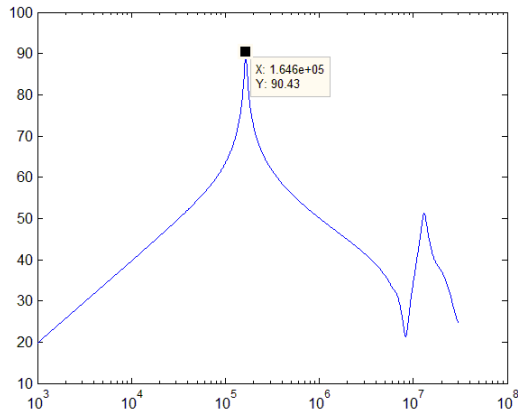


Figure 11-56 A 100 turn KoolM $\mu$  core with 100 turns of Litz wire 120 x 0.1mm at 20°C

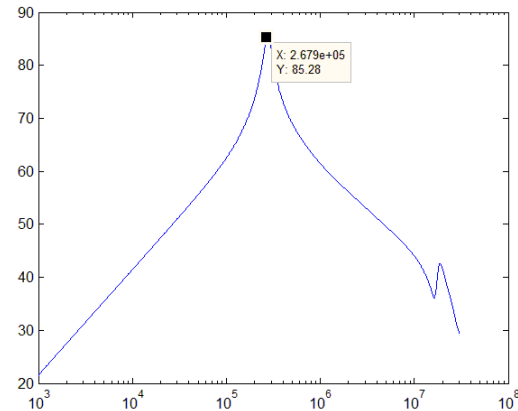


Figure 11-57 A 100 turn High Flux core with 136 turns of Litz wire 1 x 1.15 at 20°C

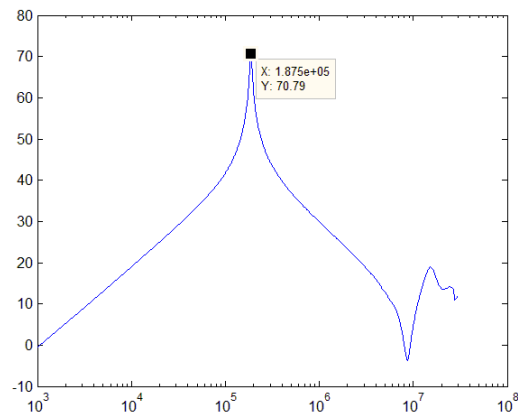


Figure 11-58 A 100 turn KoolM $\mu$  core with 100 turns of Litz wire 120 x 0.1mm at 118°C

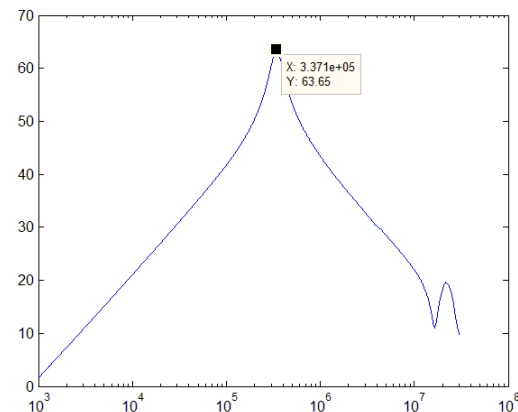


Figure 11-59 A 100 turn High Flux core with 136 turns of Litz wire 1 x 1.15 at 118°C

Comparing all the values of leakage capacitance in this section it can be seen that leakage capacitance is around 5.5 pF per turn in Litz wire this relationship is present in 50 turn, 100 and 11 turns. There was only one core with enamel which means it is not possible to draw any conclusions however in the one sample the leakage capacitance was 1.17 per turn. This could be used for a crude estimate of leakage capacitance in the case of Litz wire from Block-Trafo in small toroid cores however winding technique can change this allot.

### 11.4 References

[1] Magnetics® Technical Bulletin “Powder Core Catalog” 2011

## 12 Conclusions

This report presents design of magnetic components intended for applications with temperature up to 200°C with a focus on SiC power electronics. The effect of using SiC over conventional Si switches has been investigated theoretically, and the results are that the leakage current is reduced, the on resistance so low that it can lead to larger ringing effects, since the system is close to being undamped. High breakdown voltage leads to higher possible operation temperatures, and the drift region can be made shorter increasing  $dv/dt$ . Silicon carbide switches have lower losses, and switching time which give the possibility to increase the switching frequency. This can be used to create smaller and more compact filters which would be benefit able in down-hole applications.

Magnetic materials for high temperatures have been investigated, and powder cores and ferrites for higher temperatures are listed in chapter 4. The conclusion is that there are a large number of materials with high curie temperature, but the lamination and isolation, limits this temperature at a maximum 200°C for coated cores. This could be related to low incentives to develop magnetic materials for high temperatures due to little demand.

The losses in the magnetic cores have been investigated and several different loss models based on the Steinmetz parameters have been presented. The original Steinmetz equation do not take into account non-sinusoidal loss and it has been shown that this can underestimate the loss significantly and in some cases over half the loss is unaccounted for. The analytical data provided by the manufactures in this case Magnetics® is only accurate for High Flux while there is large deviations in MPP and  $K_{oolM\mu}$ . However some of this deviation could be related to the measurement setup and small sample sizes. New Steinmetz parameters were calculated for the  $K_{oolM\mu}$  and MPP for 5 kHz and 20 kHz. The temperature primarily affects  $K_{oolM\mu}$  by a factor of up to 20 % at 180°C while in MPP and High flux no significant effect was observed.

Windings tested in this report have indicated that at elevated temperatures enamel windings have a tendency to be damaged before the maximum operation temperature is reached, along the areas where the wires have been bent. This effect makes Litz wires or other wires with insulation that can handle bending a better option at higher temperatures. However Litz wire for 200°C do not seem to exist commercially, but Litz wire for 130°C was successfully used at 180°C and above for several days of discontinues use.

It was found that paralleling of inductors might result in smaller design, when the magnetic material is a powder cores due to the large influence of the magnetic field strength on inductance. This will also result in a better thermal design. A configuration of this have been built and tested. However more turns is necessary on the cores which would result in higher leakage capacitance and in parallel the leakage capacitance add together which means the capacitance might nearly double.

The leakage capacitance in multilayer Litz wire is quite high, but can be reduced by at least 50 % by inserting an air gap between the layers or by using bank windings. Enamel round wires have much lower leakage capacitance than a similar Litz wire bunt, and due to the properties of leakage capacitance in series the minimum leakage capacitance is not obtained at 1 turn but at  $x$  turns. The temperature does not affect leakage capacitance much after the windings have been heated up

once. Powder cores have high frequency dependence, and the inductance is drastically reduced as the frequency increases above 1-2 MHz.

An analytical design tool for optimized design of high temperature inductors have been developed and used to design prototypes. The software has quite high correlation with the measured values but due to the materials permeability deviation of 8%, the accuracy depends allot on the real permeability of the materials. The primary use for the software is output inductors with sinusoidal AC waveform but by changing the input parameters both AC and DC designs can be obtained.

### 13 Further Work

The software should be improved with a better iterative solver to speed up some iterating loops, and dowels equations should be updated so they take non sinusoidal waveforms into account. Core losses should also take into account non sinusoidal waveforms. The ferrite part of the analytical tool was not complete and tested by the end of the thesis due to time constraints, this part should be completed. The thermal models should be fully implemented and the analytical approaches to effects of using SiC over Si should be verified by experiments and if any significant effects are discovered should be included into the analytical tool. In a toroid configuration the number of layers on the inner surface is larger than on the outer, this effect should be further investigated to see how it affects the losses.

It was discovered that enamel windings with a diameter of 1.15 mm have a tendency to be damaged below the rated temperature where the winding have been bent, this is likely caused by stresses in the insulation during the bending which at higher temperature results in insulation failure, this should be investigated further.

An investigation into larger filters could be performed and the design further extended to 100 kW it might be possible to use several smaller inductors to build the large filter.

Further investigation of paralleling inductors should be conducted and rules to when it would be better to parallel found. The loss up to 100 kHz should be investigated further with a larger sample sizes and higher temperature with a more accurate tool than in this thesis. It was only possible to test one sample of each core material in the core loss characterization due to time constraints, and therefore it was not possible to rule out that there might be large deviations among the samples, this should be further investigated

The next step after the analytical tool is completed is to design a SiC circuit. This requires building the gate driver and passive components and test the full system. Finally a three phase SiC circuit should be built and tested.

## A Appendixes

### Definitions:

Al	Nominal inductance	$nH \cdot N^{-2}$
le	Mean magnetic path	cm
Ae	Core cross section	$cm^2$
$\mu$	Permeability	$Wb \cdot m^3 A^{-1}$
I	Current	A
$I_{dc}$	Direct current	A
$I_{ac}$	Alternating fundamental current	A
$I_{ac ripple}$	High frequency ripple current	A
$V_e$	Core volume	$m^3$
$B_{peak}$	Maximum flux density	T
$\rho$	Resistivity	$\Omega \cdot m$
$\rho_0$	Resistivity at 20 degrees	$\Omega \cdot m$
$\alpha_r$	Temperature coefficient	1
$A_{wire}$	Cross section of the wire	$m^2$
$A_w$	Area of the core window	$m^2$
$k_{cu}$	Winding factor	1
MLT	Mean length per turn	m
$R_y$	Core outer radius	m
$R_i$	Core inner radius	m
$D_y$	Core outer diameter	m
$D_i$	Core inner diameter	m
H	Core height	m
$N_{cores}$	The number of cores stacked	1
S	Surface	$m^2$
P	Power loss	W
$T_{increase}$	Temperature increase	K
N	Number of turns	1
Al	Nominal Inductance	$nH/N^2$
$\mu_T correction$	Permeability correction for temperature	1
$\mu_H correction$	Permeability correction for magnetizing field	1
$\mu_F correction$	Permeability correction for frequency	1
$\mu correction$	Total permeability correction	1
$K_l$	Number of layers	1
$R_w$	Wire radius	m
$D_w$	Wire Diameter	m

## B Appendix Software for design of Powder cores Inductors

Optimizing the volume in magnetic components requires a case to case design with appropriate choice of materials, cooling, and winding configuration. This is usually done by selection from a chart based on the energy storage, which is provided by manufacturers. This is a simple and fast selection process but is not optimized and focuses on the saturation and thermal limit. In cases with a wide range of switching frequencies, temperature changes, and saturation flux where little information is given and with the permeability changing due to different factors a computerized selection process is preferred.

Several magnetic optimizing programs are available but all they are based on normal operation temperatures which are below 130 C and therefore a new program was created. In the following sections the main equations and principles found in the program will be given.

### I. Turns

The number of turns:

$$N = \sqrt{\frac{L}{Al \cdot 10^{-9}}} \quad \text{Equation 14-1}$$

### II. Fill factor

$$k_{cu} = \frac{NA_{wire}}{A_w} \quad \text{Equation 13-2}$$

### III. Mean length per turn

Mean length per turn (MLT) can be calculated from the core dimensions assuming the area of a single winding can be modeled as a square.

$$MLT_i = 2(R_y - R_i + H \cdot N_{cores}) \quad \text{Equation 13-3}$$

The windings themselves increase the MLT. This was approximated by assuming that the MLT increases by one 4<sup>th</sup> of a circle in each corner multiplied with the wire radius. This was approximated by Equation 13-4 which resulted in an improvement of 8% compared to using square corners see appendix F where the initial approximation gave an error of 43 %.

$$MLT = MLT_i + \pi((K_l - 1)D_w + D_w) \quad \text{Equation 13-4}$$

The resulting 35 % deviation from the real value is likely due to that more windings per layer fit into the outer diameter of a toroid compare to the inner. This approximation is not enough in a toroid due to the difference in circumference from the outer to the inner part of the core you can fit allot more turns at the outside leading to this part of the winding growing slower than the inner. See Figure 13-1 Toroid winding configuration.



This effect was approximated by using partly equation 10 and assuming that the corner diameter in the outer diameter only is increasing by  $\frac{R_i}{R_y}$  compared to the inner.

$$MLT = MLT_i + \frac{\pi((K_l-1)D_w+D_w)}{2} + \frac{\pi\left(\left(\frac{K_l R_i}{R_y}-1\right)D_w+D_w\right)}{2} \quad \text{Equation 13-5}$$

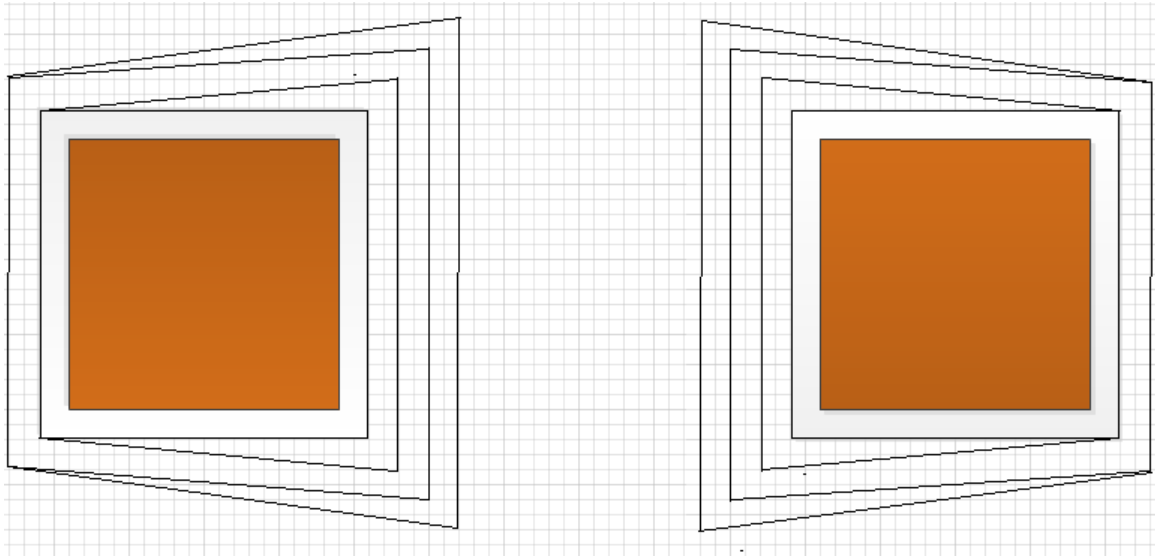


Figure 13-1 Toroid winding configuration

Equation 13-5 assumes square fitting of the wires but this might not be the case therefore it was assumed that hexagonal fitting is most likely see Figure 13-2 for square and hexagonal fitting.

The large number of factors affecting MLT means that a simple approximation is necessary and according to [5] Equation 13-6 is a good approximation which according to the real wound core in appendix F only have a 12.4 % deviation.

$$MLT = 0.8(OD + 2H) \quad \text{Equation 13-6}$$

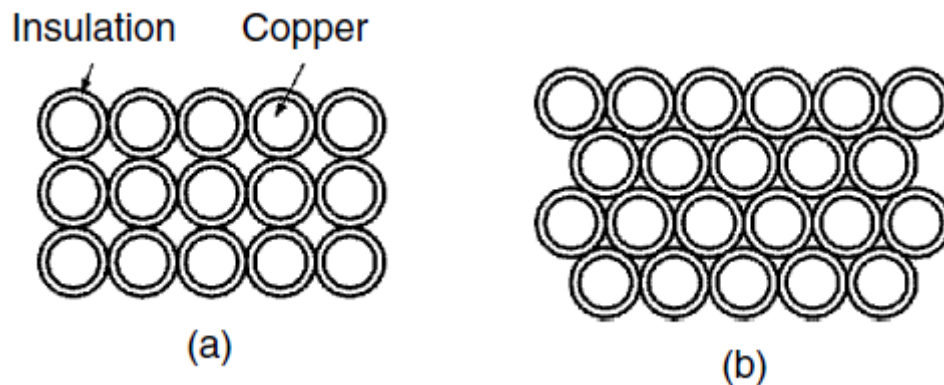


Figure 13-2 (a) Square fitting (b) hexagonal fitting [4].

#### IV. Hdc

The magnetic field strength have a large influence on the permeability.

$$H = \frac{NI_{dc}}{le} \quad \text{Equation 13-7}$$

#### V. Flux density

The maximum flux which is used to calculate the losses is found by using amperes law Equation 13-8. This is done for the ripple frequency and the fundamental frequency. According to [3] for transformers this is set with a 10 – 20 % safety margin between the saturation flux and Bpeak.

$$B = \frac{\mu NI_{ac,ripple}}{le} \quad \text{Equation 13-8}$$

#### VI. Permeability correction

The powder cores permeability need to be adjusted especially for dc bias and frequency and in higher temperature operation.

$$\mu_T \text{ correction} = 1 + (a + bT + cT^2 + dT^3) \quad \text{Equation 13-9}$$

$$\mu_H \text{ correction} = (a + bH + cH^2 + dH^3 + eH^4) \quad \text{Equation 13-10}$$

$$\mu_F \text{ correction} = 1 + (a + bF + cF^2 + dF^3 + eF^4) \quad \text{Equation 13-11}$$

$$\mu \text{ correction} = \mu_T \text{ correction} \cdot \mu_H \text{ correction} \cdot \mu_F \text{ correction} \quad \text{Equation 13-12}$$

The parameter which is the largest contributor to permeability change in powder cores is the dc-bias experienced at peak fundamental current. The roll off in permeability follows the initial permeability leading to that high permeability cores have a larger change with dc bias. These equations are only accurate at permeability changes above 40 %.

#### VII. The power handling capability of the core

The energy storage capability of the core is related to the equation bellow and the program starts by checking that the chosen core can handle the energy requirement.  $\mu$  depends on allot of factors therefore a maximum roll off in permeability was hardcoded to be 1% meaning all cores which will have a roll off larger than 50% is not checked. The maximum peak flux cannot be above the saturation flux density therefore  $B_{peak}$  is given.

$$\mu I^2 L = V_e B_{peak}^2 \quad \text{Equation 13-13}$$

## VIII. Resistance

Resistance of copper is a function of temperature and the dc resistance is taken into account by the following formulas:

$$\rho = \rho_0(1 + \alpha_r(T - 20))$$

$$R_{dc} = \frac{1}{\rho} \cdot \frac{l}{A_{wire}}$$

$$\rho_0(\Omega m) = 1.68 * 10^{-8} \alpha(k^{-1}) = 0.0039, l \text{ length of wire}$$

The Ac resistance is a function of frequency, temperature, layers and is described in [2]. The factor m is the number of layers.

$$D_{pen} = \text{sqrt}\left(\frac{\rho}{\mu\pi f}\right) \quad \text{Equation 13-14}$$

$$x = \frac{r_{wire}}{D_{pen}} \quad \text{Equation 13-15}$$

$$M = x \left( \frac{\sinh(2x) + \sin(2x)}{\cosh(2x) - \cos(2x)} \right) \quad \text{Equation 13-16}$$

$$D = \frac{2x(\sinh(x) - \sin(x))}{\cosh(x) + \cos(x)} \quad \text{Equation 13-17}$$

$$Fr = M + D(m^2 - 1)/3 \quad \text{Equation 13-18}$$

The ac resistance is finally found by Equation 13-19.

$$R_{ac} = Fr \cdot R_{dc} \quad \text{Equation 13-19}$$

The ac resistance can be calculated for each frequency and this is done for the fundamental and the switching frequency.

## IX. Power Loss

The power losses leads to heating of the design and depending on the shape of the core a couple of guidelines should be noted. In the case of a toroid shape it is easy to dissipate great copper loss since the windings are exposed to the outside air or liquid flow. In a core loss dominated design the losses are trapped inside of the windings leading to increased temperature and this should be avoided if possible by changing the configuration.

### Copper loss

The magnetic field in inductors and transformers are produced by windings normally consisting of copper conductors, copper has high conductivity but the winding losses are still large and have to be included in an accurate model. The copper losses is calculated based on the length of the wire

multiplied with the resistance, there are 3 components calculated dc, ac and ac ripple and the losses are finally summed.

### Core losses

The core losses are calculated based on Steinmetz equation and the fundamental losses and high frequency losses are summed. This is due to the fundamental flux density being a magnitude larger than the high frequency ripple.

## X. Surface area

The surface area of the core is increased due to the windings which are added and this surface increase is estimated by the following formulas.

$$R_{new} = k_{cu}^{0.5} * R_i \quad \text{Equation 13-20}$$

$$R_y = R_{yold} + R_{new} \quad \text{Equation 13-21}$$

$$R_i = R_{iold} - 2R_{new} \quad \text{Equation 13-22}$$

$$H = H_{old} + 2R_{new} \quad \text{Equation 13-23}$$

$$S = 2\pi(R_y^2 - R_i^2) + 2\pi(R_y + R_i) \quad \text{Equation 13-24}$$

## XI. Thermal

The temperature increase is estimated by a best fit curve based on empirical data

$$T_{increase} = \left(\frac{P}{S}\right)^{0.833} \quad \text{Equation 13-25}$$

## XII. Layers

The windings need to be configured into. This factor is important to estimate the winding losses due to proximity effects. This is done by an iterative process which take the inner diameter of the core removes the diameter of the wire and calculates how many turns which goes into that layer, then the process is repeated until all turns are located. Due to that it is not possible to perfectly model the reality where turns is not fitted perfectly and you have toroid where windings will not perfectly follow a loop as mentioned above a factor of  $1.1^{K_l}$  was added based on data from appendix F.

## XIII. Leakage inductance

The leakage inductance is created due to stray flux which is not enclosed in the magnetic material this inductance adds to the total inductance of the core and an estimated formula with up to 50 % deviation is provided by the manufacturer [1] see Equation 13-26 however the leakage inductance in toroid power cores are very small.

$L_{lx}$  = Leakage inductance  $\mu\text{H}$

N = Turns

Ae = Core cross section mm<sup>2</sup>  
le = Core magnetic path mm

$$L_{lx} = \frac{0.292N^{1.065}Ae}{le} \quad \text{Equation 13-26}$$

The way this inductance is used by the program is that the leakage inductance is transferred into Al and added to the core Al.

#### **XIV. Stacking cores**

The magnetic cores can be stacked and by that overall gaining a smaller volume at a lower radius or similar this is implanted as simple scaling up the input data from the cores so Ae, Ve, H is multiplied with the number of cores wanted, and saved back into the data changing the data for all equations in the program.

#### **XV. Iterative process**

The core optimizing process takes in tables containing the characteristics of commercial cores and redesigns the inductors magnetic arrangement to fulfill the input parameters. This is performed until the temperature stabilizes so that the temperature change from on step to the next is lower than the input constraint. The final magnetic arrangement is checked against the input parameters and only if these are fulfilled the core will be saved.

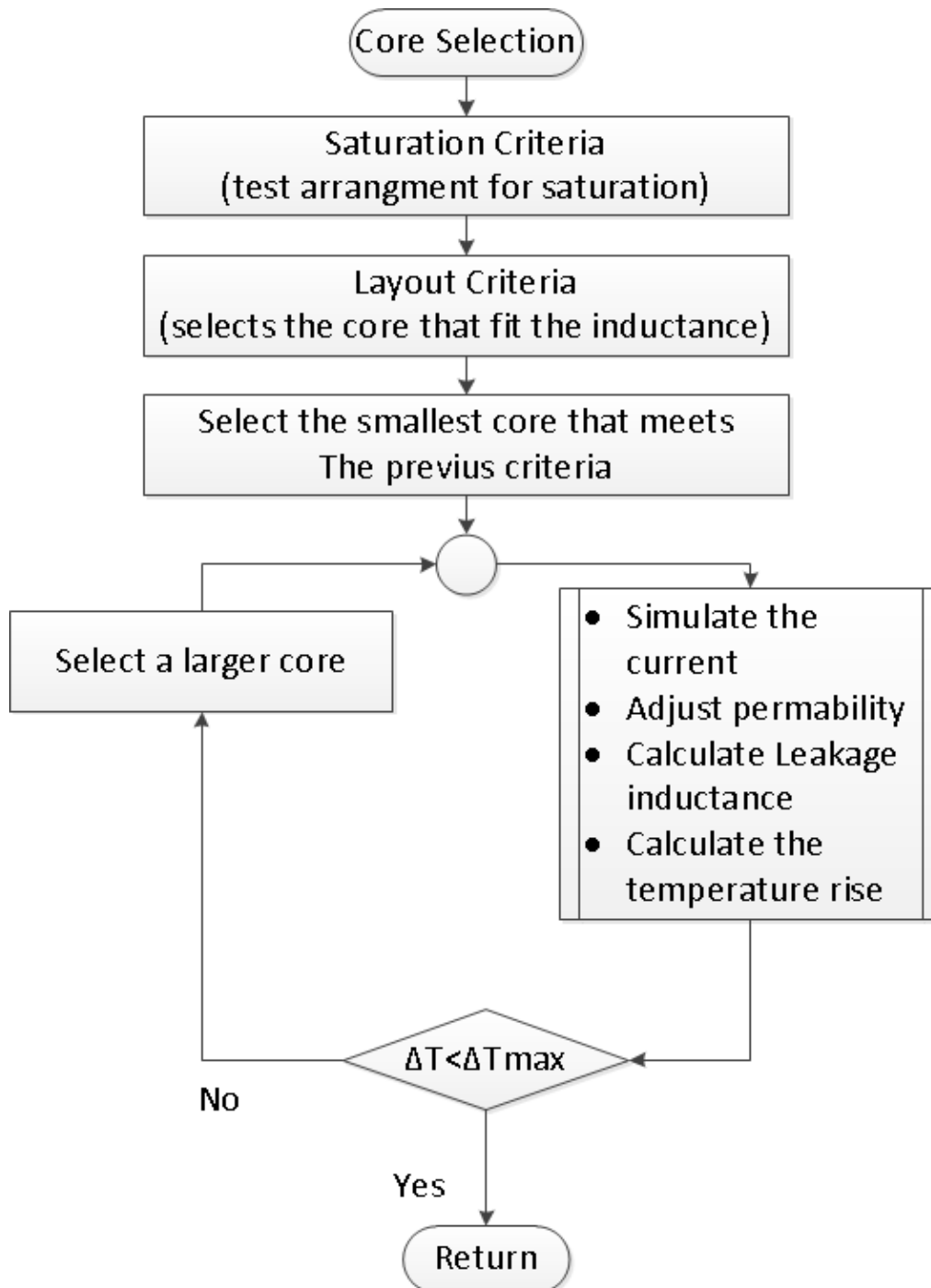


Figure 13-3 Simple flow chart of the Iterative process

## XVI. References

- [1] "Magnetics® powder catalog 2012".
- [2] R. Lund Memo "Output Filter Considerations In High Switching Inverters"
- [3] Ortiz, G.; Biela, J.; Kolar, J.W.; , "Optimized design of medium frequency transformers with high isolation requirements," *IECON 2010 - 36th Annual Conference on IEEE Industrial Electronics Society* , vol., no., pp.631-638, 7-10 Nov. 2010
- [4] A. Bossche, V. Valchev Inductors and Transformers for Power Electronics 2005
- [5] C. McLyman Transformer and Inductor Design Handbook

## C Appendix Software to design Ferrite Inductors

The magnetic materials chosen for high temperature operation is the R, P and T materials from magnetics®. The manufacturer has provided data about the operation up to 125 degrees Celsius and above this the information should not be used, due to this measurements of the permeability and losses with varying temperature should be performed. According [2] the change in permeability is not critical due to the air gap limiting this property and the temperature shift is low. Temperature does affect the losses extensively. Most of the equations in the previous appendix is used for ferrite inductors also and will not be repeated.

### I. Energy storage capability

The analytical design for soft ferrites is performed in the python program following Equation 13-27 which is based on the energy storage capability of the core.  $B_{peak}$  was equaled to the maximum saturation flux density. Note that the saturation flux density depends on the temperature but this has not been included.

$$\mu_e = V_e \cdot \frac{B_{peak}^2}{\mu_0 I^2 L} \quad \text{Equation 13-27}$$

### II. Permeability

The effective permeability is used to calculate the necessary air gap with Equation 13-28

$$\frac{1}{\mu_e} = \frac{1}{\mu_i} + \frac{l_g}{l_e} \quad \text{Equation 13-28}$$

The stability of the initial core permeability has less importance in ferrites compared to powder cores due to the air gap which stabilizes the permeability.

Inserting values for a R material with  $\mu_i = 2300$   $l_g = 0.26\text{mm}$  and  $l_e = 138\text{mm}$  into Equation 13-28 yields the results in Table 13-1. For permeability which have changed to 25% 50% 150% and 175% of its original value. It can be seen that the effective permeability change much less than the core permeability.

Table 13-1 The permeability stability in a ferrite air gap 0.26mm  $l_e$  138mm and  $\mu$  2300

Permeability deviation	Value	$\mu_e$
$\mu(0\%)$	= 2300	431.25
$\mu(25\%)$	= 575	276
$\mu(50\%)$	= 1150	363.15
$\mu(150\%)$	= 3450	460
$\mu(175\%)$	= 4025	468.93

The turns can then be calculated and rounded up or down to nearest integer note that this can cause large change of the inductance in the case of few windings and if it is rounded up unnecessary windings results in larger losses.

Turns

$$N = \text{round}\left(\sqrt{\frac{L \cdot l_e}{\mu_e \mu_0 A e}}\right)$$

The flux density depends on N so the rounding changes the flux density and this is recalculated with the change in windings this could result in going above the saturation flux density but the resulting output information should clear up if this would pose a problem.

The losses and other properties are calculated in the same manner as in powder cores.

### III. References

- [1] C. McLyman Transformer And Inductor Design Handbook 3e 2004
- [2] Magnetics® Technical Bulletin “Using Magnetic Cores at High Temperatures”



## D Appendix Measurements & Calculations

### I. Measurements Up to 100 kHz 20°C

The 100 kHz measurements were performed with an oscilloscope with a power module that calculates the power based on the 2500 measurement point taken in by the oscilloscope. The signal was generated by a function generator and the voltage and frequency adjusted until there was less than 1% error between the wanted numbers and the real values. An Amplifier increased the current up to a usable level and the magnetic cores which is described in Table 10-3 was connected between the outputs. The winding losses was estimated based on the dc resistance and the cycl rms current this could be done since the windings are Litz wire and therefore would have a close resistance to the dc resistance. In the measurements the temperature effect on resistance was not taken into account but the measurements was performed with low  $\Delta T$  in the material due to the low power loss in most samples.

Table 13-2 measurements from 5 – 100 kHz at 20°C

Core	Flux Density [mT]	Frequency [kHz]	Winding losses [W]	Brochause [mW/cm <sup>3</sup> ]	Oscilloscope [mW/cm <sup>3</sup> ]	Power meter [mW/cm <sup>3</sup> ]	Analytical [mW/cm <sup>3</sup> ]	Tc +/-1C	Ta +/-1C	Tdc comparison
MPP	25	5	-	1.66	-	-	0.55			
MPP	50	5	0.24	6	10.3	10.4	1.719			
MPP	75	5	0.51	21.6	22.16	31.41	4.3			
MPP	100	5	0.88	89	35.2	46.15	8	26.0	22	35
MPP	25	20	0.0593		6.58	9	3.61			
MPP	50	20	0.237		29.67	50.19	16.58			
MPP	75	20	0.521		72.37	114	40.47			
MPP	100	20	0.966		132.3	200.9	76.22	35.7	22	47
MPP	25	50	0.0586		18.29		16			
MPP	50	50	0.2333		155.55		73.87			
MPP	75	50	0.517		346.8		180	43.4	22	57
MPP	100	50	-		-		-			
MPP	25	100	0.063		81.21		49.46			
MPP	48	100	0.617*		354.67		228	48.1	22	
MPP	75	100	-		-		-			
MPP	100	100	-		-		-			

Core	Flux Density [mT]	Frequency [kHz]	Winding losses [W]	Brochause [mW/cm <sup>3</sup> ]	Oscilloscope [mW/cm <sup>3</sup> ]	Power meter [mW/cm <sup>3</sup> ]	Analytical [mW/cm <sup>3</sup> ]	Tc +/-1C	Ta +/-1C
------	-------------------	-----------------	--------------------	---------------------------------	------------------------------------	-----------------------------------	----------------------------------	----------	----------

KoolMμ	25	5	0.0669	2	3.71	3.33	0.37		
KoolMμ	50	5	0.25	8	16.28	15.72	1.73		
KoolMμ	75	5	0.615	28	32.38	36.79	4.22	28.7	22
KoolMμ	25	20	0.0628		9.44	14.28	3.6		
KoolMμ	50	20	0.2446		43.8	65.12	16.58		
KoolMμ	75	20	0.539		109.47	148.46	40.47	33.4	22
KoolMμ	25	50	0.0608		28.12		16		
KoolMμ	50	50	0.2433		124.32		73		
KoolMμ	75	50	0.5574		310.8		180	50	22
KoolMμ	25	100	0.0642		62		49		
KoolMμ	44	100	0.5942*		145.95*		228	48.6	22
					*				
Core	Flux Density [mT]	Frequency [kHz]	Winding losses [W]	Brochause [mW/cm <sup>3</sup> ]	Oscilloscope [mW/cm <sup>3</sup> ]	Power meter [mW/cm <sup>3</sup> ]	Analytical [mW/cm <sup>3</sup> ]	Tc +/-1C	Ta +/-1C
HighFlux	25	5	0.0190		0.4858	5.06			
HighFlux	50	5	0.0687		3.34	7.53			
HighFlux	75	5	0.152		9.82	16.32			
HighFlux	100	5	0.2717		18.38	23.68			
HighFlux	125	5	0.4176		29.24	39.12			
HighFlux	150	5	0.6209	109	44.59	52.79		29.7	22 35
HighFlux	25	20	0.0191		7.8	5			
HighFlux	50	20	0.0702		39.71	36.1			
HighFlux	75	20	0.158		100.13	123.27			
HighFlux	100	20	0.279		183.28	245.9			
HighFlux	125	20	0.4259		290.14	398			
HighFlux	150	20	0.6133		447.4	575.11		43.4	22
HighFlux	25	50	0.0184		23.5				
HighFlux	50	50	0.0736		124.9				
HighFlux	75	50	0.1626		320				
HighFlux	100	50	0.2794		574				
HighFlux	125	50	0.4276		906.6				
HighFlux	150	50	0.6133		1418			80.5	22
HighFlux	25	100	0.0292		65.99		61.11		
HighFlux	50	100	0.0765		309		300		
HighFlux	75	100	0.1721		768.1		764		
HighFlux	100	100	0.2753		1949		1482	65.3	22

\*Winding number was decreased \*\*Most likely measurement error \*\*\*Damage to the windings when they were adjusted.

Core	Flux Density [mT]	Frequency [kHz]	Winding losses [W]	Brochause [mW/cm <sup>3</sup> ]	Oscilloscope [mW/cm <sup>3</sup> ]	Power meter [mW/cm <sup>3</sup> ]	Analytical [mW/cm <sup>3</sup> ]	Tc+/-1C	Ta+/-1C	Tdc comparison
MPP	25	5	-	1.66	-	-	0.55			
MPP	50	5	0.24	6	10.3	10.4	1.719			
MPP	75	5	0.51	21.6	22.16	31.41	4.3			
MPP	100	5	0.88	89	35.2	46.15	8	26.0	22	35
MPP	25	20	0.0593		6.58	9	3.61			
MPP	50	20	0.237		29.67	50.19	16.58			
MPP	75	20	0.521		72.37	114	40.47			
MPP	100	20	0.966		132.3	200.9	76.22	35.7	22	47
MPP	25	50	0.0586		18.29		16			
MPP	50	50	0.2333		155.55		73.87			
MPP	75	50	0.517		346.8		180	43.4	22	57
MPP	100	50	-		-		-			
MPP	25	100	0.063		81.21		49.46			
MPP	48	100	0.617*		354.67		228	48.1	22	
MPP	75	100	-		-		-			
MPP	100	100	-		-		-			
KoolMμ	25	5	0.0669	2	3.71	3.33	0.37			
KoolMμ	50	5	0.25	8	16.28	15.72	1.73			
KoolMμ	75	5	0.615	28	32.38	36.79	4.22	28.7	22	
KoolMμ	25	20	0.0628		9.44	14.28	3.6			
KoolMμ	50	20	0.2446		43.8	65.12	16.58			
KoolMμ	75	20	0.539		109.47	148.46	40.47	33.4	22	
KoolMμ	25	50	0.0608		28.12		16			
KoolMμ	50	50	0.2433		124.32		73			
KoolMμ	75	50	0.5574		310.8		180	50	22	
KoolMμ	25	100	0.0642		62		49			
KoolMμ	44	100	0.5942*		145.95*		228	48.6	22	

The last high flux measurements overestimates the losses somewhat due to an increase in the resistance due to temperature however this had no significant impact on the results.

Core	Flux Density [mT]	Frequency [kHz]	Measurement 1 [mW/cm <sup>3</sup> ]	Measurement 2 [mW/cm <sup>3</sup> ]	Measurement 3	Measurement 4 [mW/cm <sup>3</sup> ]	Measurement 5 [mW/cm <sup>3</sup> ]	
HighFlux	25	5	0.649	0.564		0.68	0.7	0.89
HighFlux	50	5	4.95	4.44		4.86	4.88	4.4
HighFlux	75	5	13.5	13.08		13.76	13.72	11.19
HighFlux	100	5	25.11	25.5		26.55	26.51	21.69
HighFlux	125	5	39.24	42.5		45.49	46.11	36.25
HighFlux	150	5	61.71	57.37		66.17	66.05	55.13
HighFlux	25	20	5.57	5.63		5.16	4.94	6.31
HighFlux	50	20	32.71	34.18		30.34	30.76	31.11
HighFlux	75	20	83.53	79		71.55	74.8	79.06
HighFlux	100	20	148.7	145.9		138.8	140	153.2
HighFlux	125	20	238	243		230	226	255
HighFlux	150	20	394	395		390.5	398	389
HighFlux	25	50	18.76	21.84		18.31	16.67	22.99
HighFlux	50	50	115.8	113.1		93.25	93.47	113.3
HighFlux	75	50	293.2	295.6		255.12	250.3	287.8
HighFlux	100	50	546	548.8		467	467.2	557.7
HighFlux	125	50	858.1	858.2		744	740	931.8
HighFlux	150	50	1414	1322		1222	1227	1417
HighFlux	25	100	69	68.83		65.28	65.04	61.11
HighFlux	50	100	326	316		301.7	303.85	300
HighFlux	75	100	803	796		706.58	706	764

Core	Flux Density [mT]	Frequency [kHz]	Measurement 1 [mW/cm <sup>3</sup> ]	Measurement 2 [mW/cm <sup>3</sup> ]	Measurement 4 [mW/cm <sup>3</sup> ]	Measurement 5 [mW/cm <sup>3</sup> ]	
KoolMμ	25	5	1.33	1.41	2.40	2.44	0.37
KoolMμ	50	5	5.04	5.14	10.26	10.2	1.73
KoolMμ	75	5	8.44	8.78	20.44	20.74	4.22

KoolM $\mu$	25	20	11.15	11.59	14.3	13.92	3.6
KoolM $\mu$	50	20	53.69	50.8	66.13	65.15	16.58
KoolM $\mu$	75	20	115	119	151.9	152.92	40.47
KoolM $\mu$	25	50	36.61	36.47	43.67	43.2	16
KoolM $\mu$	50	50	153	152.9	190	184	73
KoolM $\mu$	10	100	7.34	7.9	11.85	12.58	
KoolM $\mu$	25	100	66.3	65.5	97.95	97.32	49

Core	Flux Density [mT]	Frequency [kHz]	Measurement 1 [mW/cm <sup>3</sup> ]	Measurement 2 [mW/cm <sup>3</sup> ]	Measurement 4 [mW/cm <sup>3</sup> ]	Measurement 5 [mW/cm <sup>3</sup> ]	
MPP	25	5	1.2	1.15	1.13	1.15	0.55
MPP	50	5	4.54	4.4	4.41	4.37	1.719
MPP	75	5	6.8	7.88	7.58	7.46	4.3
MPP	25	20	7.36	7.35	7.54	7.31	3.61
MPP	50	20	36.23	36.19	34.58	35.05	16.58
MPP	75	20	82.3	82.7	84.76	85.53	40.47
MPP	25	50	26.5	26.74	24.3	24.27	16
MPP	50	50	111.2	114.7	99.75	99.11	73.87
MPP	10	100	5.82	5.73	6.76	6.8	14.4
MPP	25	100	48.23	45.81	51.64	53.73	90

MPP 100 khz 25 mT 25 var 900mW

## II. Measurements Up to 100 kHz 180°C

The measurements at 100 kHz and 180°C was performed with the previous setup and a heating chamber due to the high temperature, thermal measurements would have destroyed the windings and would not be reliable with the comparisons due to the large temperature difference, the forced convection in the chamber and it was no time to get a baseline at high temperature.

Table 13-3 measurements from 5 – 100 kHz at 180°C

Core	Flux Density [mT]	Frequency [kHz]	Winding losses [W]	Brochause [mW/cm <sup>3</sup> ]	Oscilloscope [mW/cm <sup>3</sup> ]	Power meter [mW/cm <sup>3</sup> ]	Analytical [mW/cm <sup>3</sup> ]	Tc +/-1C	Ta +/-1C	Tdc comparison
MPP	25	5	0.0992		1.0	1.33	0.55		178	
MPP	50	5	0.4211		3.58	4.41	1.719		178	
MPP	75	5	0.758		7.58	11.42	4.3		178	
MPP	100	5	1.620		12.12	17.89	8		178	
MPP	25	20	0.1016		5.34	8.23	3.61		178	
MPP	50	20	0.4235		67.76	83.1	16.58		178	
MPP	75	20	0.95		164.03	201.2	40.47		178	
MPP	100	20	1.68		296.2	359.6	76.22		178	
MPP	25	50	0.107		95.65		16		178	
MPP	50	50	0.438		339.45		73.87		178	
MPP	63	50	-		-		180		178	
MPP	100	50	-		-		-		178	
MPP	25	100	0.2961		396.4		49.46		178	
MPP	33	100	0.47		841		228		178	
MPP	75	100	-		-		-		178	
MPP	100	100	-		-		-		178	
KoolMμ	25	5	0.113		2.95	2.26	0.37		177	
KoolMμ	50	5	0.39		10.77	4.98	1.73		177	
KoolMμ	75	5	1.03		26.61	10.24	4.22		177	
KoolMμ	25	20	0.1152		26.71	3.44	3.6		177	
KoolMμ	50	20	0.465		46.17	16.61	16.58		177	
KoolMμ	75	20	1.11		109	30.58	40.47		177	

<b>KoolM<math>\mu</math></b>	25	50	0.1242		29.54		16		177
<b>KoolM<math>\mu</math></b>	50	50	0.4838		134.35		73		177
<b>KoolM<math>\mu</math></b>	75	50	1.074		354.14		180		177
<b>KoolM<math>\mu</math></b>	25	100	0.0713		326.9		49		177
<b>KoolM<math>\mu</math></b>	44	100	-		-		228		177
<b>Core</b>	<b>Flux Density [mT]</b>	<b>Frequency [kHz]</b>	<b>Winding losses [W]</b>	<b>Brochouse [mW/cm<sup>3</sup>]</b>	<b>Oscilloscope [mW/cm<sup>3</sup>]</b>	<b>Power meter [mW/cm<sup>3</sup>]</b>	<b>Analytical [mW/cm<sup>3</sup>]</b>	<b>T<sub>c</sub>+/-1C</b>	<b>T<sub>a</sub>+/-1C</b>
<b>HighFlux</b>	25	5	0.0458		1.28	0.36	0.89		175
<b>HighFlux</b>	50	5	0.183		6.34	8	4.4		175
<b>HighFlux</b>	75	5	0.4253		18.22	20.39	11.19		175
<b>HighFlux</b>	100	5	0.799		32.23	24.34	21.69		175
<b>HighFlux</b>	125	5	1.193		47.33	49.74	36.25		175
<b>HighFlux</b>	150	5	0.905*		87.73	70.86	55.13		175
<b>HighFlux</b>	25	20	0.028		15.38	10.13	6.31		175
<b>HighFlux</b>	50	20	0.1074		67.6	39.17	31.11		175
<b>HighFlux</b>	75	20	0.2368		162.44	121.24	79.06		175
<b>HighFlux</b>	100	20	0.4125		271	237	153.2		175
<b>HighFlux</b>	125	20	0.6419		421	399	255		175
<b>HighFlux</b>	150	20	0.9345		642	594	389		175
<b>HighFlux</b>	25	50	0.0306		72.62		22.99		175
<b>HighFlux</b>	50	50	0.1212		317		113.3		175
<b>HighFlux</b>	75	50	0.2646		765		287.8		175
<b>HighFlux</b>	100	50	0.4681		1374		557.7		175
<b>HighFlux</b>	125	50	0.7028		2124		931.8		175
<b>HighFlux</b>	150	50	1.0549		3312		1417		175
<b>HighFlux</b>	25	100	0.0318		279		61.11		175
<b>HighFlux</b>	50	100	0.1298		1180		300		175
<b>HighFlux</b>	75	100	0.4969		2314		764		175
<b>HighFlux</b>	100	100	-		-		1482		175

\*Winding was changed

### III. Non-sinusoidal losses

The non-sinusoidal losses were investigated using the waveform generator and amplifier approach however the error in the setup caused large deviations and the testing was stopped. The initial values measured can be seen below but no conclusion can be taken since the highest loss is obtained differently at each measurement point.

Core	Flux Density [mT]	Waveform	Frequency [kHz]	Winding losses [W]	Core Losses [mW/cm <sup>3</sup> ]	Power meter [mW/cm <sup>3</sup> ]	Analytical [mW/cm <sup>3</sup> ]	Tc +/-1C	Ta +/-1C	Tdc comparison
High Flux	100	Sinus	9675	0.338	58.065					
High Flux	100	Square	9675	0.331	71.31					
High Flux	100	Triang.	9675	0.4015	57.22					
High Flux	100	Sinus	20 000	0.3785	143.24					
High Flux	100	Square	20 000	0.2595	131.21					
High Flux	100	Triang.	20 000	0.417	166.93					
High Flux	100	Sinus	50 000	0.3188	480					
High Flux	100	Square	50 000	0.283	512					
High Flux	100	Triang.	50 000	0.421	635					
High Flux	75	Sinus	100 000	0.2233	796					
High Flux	75	Square	100 000	0.178	677					
High Flux	75	Triang.	100 000	0.181	611					



## V. Filter for Buck Converter

In the filter section four different inductors was designed for filter purposes see below for a repeat of the main values. In this section the software will be used to calculate the physical size and configuration of the inductor and measured values will be included.

Buck filter specification						
$V_o$ [V]	F [kHz]	D	$\Delta I_L$ [A]	$\Delta V_o$ [V]	L [mH]	C [ $\mu$ F]
30	5	0.5	3	2.27	1	33
30	10	0.5	1.2	0.4545	1.25	33
100	10	0.5	4	1.5152	1.25	33
30	10	0.5	0.6	0.2273	2.5	33
100	10	0.5	2	0.7576	2.5	33
30	10	0.5	0.4286	0.1623	3.5	33
100	10	0.5	1.428	0.54	3.5	33
30	5	0.5	0.66	0.5	4.5	33
100	5	0.5	2.22	1.68	4.5	33

The resistive load is set to 10 $\Omega$  and the input parameters to the inductor software are recalculated to being the dc equivalent. The temperature is set to 25°C and only the cases which fit with available core materials will be used.

	Inductor 1	Inductor 2	Inductor 3
Dc Bias	3 A	2 A	5A
Ambient temp.	25°C	25°C	25°C
Peak inductance	1.25 mH	2.5 mH	1 mH
Current Peak	0.6 A	0.3 A	1.5 A
Average output Current	3 A	2 A	5 A
Ripple current	100	100	100
Fundamental frequency	1	1	1
Switching frequency	10 000 Hz	10 000 Hz	5 000 Hz
Current Density	200	200	200
Number of strands in bundle	120	120	120
Strand diameter	0.1 mm	0.1 mm	0.1 mm
Bundle diameter	1.55 mm	1.55 mm	1.55 mm

Table 13-4 Inductor analytical data and measured values

Inductor 1	Analytical prediction	Measured values		Inductor 2	Analytical prediction	Measured values	
<b>Core Data</b>	125Mμ 0077715A7			<b>Core Data</b>	160 High Flux C058583A2		
<b>Linitial</b>	1.52	1.646	mH	<b>Linitial</b>	2.91 mH	2.57	mH
<b>Lpeak</b>	1.31	1.035	mH	<b>Lpeak</b>	2.53 mH	1.68	mH
<b>I peak</b>	0.6	0.72	A	<b>I peak</b>	0.3	0.444	A
<b>Turns</b>	98	100	-	<b>Turns</b>	169	170	-
<b>Copper loss</b>	0.52810	-	W	<b>Copperloss</b>	0.276112	-	W
<b>CoreLoss</b>	0.13924	--	W	<b>CoreLoss</b>	0.233555	-	W
<b>Total Loss</b>	0.66734	1.2	W	<b>Total Loss</b>	0.509667	0.494	W
<b>Temperature</b>	4.1312	12	°C	<b>Temperature</b>	4.834313	10	°C
<b>MyCorrection</b>	0.85940	0.628	-	<b>MyCorrection</b>	0.868757	0.653	-
<b>Fill factor</b>	0.24658	0.25	-	<b>Fill factor</b>	0.80201	0.83	-

Table 13-5 Inductor analytical data and measured values

Inductor 3	Analytical prediction	Measured values	
<b>Core Data</b>	125 HighFlux C058548A2		
<b>Linitial</b>	1.77 mH	2.01	mH
<b>Lpeak</b>	1.0 mH	0.993	mH
<b>I peak</b>	1.5	1.46	A
<b>Turns</b>	118	120	-
<b>Copper loss</b>	2.83		W
<b>CoreLoss</b>	0.076		W
<b>Total Loss</b>	3.19	4.2	W
<b>Temperature</b>	38	24	°C
<b>MyCorrection</b>	0.56	0.49	-
<b>Fill factor</b>	0.34		-

## VI. Dv/dt output inductor for differential noise

-The drive specification can be viewed in the table below and dv/dt and sinus filter is calculated in the following sections.

Drive Specification	
$V_{dc}$	600 V
$S$	3k VA
$f_{sw}$	100 KHz
$f_{fund}$	50 Hz
$t_{r max}$	1 Kv/μs
$I_1$	4.71 A    PWM ma = 1 @ 367.2V <sub>LL,rms</sub>
$T_{amb}$	150 °C

## VII. Sinus output filter

Sinus output filter same as above just with lower  $\omega_0$  and inductance in the 1-10% range

$$L_f > 0.143 * 0.01$$

$$L_f > 1.43 \text{ [mH]}$$

For a sinus output filter the resonance frequency is chosen below the switching frequency.

Recommended at  $\omega_0 = \frac{f_{sw}}{3}$

$$\omega_0 < 2\pi * 33333 \text{ Hz}$$

$$C_f = \frac{1}{L_f * \omega_0^2}$$

$$C_f = \frac{1}{1.43 * 10^{-3} * (33333 * 2\pi)^2}$$

$$C_f = 1.59 * 10^{-8} \text{ [F]}$$

See Table 13-6 with recommended L from 0.25%, 1%, 2%, 3%, 6%, 10% for dv/dt filter and 1%, 2%, 3%, 6%, 10% for sinus filter.

Table 13-6 some values for LC in different filters

	L	C	R	P <sub>loss</sub>	$\omega_0$
<b>dv/dt filter 0.25%</b>	0,000358	7,77E-09	858,3916	150,98	600000
<b>Sin filter 1%</b>	0,001431	1,97E-08	0	0	188495,6
<b>1 %</b>					
<b>dv/dt filter</b>	0,001431	1,94E-09	3433,566	37,74501	600000
<b>Sin filter</b>	0,001431	1,97E-08	0	0	188495,6
<b>2 %</b>					
<b>dv/dt filter</b>	0,002861	9,71E-10	6867,133	18,8725	600000
<b>Sin filter</b>	0,002861	9,84E-09	0	0	188495,6
<b>3 %</b>					
<b>dv/dt filter</b>	0,004292	6,47E-10	10300,7	12,58167	600000
<b>Sin filter</b>	0,004292	6,56E-09	0	0	188495,6
<b>6 %</b>					
<b>dv/dt filter</b>	0,008584	3,24E-10	20601,4	6,290835	600000
<b>Sin filter</b>	0,008584	3,28E-09	0	0	188495,6
<b>10 %</b>					
<b>dv/dt filter</b>	0,014307	1,94E-10	34335,66	3,774501	600000
<b>Sin filter</b>	0,014307	1,97E-09	0	0	188495,6

Assuming 10% Ac 0% Dc at inverter frequency

---

<b>Dc-Bias at peak</b>	<b>5.99 A</b>
<b>Ac-Current 10%</b>	0.471A
<b>Fundamental freq</b>	50 Hz
<b>f<sub>sw</sub></b>	100 KHz
<b>L</b>	0,001431

---

## VIII. Parallel connection of inductors in a buck converter

Table 13-7 KoolM $\mu$  70 turns inductance at dc bias from 0-16 A

Dc Bias [A]	$\Delta I$ [A]	$V_{pp}$ [V]	F [Hz]	L [ $\mu$ H]	% of initial value
0				691	100
2	2.56	67	10 078	649	93.9
4	3.16	67	10 078	525	76
6	4.33	67	10 078	383	55.5
8	5.72	67	10 078	290	42
10	8.08	67	10 078	205	29.75
12	10	67	10 078	166	24
14	12.2	67	10 078	136	19.7
16	14.4	67	10 078	115	16.6

Table 13-8 KoolM $\mu$  two 100 turns inductors parallel connected

Dc Bias [A]	$\Delta I$ [A]	$V_{pp}$ [V]	F [Hz]	L [ $\mu$ H]	Dc current L1	Dc current L2	% of initial value
0	3.6	20.4	1972	718			100
2	2.08	68	10 078	810	0.937	0.990	112
4	2.42	68	10 078	697	1.906	2.016	97
6	3	68	10 078	562	2.9	3.06	78.3
8	3.86	68	10 078	437	3.876	4.1	60.8
10	4.76	68	10 078	354	4.85	5.125	49.3
12	5.8	68	10 078	290	5.836	6.165	40
14	7.04	68	10 078	239	6.81	7.17	33.2
16	8.56	68	10 078	197	7.85	8.26	27.4

Table 13-9 HighFlux 40 turns inductance at dc bias from 0-16 A

Dc Bias [A]	$\Delta I$ [A]	$V_{pp}$ [V]	F [Hz]	L [ $\mu$ H]	% of initial value
0	2.68	3.2	1972	151.7	100
2	10.6	69	10075	160.1	105.5
4	11.2	68.3	10075	151.3	99.7
6	13.4	67.5	10075	125	82.4
8	16.6	67	10075	100	65.91
10	20.6	66.5	10075	80	52.7
12	27.2	66	10075	60.2	39.68

Table 13-10 HighFlux two 50 turns inductors parallel connected

Dc Bias [A]	$\Delta I$ [A]	$V_{pp}$ [V]	F [Hz]	L [ $\mu$ H]	Dc current L1	Dc current L2	% of initial value
0	2.64	3.2	1972	151.7			100
2	10	69	10075	171.2	0.965	1.022	112.8
4	9.8	68	10075	172	1.94	2.06	113.4
6	10	67.3	10075	167	2.92	3.1	110
8	10.6	66.6	10075	155.9	3.84	4.08	102.7
10	11.4	66	10075	143.6	4.87	5.16	94.6
12	12.2	66	10075	134	5.86	6.18	88.3
14	13	65.5	10075	125	6.74	7.11	82.4
16	14.8	65	10075	108	7.78	8.2	71.1
18	16.2	64.5	10075	98.8	8.88	9.26	65.1
19.5	17.8	64	10075	89.2	9.5	10	58.8

## IX. N27

The N27 is a magnetic core produced by Siemens exact core data was not found and was instead measured with outer dimensions to be 102mm x 102mm (a double c core) and a cross section of 25mm x 25mm with two air gaps. The clamping pressure was not known and therefore this was ignored. The BROCHAUS MPG100 do not have a built in function to calculate C cores therefore the data have to be transformed into a toroid equivalent see chapter 10.2.1, and Table 13-11.

Table 13-11 N27 Geometric Data

Type	$A_e$	$l_e$	$V_e$	$D_y$	$D_i$	H	Density
<b>N27 C</b>	625 mm <sup>2</sup>	308 mm	166 250 mm <sup>3</sup>	-	-	-	4800 kgm <sup>-3</sup>
<b>N27 O Eq</b>	625 mm <sup>2</sup>	308 mm	166 250 mm <sup>3</sup>	73mm	123mm	25 mm	4800 kgm <sup>-3</sup>

## E Appendix Python

Python was chosen as the script language over Matlab partly to test out the scientific packages found in python(x,y) which is scientific-oriented python packages. This was a test project initiated by SmartMotor during the summer internship 2012 to see if it was possible to write a larger script without dependence on Matlab which is an expensive investment.

The conclusion is that I did not miss any part from Matlab and learned python quite fast. The main problem encountered with using python was that other software often supports Matlab and not python which in a more complex script might be beneficial.

All functions I normally use in Matlab is found in python(x,y) from for loops to graphs. Gui creation was also simplified by the tool qt designer which is made for rapid prototyping of gui's where just by dragging and dropping elements into a window a new gui can be made, and by using a several scripts the gui creation and other functions can be separated meaning new gui's can be made without changing any code in other scripts. You have to make connections for new functions but this is not complicated.

## F Mechanical measurements MLT

A magnetic Core C055251A was wound with wire size 1.12mm and 246 turns this resulted in the layer configuration 71 66 52 44 and a layer with 13. The total length equaled 14.03 meters which means the MLT = 0.0568 meters.

The initial analytical calculations resulted in an error of 22.9% and a more advanced formula decreased this error to 12.5 % which was then implanted into the software.

	Turns	Wire size	Layers	Total length	MLT
C055251A real	246	1.12 mm	71 66 52 44	14.03	0.0568
C055251A calc	246	1.12 mm	75 71 68 32	17.24	0.06982 m
match % calc/real				22.9%	22.9%
C055251A improved calc				15.76	0.06384
match % i. calc/real				12.4%	12.4%



## G Thermal Resistances

### I. Natural Convection

$$P = \alpha_{th} S_{env} (T_s - T_\infty) \quad \text{Equation 13-29}$$

$$\alpha_{th} = \frac{Nu\lambda}{L} \quad \text{Equation 13-30}$$

Horizontal

$$Nu = \left( 0.6 + 0.387 [Ra f_1(Pr)]^{\frac{1}{6}} \right)^2 \quad \text{Equation 13-31}$$

$$f_1(Pr) = \left[ 1 + \left( \frac{0.559}{Pr} \right)^{\frac{9}{16}} \right]^{-\frac{16}{9}} \quad \text{Equation 13-32}$$

$$Ra = GrPr \quad \text{Equation 13-33}$$

$$Gr = \frac{L^3 g \beta_{th} \Delta T}{\nu^2} \quad \text{Equation 13-34}$$

$$\alpha_{th,h} = \left( 0.6 + 0.387 \left[ \frac{L^3 g \beta_{th} \Delta T Pr}{\nu^2} \left[ 1 + \left( \frac{0.559}{Pr} \right)^{\frac{9}{16}} \right]^{-\frac{16}{9}} \right]^{\frac{1}{6}} \right)^2 \frac{\lambda}{L} \quad \text{Equation 13-35}$$

$$P_{cond,h} = \left( 0.6 + 0.387 \left[ \frac{L^3 g \beta_{th} \Delta T Pr}{\nu^2} \left[ 1 + \left( \frac{0.559}{Pr} \right)^{\frac{9}{16}} \right]^{-\frac{16}{9}} \right]^{\frac{1}{6}} \right)^2 \frac{\lambda S_h (T_s - T_a)}{L} \quad \text{Equation 13-36}$$

$$R_{\theta,cond} = \frac{\Delta T}{P} \quad \text{Equation 13-37}$$

$$R_{\theta,cond,h} = \frac{T_s - T_a}{\left( 0.6 + 0.387 \left[ \frac{L^3 g \beta_{th} (T_s - T_a) Pr}{\nu^2} \left[ 1 + \left( \frac{0.559}{Pr} \right)^{\frac{9}{16}} \right]^{-\frac{16}{9}} \right]^{\frac{1}{6}} \right)^2 \frac{\lambda S_h (T_s - T_a)}{L}} \quad \text{Equation 13-38}$$

Vertical

$$Nu = \left(0.825 + 0.387[Raf_1(pr)]^{\frac{1}{6}}\right)^2 \quad \text{Equation 13-39}$$

$$f_1(Pr) = \left[1 + \left(\frac{0.492}{Pr}\right)^{\frac{9}{16}}\right]^{-\frac{16}{9}} \quad \text{Equation 13-40}$$

$$Ra = GrPr \quad \text{Equation 13-41}$$

$$Gr = \frac{L^3 g \beta_{th} \Delta T}{\nu^2} \quad \text{Equation 13-42}$$

$$\alpha_{th,v} = \left(0.825 + 0.387 \left[ \frac{L^3 g \beta_{th} \Delta T Pr}{\nu^2} \left[1 + \left(\frac{0.492}{Pr}\right)^{\frac{9}{16}}\right]^{-\frac{16}{9}} \right]^{\frac{1}{6}}\right)^2 \frac{\lambda}{L} \quad \text{Equation 13-43}$$

$$P_{cond,v} = \left(0.825 + 0.387 \left[ \frac{L^3 g \beta_{th} \Delta T Pr}{\nu^2} \left[1 + \left(\frac{0.492}{Pr}\right)^{\frac{9}{16}}\right]^{-\frac{16}{9}} \right]^{\frac{1}{6}}\right)^2 \frac{\lambda S_v (T_s - T_a)}{L} \quad \text{Equation 13-44}$$

$$R_{\theta,cond} = \frac{\Delta T}{P} \quad \text{Equation 13-45}$$

$$R_{\theta,cond,v} = \frac{T_s - T_a}{\left(0.825 + 0.387 \left[ \frac{L^3 g \beta_{th} (T_s - T_a) Pr}{\nu^2} \left[1 + \left(\frac{0.492}{Pr}\right)^{\frac{9}{16}}\right]^{-\frac{16}{9}} \right]^{\frac{1}{6}}\right)^2 \frac{\lambda S_v (T_s - T_a)}{L}} \quad \text{Equation 13-46}$$

## II. Forced Convection

## III. Radiation

$$P_{rad} = 5.7 \cdot 10^{-8} \cdot E \cdot A_{eff} (T_s^4 - T_a^4) \quad \text{Equation 13-47}$$

$$R_{\theta,rad} = \frac{T_s - T_a}{5.7 \cdot 10^{-8} \cdot E \cdot A_{eff} (T_s^4 - T_a^4)} \quad \text{Equation 13-48}$$

### Example:

0077715A7 with 99 turns

$T_c, T_s$  78

Core winding resistance ignored

$T_a$  25

$\beta_{th}$	0.003081	Values found in Table 7-5 Evaluated at $\frac{T_s - T_a}{2}$
E	0.58	emissivity
$A_{eff}$	0.0058	Surface emissivity area
$A_v$	0.0062	Vertical area
$L_v$	0.0153	Vertical area
$v$	$3.26 \cdot 10^{-5}$	

$$R_{\theta,rad} = \frac{78 - 25}{5.7 \cdot 10^{-8} \cdot E \cdot A_{eff}(351.15^4 - 298.15^4)} = \frac{0.219}{A_{eff}}$$

$$Gr = \frac{L^3 g \beta_{th} \Delta T}{v^2} = \frac{0.0153^3 \cdot 9.81 \cdot 0.003081 \cdot 53}{(3.26 \cdot 10^{-5})^2} = 5398$$

$$Ra = GrPr = Gr \frac{v \rho_{th} C_p}{\lambda} = Gr \cdot 3.26 \cdot 10^{-5} \cdot 1.03 \cdot \frac{1000}{0.04432} = Gr \cdot 0.7576 = 4089.6$$

$$f_1(Pr) = \left[ 1 + \left( \frac{0.492}{Pr} \right)^{\frac{9}{16}} \right]^{-\frac{16}{9}} = 0.35$$

$$Nu = \left( 0.825 + 0.387 [Ra f_1(Pr)]^{\frac{1}{6}} \right)^2 = \left( 0.825 + 0.387 [4089.6 \cdot 0.35]^{\frac{1}{6}} \right)^2 = 4.51$$

$$\alpha_{th} = \frac{Nu \lambda}{L} = \frac{4.51 \cdot 0.04254}{0.0153} = 12.54$$

$$P_v = A_v \alpha_{th} (T_{th,s} - T_{th,\infty}) = 0.0062 \cdot 12.54 (51.5) = \mathbf{4.004 \text{ [W]}}$$

$T_c, T_s$	178	Core winding resistance ignored
$T_a$	25	
$\beta_{th}$	0.00267	Values found in Table 7-5 Evaluated at $\frac{T_s - T_a}{2}$
E	0.58	emissivity
$A_{eff}$	0.0058	Surface emissivity area
$A_v$	0.0062	Vertical area
$L_v$	0.0153	Vertical area
$v$	$3.26 \cdot 10^{-5}$	

$$Gr = \frac{L^3 g \beta_{th} \Delta T}{v^2} = \frac{0.0153^3 \cdot 9.81 \cdot 0.00267 \cdot 101.5}{(4.06 \cdot 10^{-5})^2} = 5776.54$$

$$Ra = GrPr = Gr \frac{v \rho_{th} C_p}{\lambda} = Gr \cdot 4.06 \cdot 10^{-5} \cdot 0.892 \cdot \frac{1000}{0.0474} = Gr \cdot 0.764 = 4413.47$$

$$f_1(Pr) = \left[ 1 + \left( \frac{0.492}{Pr} \right)^{\frac{9}{16}} \right]^{-\frac{16}{9}} = 0.3581$$

$$Nu = \left( 0.825 + 0.387 [Ra f_1(Pr)]^{\frac{1}{6}} \right)^2 = \left( 0.825 + 0.387 [4413.47 \cdot 0.3581]^{\frac{1}{6}} \right)^2 = 4.60$$

$$\alpha_{th} = \frac{Nu\lambda}{L} = \frac{4.6 \cdot 0.0474}{0.0153} = 14.25$$

$$P_v = A_v \alpha_{th} (T_{th,s} - T_{th,\infty}) = 12.54(51.5) = \mathbf{8.96 [W]}$$

## H Pictures from the laboratory



Figure 13-4 The loss measurement setup with a Brochause steel tester

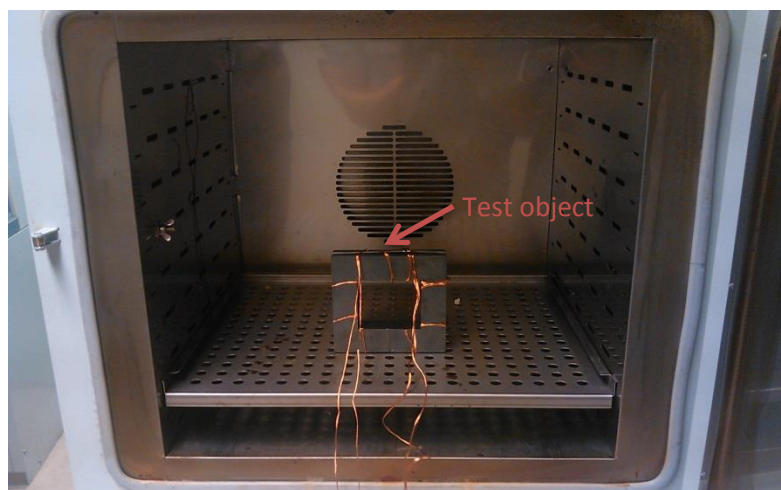


Figure 13-5 The heating chamber

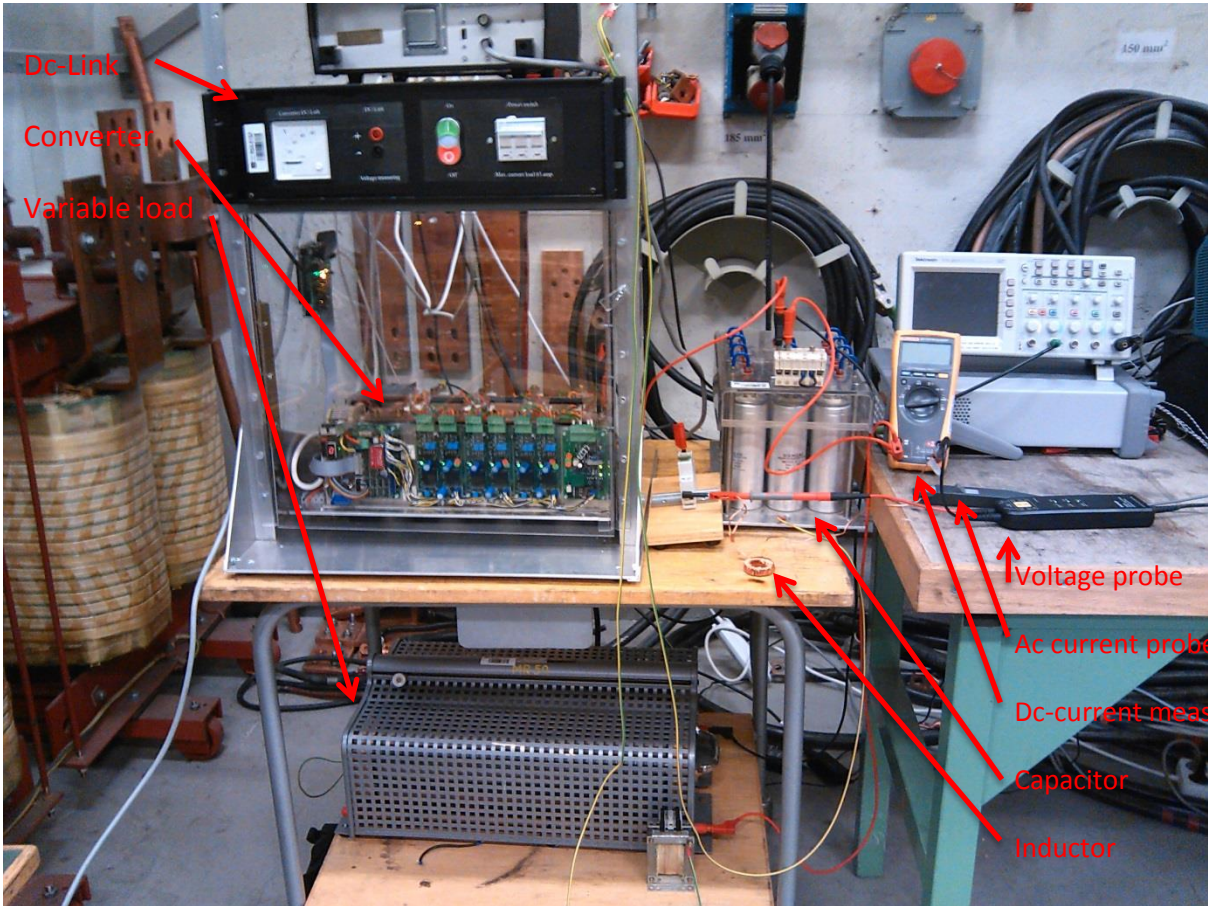


Figure 13-6 Buck converter



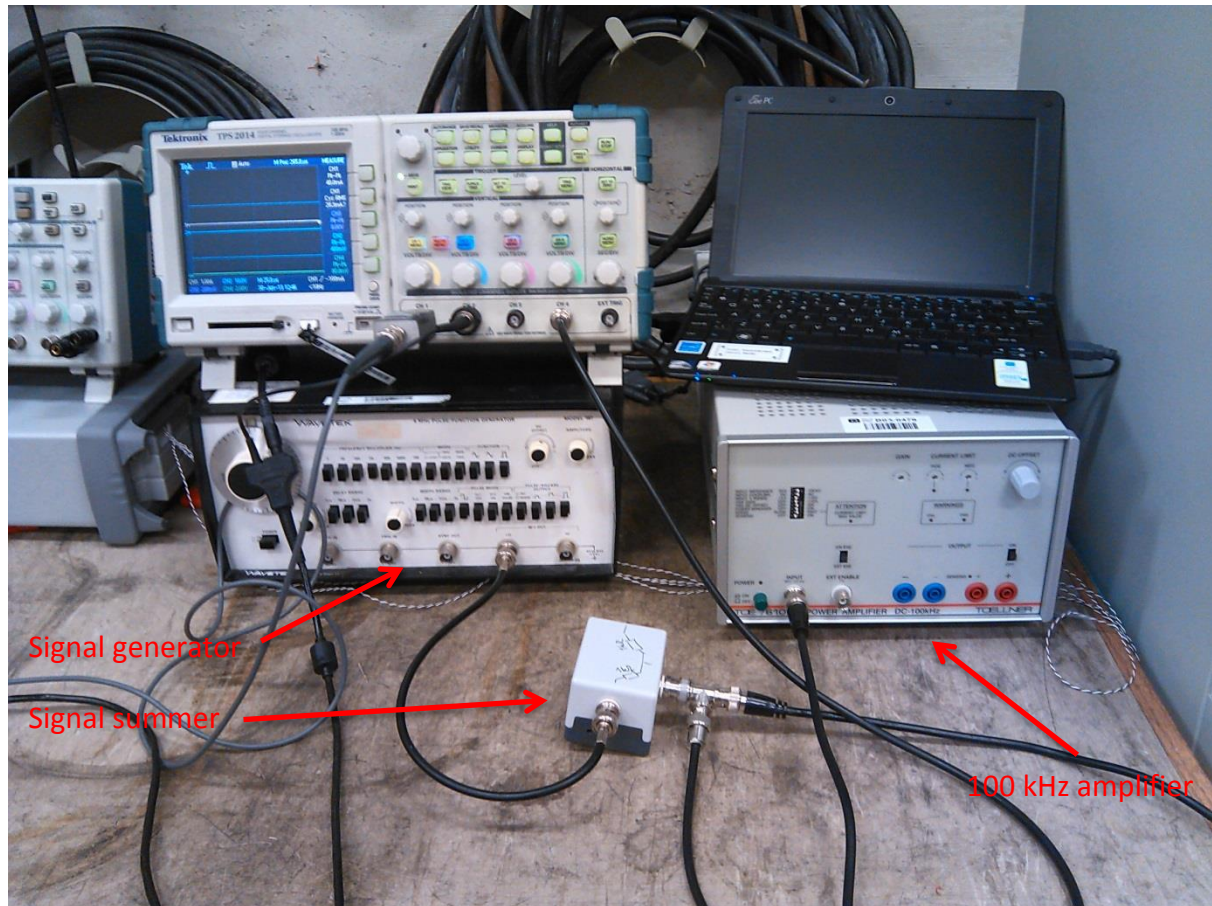


Figure 13-7 The 100 kHz amplifier setup

## I Python Source code

The python source code was uploaded to DAIM and should be found in the NTNU database.